THE UNIVERSITY OF CHICAGO

HIPPOCAMPAL CA1 AND CA3 NETWORK DYNAMICS UNDERLYING EPISODIC MEMORIES

A DISSERTATION SUBMITTED TO
THE FACULTY OF THE DIVISION OF THE BIOLOGICAL SCIENCES
AND THE PRITZKER SCHOOL OF MEDICINE
IN CANDIDACY FOR THE DEGREE OF
DOCTOR OF PHILOSOPHY

COMMITTEE ON NEUROBIOLOGY

BY
CAN DONG

CHICAGO, ILLINOIS
DECEMBER 2022

This thesis is dedicated to my grandpa, Shichun Mi and grandma Sukun Wang.

TABLE OF CONTENTS

LIST OF FIGURES

LIST OF TABLES

ACKNOWLEDGMENTS

I am extremely grateful to my advisor, mentor and friend Dr. Mark Sheffield for his guidance and support over the past six years. Mark took me as a rotation student in the summer of 2017 and there my adventure begins. As the first graduate student in the lab, it was a privilege to learn everything from him directly. Mark has taught me so much, he taught me how to build the very first rig in my life, how to design a scientific project, how to troubleshoot every small problem, how to write a manuscript and how to confidently communicate my science. During the whole journey he provided me with great support, patience and care one cannot ask for better. I feel incredibly lucky and grateful.

I want to thank the past and present Sheffield lab members - Seetha Krishnan, Antoine Madar, Douglas Goodsmith, Chad Heer, Anqi Jiang, Heather Macomber, Yuhung 'Tommy' Chiu, Madeline Klinger, Chery Cherian, Sophia Vann-Adibe, Joe Dipietro, Denisse Morales-Rodriguez, Mohamed Fawaz - for so many things: for teaching me, for helping me, for all the mindful discussions, for encouragement and for all the fun we had. I give special thanks to Seetha, for bringing so much joy in the lab and in life. I thank her for collaborating with me on the CFC project, she was my mental and experimental saver for troubleshooting over almost a year. I thank Antoine for working with me on my first manuscript, I learned a lot from his deep thought in science. I thank Chad, Chery, Madeline and Sophia for being my lab buddy in the early years of rig building and surgery practicing.)

I thank my thesis committee members: Dr. John Maunsell, Dr. Jason MacLean, Dr. Narayanan 'Bobby' Kasthuri, and Dr. Wei Wei, for their great suggestions and insights along the way, scientific-wise and career pathway-wise. It has been a great privilege for me to learn from them.

I thank my friends outside the lab who has been helping me and loving me during this long journey. I thank Xiaolin Huang and Qinpu He, who were UChicago neuroscience PhD too, for accompanying me and encouraging me. I thank Wenqing Fan, for supporting me and

trusting me since middle school. I thank Shilu Zheng, for being with me together to find our pathway in academia since college. I was lucky to have so many great friendships.

Finally, I would like to thank my family, my grandparents Shichun Mi and Sukun Wang, my parents Gang Dong and Jianghua Mi for raising me and educating me with the best love, and my parents-in-law for being understanding and supportive. Last but not least, I would love to thank my husband Hanyu Li, for sharing the excitement of new findings and easing the upset of unsuccessful tries, for supporting my choice with no hesitation and for encouraging me to be brave and confident. This thesis would not have been possible without him by my side.

ABSTRACT

When exploring new environments animals form spatial memories that are updated with experience and retrieved upon re-exposure to the same environment. The hippocampus is thought to support these memory processes, but how this is achieved by different sub-networks such as CA1 and CA3 remains unclear. My doctoral work aims at studying the CA1 and CA3 network dynamics when animals experience neutral or noxious novel environments and interpreting the underlying function of CA1 and CA3 during memory encoding and recall.

In chapter 1, to understand how hippocampal spatial representations emerge and evolve during familiarization with a neutral novel environment, we performed 2-photon calcium imaging in mice running in new virtual environments and compared the trial-to-trial dynamics of place cells in CA1 and CA3 over days. We found that place fields in CA1 emerge rapidly but tend to shift backward from trial-to-trial and remap upon re-exposure to the environment a day later. In contrast, place fields in CA3 emerge gradually but show more stable trial-to-trial and day-to-day dynamics. These results reflect the different roles of CA1 and CA3 in spatial memory processing during familiarization with new environments and constrain the potential mechanisms that support them.

In chapter 2, to study the network dynamics in CA1 and CA3 during contextual fear memory formation and recall, we implemented a novel behavioral and imaging paradigm for CFC in virtual reality where simultaneous two-photon calcium imaging of the hippocampal CA1 and CA3 was performed. We observed CFC behaviors in head-fixed mice in virtual reality similar to freely moving animals. We identified co-activated neuronal ensembles independently within CA1 and CA3 and also across CA1 and CA3 during contextual fear memory formation and recall. Interestingly, across regions co-activate events were associated with fear memory encoding and recall, suggesting synchronized activity across hippocampal sub-networks is a feature of memory encoding and recall in the hippocampus.

Overall, my thesis provide the field with a new method to access CA1 and CA3 neurons simultaneously with two-photon imaging. Moreover, we investigated the CA1 and CA3 network dynamics when neutral or fearful novel memory formed and recalled. We found distinct CA1 and CA3 place field dynamics during neutral memory formation and recall, indicating distinct role of CA1 and CA3 in memory processing. On the other hand, we found synchronized CA3-CA1 co-activation events associated with contextual fear memory formation and recall, indicating the cross-network connection is also critical for memory formation and recall.

CHAPTER 1

INTRODUCTION

Learning and memory are essential for animal survival and higher order functions and hence have been a critical and central topic in neuroscience. The fact that memory is stored in the brain only started to be accepted in mid 20th century. With more than 70 years of study of memory, it has been divided into short-term and long-term memory. Short-term memory maintains transient representation of information relevant to immediate goals. Long-term memory, as the name suggests, refers to storing information over an extended period. Short-term memory could be transferred to long-term memory. Long-term memory can be further divided into explicit and implicit memory, where explicit memory refers to all consciously available memories and implicit memory refers to the use of objects or movements of the body. In this thesis, I will focus on discussing episodic memory, memory for specific events in time, as well as supporting their formation and retrieval, which is a subdivision of explicit memory.

1.1 What does the hippocampus do?

The study of the hippocampus could be traced back to 1911 or even earlier when Santiago Ramón y Cajal drew the main connections of the hippocampus formation (Andersen 1975) (Fig. 1.1). Although the hippocampus is now well known as a critical brain region for episodic memory, this fact hadn't been accepted until a series of studies with the patient H.M (Henry Molaison) was reported. Patient H.M, who suffered from untreatable temporal lobe epilepsy, had his hippocampal formation, amygdala and parts of the multimodal association area of the temporal cortex bilaterally removed to control the seizures. Surprisingly, after the surgery, H.M lost the ability to form new memories of facts and events, whereas he still remembered his childhood events and had relatively normal cognitive functions such

as sensory, attentional and motivational processes (Scoville and Milner 1957). This finding indicates that the hippocampus is necessary during the formation and storage of the newly formed declarative memory. The finding with patient H.M started a new era of hippocampus-related studies ranging from system to cellular levels of human and other animal species to further demonstrated the role of the hippocampus in declarative memory, especially episodic memory.

In this section, I will briefly review some studies that support the hippocampus' critical role in memory encoding, storage and retrieval. Since this thesis is based on projects tested on mice, the review is focused, but not exclusively, on rodents studies.

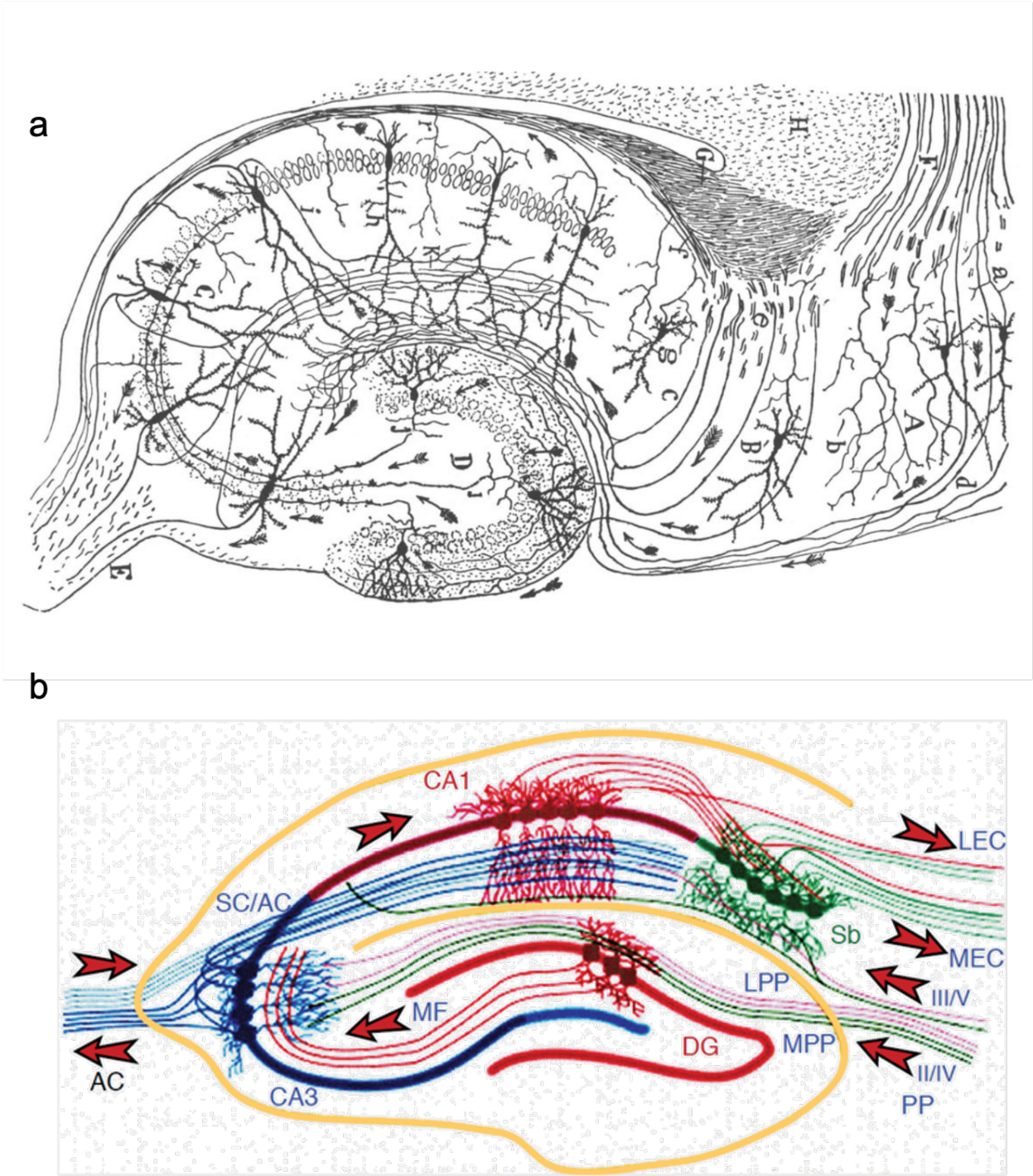

Figure 1.1: **Schematic drawing of the hippocampal formation. (a)** An anatomically faithful rendering of the cell types and their connections of the hippocampus by Ramón y Cajal (1911) of the main cells, connections, and flow of impulse traffic in the hippocampal formation. This figure is adapted from Andersen 1975, The hippocampus. **(b)** Diagrams of the hippocampus network and connectivity. (Dentate Gyrus, DG; Cornus Ammonis, CA, which can be further divided into CA3, CA2 and CA1; Subiculum, SB) This figure is adapted from Kesner 2013, Neurobiological Foundations of an Attribute Model of Memory.

In 2014, the Nobel Prize for Physiology and Medicine was rewarded to John O'Keefe and May-Britt and Edvard Moser "for their discoveries of cells that constitute a positioning system in the brain". The key brain structures that carry the 3D outside world information are the hippocampus and para-hippocampus formation. The series of studies for the 'brain GPS' started from the identification of place cells, the hippocampal neurons that fire at a specific location in a specific environment (O'Keefe and Dostrovsky 1971; O'Keefe and Conway 1978). The place cells were later to be hypothesized to be the elements of a cognitive map in the brain that represent the environment in the hippocampus and related regions (O'keefe and Nadel 1979). The view of the hippocampus as a cognitive map inspired an entire field of research on spatial representations. The following studies showed, not so surprisingly, the hippocampal neurons also have specific tuning to physical items (Wood, Dudchenko, and Eichenbaum 1999), tunes (Sakurai 2002) time (Eichenbaum 2014), or abstract cues such as reward (Gauthier and Tank 2018) or even possibility of reward (Knudsen and Wallis 2021). Along with the growing understanding of the hippocampal neuron physiology, the idea that the hippocampus could continuously provide an underlying scaffolding across space and time that allow memories to persist, get updated and be retrieved while being related and distinct has been supported by more and more studies. For example, studies have shown that place cells can rapidly form when animals enter a novel environment (Sheffield, Adoff, and Dombeck 2017), supporting the encoding of experience from the very first moment. The formed neuronal spatial ensembles presist across days partially (Ziv et al. 2013; Rubin et al. 2015; Dong, Antoine D Madar, and Sheffield 2021), indicating the hippocampus keeps updating a memory meanwhile remains the memory across time. Manipulation of hippocampal network activities (Dupret et al. 2010) or place cell activities (Robinson et al. 2020) alter the animal's memory-guided spatial behavior.

Another strong piece of evidence confirming the critical role of the hippocampus in supporting memory function came from the study of neuronal 'replay' events in the hippocam-

pus. In the 1990s, scientists found place cells spontaneously recapitulate past trajectories during rest (Wilson and B. L. McNaughton 1994; Pavlides and Winson 1989). Such 'replay' events, which later showed could also happen during active task engagement (Foster and Wilson 2006), have been proposed as a mechanism necessary for memory consolidation and planning based on previous events. The replay sequences of place cells are temporally compressed versions of trajectories that the animal made in the preceding session, usually accompanied by high-frequency local field events named sharp-wave ripple (SWR) (Ólafsdóttir, Bush, and Barry 2018). The reply duration varies between 100-300ms, about 20 times faster than the actual experience (Pfeiffer and Foster 2015). This explains how animals could go over various experiences in a short period. Before the identification of reply in the hippocampus, it was unclear how the place cells 'real-time' encoding was transformed into a stable memory. The replay events that happened during the offline rest period seem to be the perfect solution for memory consolidation (Squire et al. 2015). Indeed, studies have shown that electrical interruption of sharp-wave ripple could impair performance of a spatial memory task (Dupret et al. 2010). The replay events are also preferentially activated for the novel spatial experiences (Foster and Wilson 2006). All these finds indicate reply is important for stabilizing experiences to be transformed into memories within the hippocampus or in downstream cortical regions.

With more than 50 years of studying the hippocampus and memory, advances in genetic approaches have led to activity-dependent memory tagging systems in rodents model, which allow for examination of the memory storage mechanism. The discovery of engram cells first in the hippocampus and later in other brain regions explains how memory is stored in the brain. By labeling immediate early genes that indicates neuronal activation, scientists found a group of neuron in the hippocampus that were activated after the animal went through a contextual fear-conditioned task (X. Liu et al. 2012). Scientists found that the activation is context-specific, meaning different contexts related to the contextual fear memory will

activate different neurons. These neurons are named engram cells. Loss-of-function and gain-of-function experiments on the engram cells lead to loss or gain of the behavior that expresses the contextual fear memory, respectively. These experiments provide direct evidence for the existence of the engram cells, which indicated memory could be stored in the hippocampus (X. Liu et al. 2012; Ramirez et al. 2013; Tonegawa et al. 2015).

Besides all the experimental work, a lot of effort has been devoted by theoretical neuroscientists to build models to explain how the hippocampus as a whole with distinct sub-networks could support memory encoding and retrieval. The anatomical structure that supports hippocampal computation and the role of hippocampal sub-networks in the theoretical studies will be reviewed in the later sections.

With a decent number of studies on the hippocampus place cells and engram cells, the field is wondering how the hippocampus coordinates to simultaneously encode and store memory. There is no study yet that could reveal the mechanism of hippocampal neurons becoming place cells or engram cells. A recent study showed that engram cells and place cells are not exactly the same group of neurons. Engram cells that are place cells have different place fields across days in the same environment (Tanaka et al. 2018). Another study showed engram cells display higher repetitive activity (but not necessarily spatial related) during novel context learning, and sub-ensembles of the engram cells prefer to be reactivated during sleep and during memory retrieval (Ghandour et al. 2019). More studies are required to unravel the mechanisms of memory encoding, storage and retrieval. However, with no doubt, hippocampus formation is critical for the function of memory.

1.2 The anatomy inspired hippocampal network function

The hippocampus is a cortical structure (archicortex) with a simpler and more orderly organization than the neocortex. It's a structure conserved across mammals, birds and some reptiles (Allen and Fortin 2013) (Fig. 1.2). Being a critical part of the medial temporal

lobe for episodic memory and evolutionarily older than the neocortex, the structure of the hippocampus is different from the neocortex: The mammalian hippocampus is a three-layer structure that can be divided into two separate regions: the dentate gyrus (DG) and the cornus ammonis (CA, which can be further divided into CA3, CA2 and CA1 that are connected to the neocortical through subiculum and other parahippocampal regions). Unlike the neocortex, the connection of hippocampus sub-regions is predominately unidirectional, from DG to CA3 and CA2 and then CA3 and CA2 to CA1 (Van Strien, Cappaert, and M. Witter 2009). (Notice: The long and curved form of the hippocampus runs along a dorsal-to-ventral axis in rodents. The afore-mentioned basic intrinsic circuitry is maintained throughout the long axis, however, the anatomic connection heterogeneity exists in the dorsal and ventral hippocampus. The dorsal hippocampus encodes spatial and cognitive information while the ventral hippocampus process emotion-related information (Tao et al. 2021a). Here , I will focus on the dorsal part of the hippocampus.)

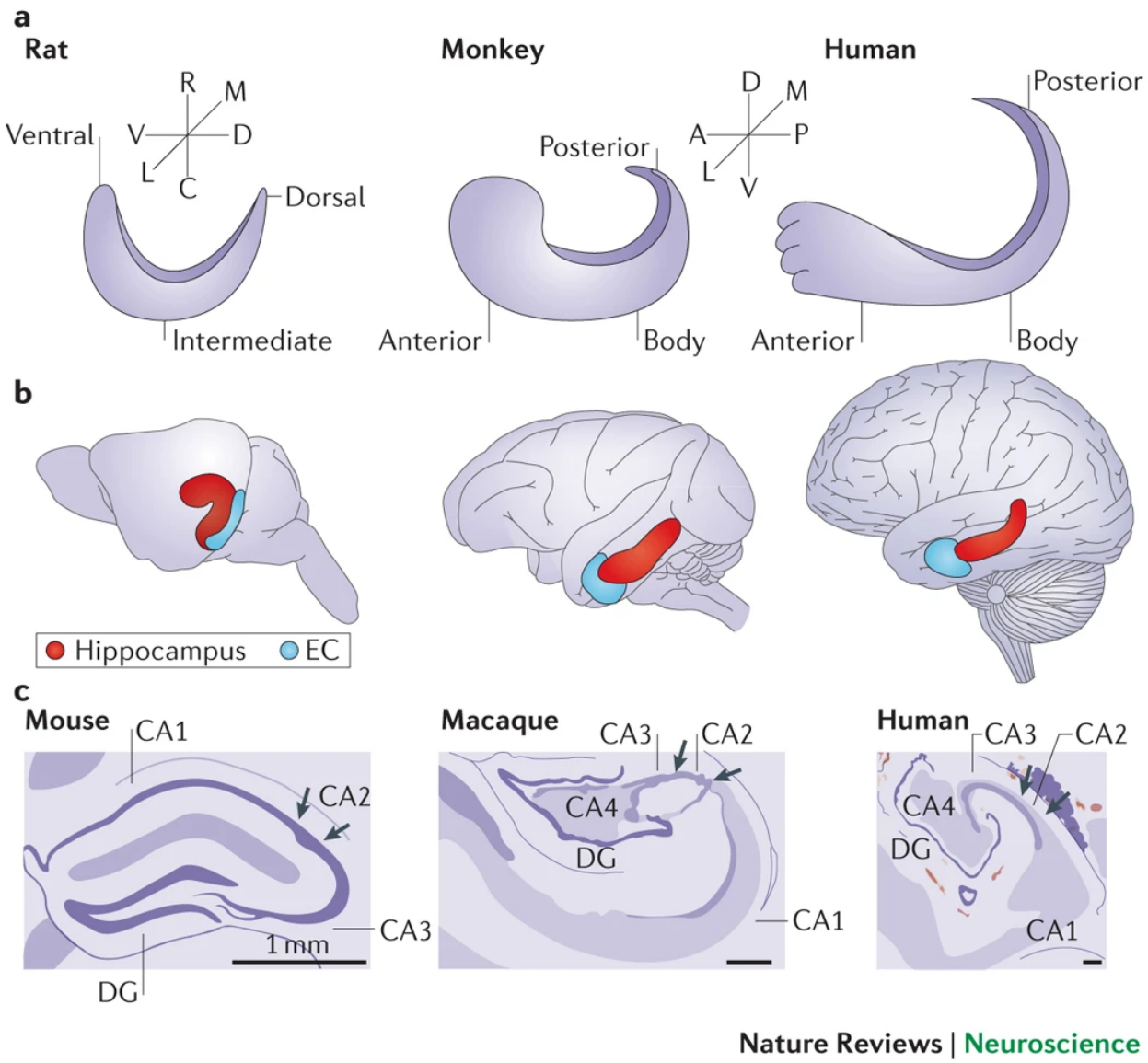

Figure 1.2: **Cross-species comparison of hippocampal anatomy.** **(a)** Schematic illustrations of the orientation of the hippocampal long axis in rats, macaque monkeys and humans. **(b)** The hippocampus (red) with the entorhinal cortex (blue) showed in the brains of rats, macaque monkeys and humans. **c** with the entorhinal cortex (EC) shown in blue. Figure is adapted with permission from (Strange et al. 2014).

The special unidirectional connection within the hippocampus, along with the interaction between the hippocampus with its neighboring entorhinal cortex has formed the classic framework for episodic memory storage and recall, which is the basic framework for the hippocampal indexing theory (Teyler and Rudy 2007; Rolls 2018). In this theory, the hip-

pocampus storage memory is an index that connects to the memory stored in the neocortex. The canonical model of this cortico–hippocampal memory framework posits that the large number and sparse activity of granule cells in the dentate gyrus (DG) provides orthogonalization of similar cortical inputs leading to pattern separation (McHugh et al. 2007; Hainmueller and Bartos 2020), the DG providing input to the recurrent CA3 network to facilitate auto association and pattern completion (McHugh et al. 2007; Cayco-Gajic and Silver 2019; Kesner and Rolls 2015), and finally, CA1 broadcasting the result to the cortex (Soltesz and Losonczy 2018; Goode et al. 2020) (Fig. 1.3 a).

The hippocampus was thought to be a good candidate for storing and recalling of activity patterns by theorists due to the within-population recurrent connection. The CA3 pyramidal neurons not only project massively to the CA1 region, but the same axons also project to other CA3 populations. Studies with single cell tracing showed that 30-75% of synapses are formed by a pair of CA3 pyramidal neuron (X.-G. Li et al. 1994). More recent patch clamp recording reported 0.92% of connected neurons within the population, much higher than random connection (Guzman et al. 2016). Based on the anatomy, theorists have built a computational model for CA3 that works as an auto-association network (Rolls 2010). These networks are good at storing and recalling patterns from partial cues which fit with the idea the CA3 work on pattern completion to store the 'index'. However, given the limited number of CA3 neurons, how CA3 could store all different patterns is a problem. To avoid interference, the idea in the index theory is the DG will be in charge of a process called 'orthogonalization', where the highly sparsely activated DG granule cells will transform similar cortical input patterns into separated outputs to CA3 (Rolls 2010), and the CA1 neurons are viewed as 'translators' to the entorhinal cortex.

The index theory has been supported by some studies (Treves et al. 2008; Jackson 2013). However, , there are some shortcomings. First, the whole theory simplifies the role of CA1 neurons, which receive complicated projections from cortical and subcortical regions such as

ventral tegmental area (VTA) and locus coeruleus (LC) which are involved neuromodulation of neuron activities (J. E. Lisman and Grace 2005; Breton-Provencher, Drummond, and Sur 2021). Second, it is unclear how the hippocampal subregions process new information while storing the old experience.

There are other theories trying to explain the role of the hippocampus in episodic memory based on anatomical and experimental studies of the prefrontal cortex (PFC) and the hippocampus (Eichenbaum 2017). This theory emphasized the direct and indirect connection between the hippocampus and the mPFC (Jay, Glowinski, and Thierry 1989; Hoover and Vertes 2007) (Fig.1.3 b). It proposes that memory is stored in the mPFC through the ventral hippocampus pathway and thalamic nucleus reuniens (RE) and the mPFC provides top-down control during memory retrieval when new information is processed through the hippocampus (Hallock, A. Wang, and Griffin 2016; Place et al. 2016; Navawongse and Eichenbaum 2013). The role of mPFC and RE in memory formation is still under studied, and there are some shortcomings of this theory too: what is the role of the hippocampus? It can't simply act as a memory encoding network given all the evidence discussed above. There are also other theories that won't be discussed in this thesis, for example, the CRISP theory (Cheng 2013).

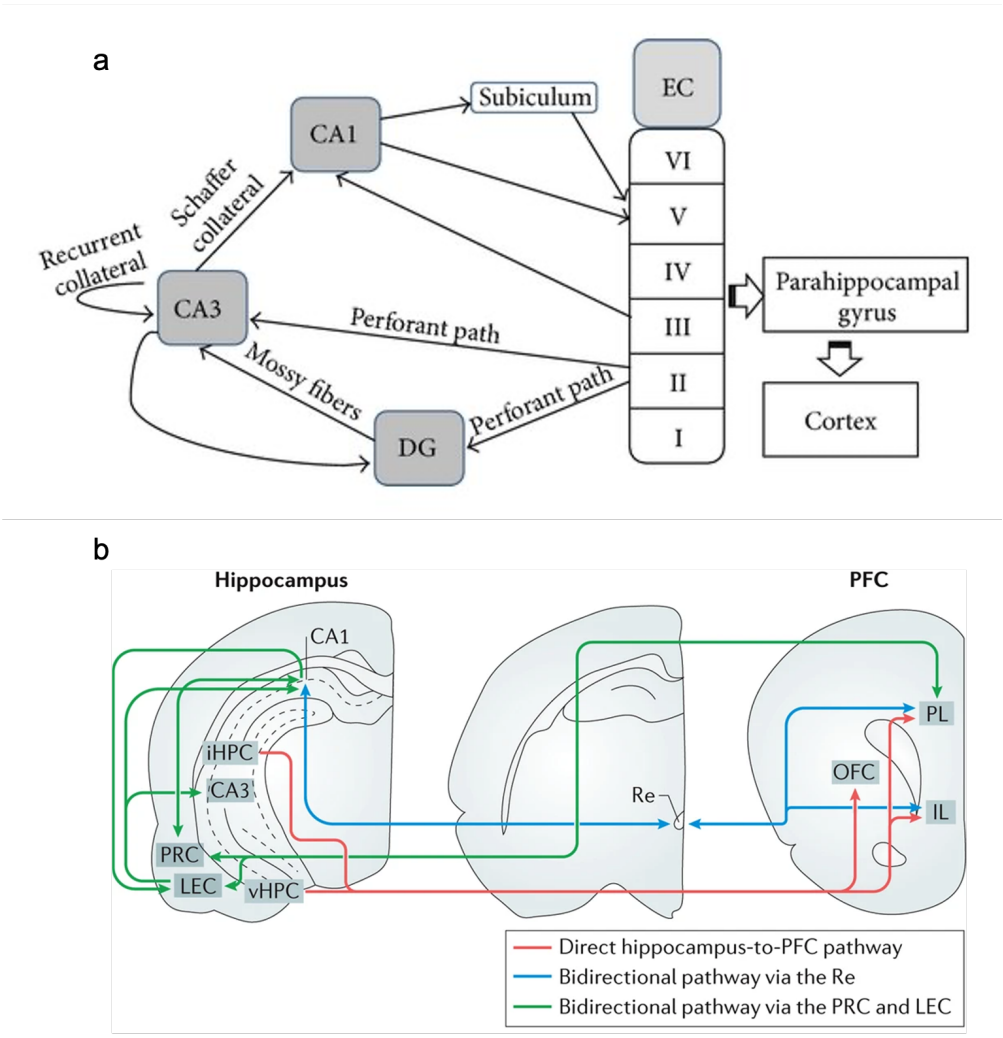

Figure 1.3: **Anatomy of the hippocampal network. (a)** The diagram illustrates the monosynaptic and the trisynaptic pathways in the hippocampus. The monosynaptic pathway consists of a direct projection from the EC to CA1 or CA3, whereas the trisynaptic pathway consists of sequential projections from EC to DG, CA3, and then to CA1. EC: entorhinal cortex; DG: dentate gyrus; CA: cornu ammonis. The figure is adapted with permission from (Yau, A. Li, and So 2015). **(b)** Indirect and direct prefrontal-hippocampal pathways. The ventral hippocampus (HPC) (as well as some more dorsal regions of the hippocampus such as the intermediate hippocampus (HPC)) sends direct connections to different regions of the prefrontal cortex (PFC), including the orbital PFC (OFC), the prelimbic cortex (PL) and infralimbic cortex (IL). In addition, two bidirectional connections between the PFC and the hippocampus exist: one via the thalamic nucleus reuniens (Re) to hippocampal area CA1 and the other via the perirhinal cortex (PRC) to hippocampal area CA1 and lateral entorhinal cortex (LEC) to hippocampal areas CA1 and CA3. Figure is adapted with permission from (Eichenbaum 2017)

Explaining how the hippocampus and related cortical regions supported memory might be one of the ultimate goals of understanding memory. The debating of different theories requires more experimental data to test different predictions and to support the building of more scientific models and simulations.

1.3 Hipoocampal CA1 and CA3

As one of the two main parts of the hippocampus, the CA (cornus ammonis), specially the CA1 and CA3 regions, has been extensively studied over the past 70 years. Both CA1 and CA3 consist of a layer of densely packed pyramidal cells (Fig.1.1 b). In mice, the CA3 neurons (140000 neurons) massively project to CA1 neurons (300000 neurons (Keller, Erö, and Markram 2018)). Although in both CA1 and CA3 the majority of the neurons are pyramidal neurons, the associational connection in CA3 (CA3-CA3 projection) is a characteristic to CA3. CA3 axons that project to CA1 neurons through the schaffer collaterals also send secondary axons to CA3 neurons. The CA3 neurons also project collaterally to CA1 and CA3 neurons through the commissural pathway, whereas the interhemispheric connections in CA1 are rather uncommon (Menno P Witter 2007; Tao et al. 2021a). The CA1 neurons, although lacking the recurrent connections of CA3, receive various input from EC, VTA etc. Given different neuronal connection and complex dendritic computation perform by the pyramidal neurons (Behabadi and Mel 2014), the CA1 and CA3 neuron activity dynamics are likely to be distinct.

With the development of behavioral and neuronal activity recording techniques, knowledge about hippocampal neuronal dynamics in behaving animal has been largely improved. A lot of the studies were done in dorsal hippocampal CA1 place cells because of the relatively easy access of the CA1 neurons and the fact that navigational task provided relatively simple behavior to relate with the neuronal dynamics. For example, scientists gained more insight into place cell dynamics during spatial representation emergence , development and retrieval.

Upon exposure to a novel environment, CA1 place fields emerged rapidly even on the first pass through of the place field (Sheffield and Dombeck 2015). In familiar environments, it has been shown that PFs in both CA1 and CA3 tend to shift backwards with experience and become negatively skewed to varying degrees depending on the behavioral paradigm used (Mehta, Quirk, and Wilson 2000; I. Lee, Rao, and Knierim 2004). Studying of the CA1 place cell formation mechanism has led to two possible candidate mechanisms for PF shifting: the spike-timing dependent plasticity (STDP) and the behavior time-scale plasticity (BTSP) (Buchanan and Mellor 2010; Bittner, Milstein, et al. 2017). Scientist identified place cell 'replay' during rest or sleep in rodents, indicating memory consolidation. (Foster 2017). When revisiting the same environment across days, only about 15-25% of CA1 PFs are stable, indicating that CA1 spatial representation are dynamic across days (Ziv et al. 2013). With all these finding, CA1 place cells seem play a critical role of spatial representation and memory function. However, how the CA1 place cells show 'one shot' learning and the actual mechanisms for place field development and across day activity pattern changes are still under debate.

Comparing with CA1, less is known about CA3 dynamics in memory encoding and retrieval. Some studies showed CA3 place field formation is slower than CA1 indicating distinct dynamics of CA1 and CA3 neurons during spatial representation (S. Leutgeb, J. K. Leutgeb, et al. 2004; Hainmueller and Bartos 2018)but in a relatively long time window (ten minutes per test) so no details about the CA3 place field emergence and development dynamics has been revealed as in CA1. Given CA3 is upstream to CA1, it is vital to systematically study CA3 neuron dynamics and compare them with CA1. Studying CA3 neuron dynamics will not only determine the distinct function of CA1 and CA3 in memory encoding and retrieval, but also provide the field with new data to build more reasonable models for hippocampal related memory.

CHAPTER 2

DISTINCT PLACE CELL DYNAMICS IN CA1 AND CA3 ENCODE EXPERIENCE IN NEW ENVIRONMENTS

This chapter is a full reprint of **"Distinct place cell dynamics in CA1 and CA3 encode experience in new environments"** (Dong, Antoine D Madar, and Sheffield 2021), in which I was first author. The work is included with permission from all authors.

2.1 Abstract

When exploring new environments animals form spatial memories that are updated with experience and retrieved upon re-exposure to the same environment. The hippocampus is thought to support these memory processes, but how this is achieved by different subnetworks such as CA1 and CA3 remains unclear. To understand how hippocampal spatial representations emerge and evolve during familiarization, we performed 2-photon calcium imaging in mice running in new virtual environments and compared the trial-to-trial dynamics of place cells in CA1 and CA3 over days. We find that place fields in CA1 emerge rapidly but tend to shift backwards from trial-to-trial and remap upon re-exposure to the environment a day later. In contrast, place fields in CA3 emerge gradually but show more stable trial-to-trial and day-to-day dynamics. These results reflect different roles in CA1 and CA3 in spatial memory processing during familiarization to new environments and constrain the potential mechanisms that support them.

2.2 Introduction

The hippocampus plays a critical role in episodic memory by rapidly forming, updating, and retrieving patterns of activity that represent specific memories(Parisi et al. 2019; Kitamura et al. 2017). The CA1 subnetwork is considered the main output of the hippocampus that

transmits information to the cortex and other regions(Goode et al. 2020), but the computational role of CA1 in memory processing remains unclear. Theoretical studies generally highlight networks upstream of CA1, such as CA3 and the medial entorhinal cortex (MEC) as being attractor networks that encode and retrieve representations associated with different environments(Goode et al. 2020; Latuske et al. 2018; Knierim and Zhang 2012; Jeffery 2011; Kesner and Rolls 2015). These representations could then simply be inherited by CA1 (Solstad, E. I. Moser, and Einevoll 2006; Neher, Amir Hossein Azizi, and Cheng 2017; Mankin, Diehl, et al. 2015). However, given the many forms of synaptic plasticity at CA1 synapses (Magee and Grienberger 2020; Buchanan and Mellor 2010), the complex dendritic computations performed by CA1 neurons (Sheffield and Dombeck 2015; Sheffield and Dombeck 2019; Sheffield, Adoff, and Dombeck 2017) and the diversity of CA1 interneurons (Pedrosa and Clopath 2020; Tamas F Freund and Buzsáki 1996), CA1 activity dynamics are unlikely to be purely inherited from upstream regions. Establishing the difference in activity dynamics between CA1 and its inputs will help reveal how information is processed by CA1, which computations are specific to CA1, and what the role of its inputs are.

Spatial memories are thought to be encoded and retrieved in the hippocampus through the activity of place cells(Hainmueller and Bartos 2018; Dupret et al. 2010; C. Kentros 2006; C. G. Kentros et al. 2004; Robinson et al. 2020) – cells with spatially selective firing fields called place fields (PFs). All hippocampal subnetworks (CA1, CA2, CA3, and dentate gyrus) express PFs during navigation (Mankin, Diehl, et al. 2015; Hainmueller and Bartos 2018). Importantly, CA1 pyramidal neurons develop PFs rapidly during exploration of a novel environment (Frank, Stanley, and Brown 2004). Understanding how hippocampal representations emerge so rapidly during one-shot events is critical to refine theories of memory. However, the specific dynamics and underlying mechanisms of PF emergence in CA1 have only recently come into focus, and even less is known about PF emergence in CA3, the main input region to CA1 (Magee and Grienberger 2020; Sheffield and Dombeck

2019; Sheffield, Adoff, and Dombeck 2017; Bittner, Milstein, et al. 2017; Cohen, Bolstad, and A. K. Lee 2017; Epsztein, Brecht, and A. K. Lee 2011; S. Leutgeb, J. K. Leutgeb, et al. 2004). An important step forward came from analyzing PFs on a trial-to-trial basis during the very first moments in a novel environment (Sheffield, Adoff, and Dombeck 2017). Such trial-to-trial resolution showed that many neurons in CA1 develop a PF on the first trial and engage synaptic plasticity mechanisms in the form of increased dendritic branch spike prevalence (Sheffield and Dombeck 2019; Sheffield, Adoff, and Dombeck 2017). Determining the dynamics of PF emergence in CA3 under the same conditions in novel environments will generate new insights into the mechanisms of PF emergence in CA1 and reveal the extent to which CA1 PF emergence is inherited from CA3 PFs.

In addition to how spatial representations emerge, understanding how they evolve during familiarization to a novel environment (a form of spatial learning) is also critical to refine theories of learning and memory. Little is known about trial-to-trial PF dynamics in CA1 or CA3 with most studies focusing on mean PF dynamics across conditions (Hainmueller and Bartos 2018; Ziv et al. 2013; Geiller et al. 2017). In familiar environments it has been shown that PFs in both CA1 and CA3 tend to shift backwards with experience and develop negatively skewed PFs to varying degrees depending on the behavioral paradigm used (Geiller et al. 2017; I. Lee, Rao, and Knierim 2004; Roth et al. 2012; Mehta, Quirk, and Wilson 2000). This is thought to be an experience-dependent process that requires NMDA receptor-dependent long-term synaptic plasticity (Ekstrom et al. 2001). How soon these phenomena appear during the familiarization process, and whether they are inherited by CA1 from CA3, remains unclear (Roth et al. 2012). Tracking large numbers of CA1 and CA3 neurons under the same conditions during familiarization to novel environments will help better understand these phenomena.

Memory retrieval is thought to be achieved by reinstating the same neuronal activity that occurred during learning (Mankin, Diehl, et al. 2015; Reijmers et al. 2007; X. Liu et al. 2012).

However, evidence from recordings of large ensembles of place cells has shown that many PFs in CA1 are unstable across exposures to the same familiar environment (Sheffield and Dombeck 2015; Hainmueller and Bartos 2018; Ziv et al. 2013; Kinsky et al. 2018; Rubin et al. 2015; Jeantet and Cho 2012; Mankin, Sparks, et al. 2012). Again, as with PF emergence and trial-to-trial dynamics, a lot less is known about the stability of CA1 and CA3 PFs during re-exposure to a novel environment. This has left unclear how familiarization influences PF stability. CA1 PFs might be expected to be less stable across days than CA3 PFs as CA1 has been shown to integrate stable spatial information from CA3 with time signals from CA2 upon re-exposures to the same familiar environment (Mankin, Diehl, et al. 2015). Further support for the idea of reactivation of stable PFs in CA3 comes from its hypothesized role in pattern completion (Kesner and Rolls 2015), although recent experimental findings tracking PFs in novel environments across days suggest otherwise (Hainmueller and Bartos 2018). Lastly, trial-to-trial retrieval dynamics of single PFs during re-exposure to a novel environment are not known because of the technical difficulty of tracking the same place cells across days (Roth et al. 2012). Overall, how PFs emerge, evolve and stabilize during familiarization to a novel environment is unclear, both in CA1 and CA3.

In this work we use 2-photon $Ca2^{+}$ imaging to longitudinally record from large populations of CA1 and CA3 pyramidal neurons in head-fixed mice running unidirectionally on a treadmill to repeatedly traverse visually enriched virtual linear environments with consistent behavior. We track neurons from the very first moments in a novel environment and across days to compare the emergence and ongoing dynamics of PFs. We find that PFs initially emerge much faster in CA1 than CA3, but CA1 PFs on average continuously shift backwards with experience. CA3 PFs emerge relatively slowly but are subsequently more reliable than CA1 PFs across trials, displaying less backward shifting. We also find that PF backward shifting decreases with familiarization across trials and across days. Upon re-exposure to the novel environment on the second day, stable PFs in CA3 reactivate rapidly on the first

trial, whereas CA1 PFs demonstrate a higher propensity to remap across days. Our findings demonstrate major differences in the initial emergence, shifting, and stability of PFs in CA1 and CA3 during familiarization to a novel environment. The distinct features of CA1 PFs compared to CA3 PFs suggests the CA1 performs significant computations on its spatial inputs from CA3 to support a distinct role in spatial memory processing.

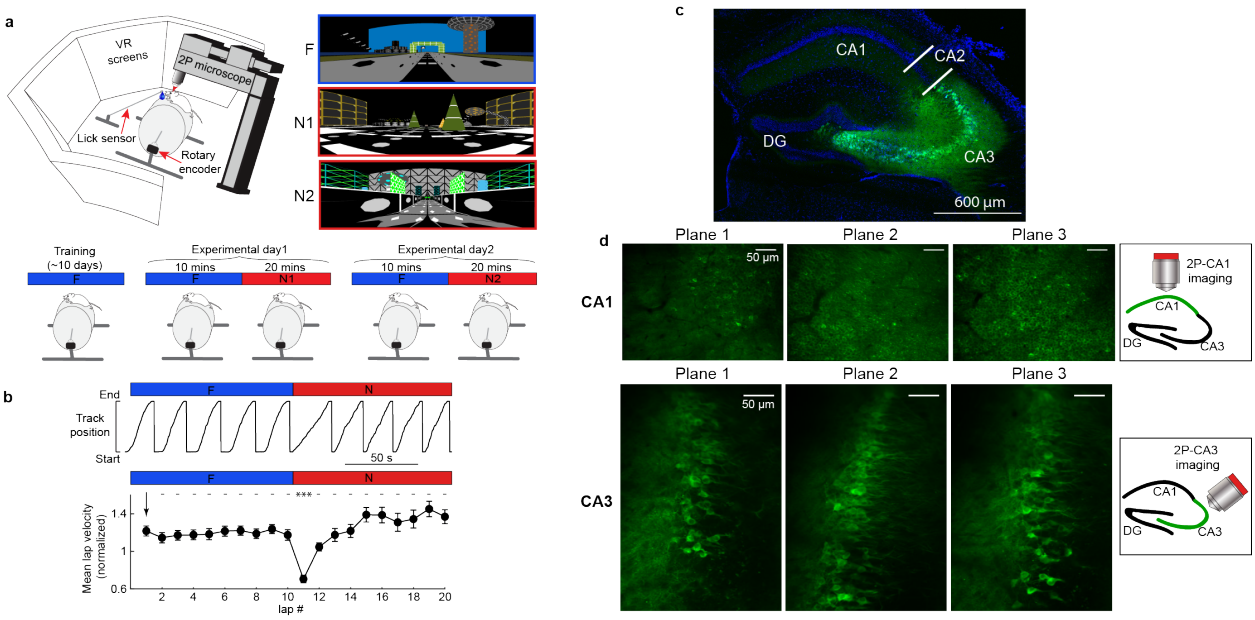

Figure 2.1: **Experimental Setup: a,**, Top left, depiction of the virtual reality (VR) set up. Top right, the familiar (F) and two novel (N1 and N2) environments. Bottom: Scheme of the experimental procedure. **b,** Top: Single mouse behavior showing track position versus time during an F to N switch. Bottom: Summary data across all mice of mean lap velocity during F and N (n = 20 sessions in 11 mice). Lap velocity is normalized to the mean lap velocity in each mouse ±SEM, and each lap is compared to the first lap in F using a one-way ANOVA with Tukey HSD post hoc test. ***, $P < 0.001$, P = 6.27e-15. **c**, Brain slice showing specific CA3 expression of cre-dependent GCaMP6f (green) and DAPI for nuclei (blue) from a Grik4-cre transgenic mouse. **d,** Example field of views (FOV) from multiplane imaging in CA1 (top) and CA3 (bottom). Right: scheme of the position for the objective during imaging.

2.3 Results

2.3.1 Place field emergence in a novel environment in CA1 and CA3

We expressed GCaMP6f in either dorsal CA1 or CA3a (referred to as CA3 from here on) of different mice (Fig. 2.1c, d). The Grik4-cre line (Nakazawa et al. 2002) was used to restrict expression to CA3 pyramidal neurons (Fig. 2.1c). Importantly, these mice show CRE expression in nearly 100 % of pyramidal cells in CA3 which means our recordings were not biased to a sub-population of CA3 pyramidal cells(Nakazawa et al. 2002) . Using 2-photon microscopy we then recorded calcium transients from pyramidal cell populations in both regions (Supplementary Fig. 2.7) (Sheffield and Dombeck 2015; Sheffield, Adoff, and Dombeck 2017). On experimental day 1 mice were exposed to a familiar (F) environment before being switched to a novel environment (N1) (Fig. 2.1a)(Sheffield, Adoff, and Dombeck 2017). On experimental day 2, mice experienced the same F-to-N switch but to a different N environment (N2; Fig. 2.1a). N1 and N2 were grouped together and are referred to as N. Mice momentarily slowed down after the transition between environments (Fig. 2.1b), confirming their perception of the switch to N. Because mice were restricted to running in 1 dimension on a custom-built treadmill, this paradigm led to many repeated traversals in both environments with matched behavior, allowing lap-by-lap PF dynamics to be measured systematically and compared across F and N environments without confounds caused by changes in behavior.

As has previously been reported, both CA1 and CA3 place cells globally remapped upon exposure to N (Fig. 2.2a, b) and displayed altered PF properties compared to F (Supplementary Fig. 2.8) (Latuske et al. 2018; Jeffery 2011; Sheffield, Adoff, and Dombeck 2017; Hainmueller and Bartos 2018; Colgin, E. I. Moser, and M.-B. Moser 2008; Muller and Kubie 1987; Bostock, Muller, and Kubie 1991; Fyhn et al. 2007). For instance, PF widths were on average larger and PF precision lower in N than F in both CA1 and CA3. Out-of-field PF

firing also increased in N versus F as did PF transient occupancy. Crucially, we wanted to observe the real-time emergence dynamics of new place cells in CA1 and CA3 to examine potential differences. Therefore, emergence of new PFs in N was quantified on a lap-by-lap basis (Fig. 2.2c-e). Some PFs formed instantly, i.e. on the first lap (Instant PFs; Fig. 2.2c; left), while others were delayed by several laps (Delayed PFs; Fig. 2.2c; right). Similar to previous observations, many CA1 PFs formed rapidly (Sheffield and Dombeck 2019; Sheffield, Adoff, and Dombeck 2017; Frank, Stanley, and Brown 2004), with a high proportion of instant PFs (30 %; Fig. 2.2d, e). Unexpectedly, only 9 % of CA3 PFs were instant and the distribution of PF onset lap number was more uniform, indicating CA3 PFs form more gradually than CA1 PFs (Fig. 2.2d, e; Supplementary Fig. 2.8c, d). Supporting this, CA1 place cell activity decoded position on the first lap better than CA3 place cell activity (Fig. 2.2f-h, Supplementary Fig. 2.9). These data suggest that in a novel environment, CA1 instantly forms a well-organized map, whereas CA3 forms a map gradually with experience.

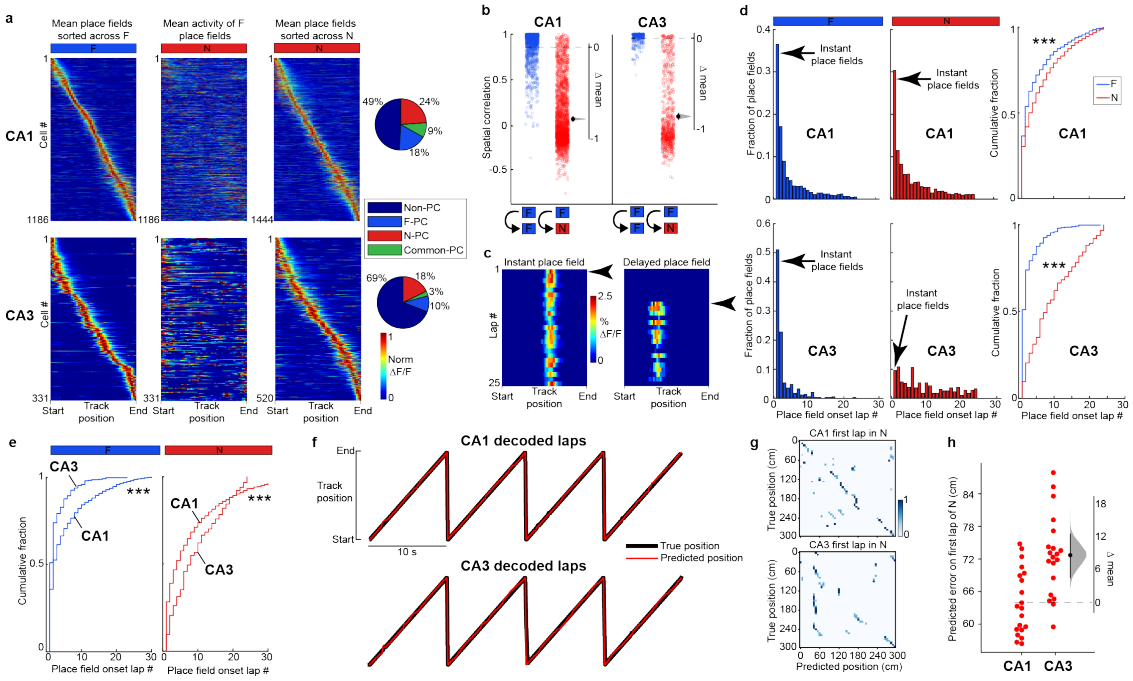

Figure 2.2: **Place field emergence in novel environments is rapid in CA1 but gradual in CA3.**

Figure 2.2, continued: **a**, Left: mean place fields (PFs) in F sorted by track position. Middle: mean activity of the same neurons on the left in N. Right: mean place fields in N sorted by track position. Far right: Percentage of place cells in F and N or common to both from all active neurons. CA1, top panels; CA3, bottom panels. $\Delta F/F$ activity is normalized to each neurons' maximum transient amplitude. n = 7 sessions in 4 mice for CA1, n = 13 sessions in 7 mice for CA3. Only place cells with single PFs are displayed, but place cells with multiple PFs are included in the pie charts and later analyses. **b**, Pearson's correlation coefficient of each cell's average activity map within F (blue, CA1 n = 1392, CA3 n = 320 neurons with activity in both halves of the F session) and between F and N (red, CA1 n = 2283, CA3 n = 698 neurons with activity in both sessions and a PF in one of them). Bootstrapped mean difference (Δ) with distribution of the mean (gray) and 95 % confidence interval (error bar) on the right of each plot (see Methods). **c**, Example of an instant PF (left) and delayed PF (right) in N. Arrows indicate PF onset lap. **d**, Histograms of PF onset laps in F (left, CA1 n = 1643 PFs, CA3 n = 336 PFs) and N (middle, CA1 n = 1712 PFs, CA3 n = 532 PFs) and cumulative fraction plots for F and N (right). Wilcoxon rank sum test, two-sided. ***, $P < 0.001$, CA1, P= 3.89e-18, CA3, P= 1.64e-55. **e**, Cumulative fraction plots for CA1 and CA3 PF onset lap in F (left) and in N (right). Wilcoxon rank sum test, two-sided. ***, $P < 0.001$, F, P= 2.94e-13, N, P= 7.40e-13. **f**, Example mouse showing true track position (black) on laps 37-40 and the predicted position (red) decoded by an LSTM decoder (see Methods). CA1, top; CA3, bottom. **g,** Confusion matrix between the predicted (x-axis) and the true (y-axis) position for the first lap in N. **h,** Predicted error on the first lap in N for CA1 and CA3. Each dot represents the decoding error for one decoder trial built based on the activity of 200 randomly chosen place cells from CA1 (left) or CA3 (right). n = 20 decoder trials. Bootstrapped mean difference (Δ) with 95 % CI (error bar) on the right.

2.3.2 Trial-to-trial place field dynamics in a novel environment

To examine and compare how PFs evolve in CA1 and CA3 during spatial learning, we tracked new PFs throughout familiarization to N. We compared the first and second half of the session and found CA3 PFs were more stable than CA1 PFs within a session in N (Fig. 2.3). Next, we computed each PF's center of mass (COM) on a lap-to-lap basis (Fig. 2.3b): in CA1, approximately half of the PFs significantly shifted during the session, but only a third in CA3 (Fig. 2.3c). The direction of shift could go backward or forward relative to the direction of the animal's motion (Fig. 2.3b-d) but most PFs shifted backwards, with a larger skew in CA1 than CA3 (Fig. 2.3c-d). As a population, CA1 PFs shifted backwards much faster than CA3 PFs (Fig. 2.3e). This difference is not an artifact of a lower sample size of CA3 PFs as shown by downsampling 1000 times the CA1 dataset (Fig. 2.3e). Removing transients prior to the onset of a robust PF (as we do for defining PF onset lap, see methods) did not alter our conclusions (Supplementary Fig. 2.4a-b). Individual PF shifting dynamics were not related to PF onset lap or velocity (Supplementary Fig. 2.5 and 2.6). Backward and forward shifting PFs occurred at all positions, with large shifts weakly biased towards the end of the track for CA1 (Supplementary Fig. 2.13). Backward shifting PFs have been previously reported and may be accompanied with an increase in PF width and the development of a negative skew with experience, although reports are conflicting (Geiller et al. 2017; I. Lee, Rao, and Knierim 2004; Roth et al. 2012; Mehta, Quirk, and Wilson 2000; Ekstrom et al. 2001; Mehta, Barnes, and B. L. McNaughton 1997). We found that, in a novel environment, PF width tended to increase through the first 10 laps in CA1 but not in CA3 (Supplementary Fig. 2.14). PFs also started with a positive skew that decreased with experience in CA1 but not in CA3 (Supplementary Fig. 2.14). Note that under calcium imaging, as compared to electrophysiology, PFs are generally positively skewed rather than symmetric as an artifact of calcium transient decay times (Dombeck et al. 2010). An evolution towards less positively skewed and larger PFs suggests that PFs

start earlier on the track (see example in Supplementary Fig. 2.14a), consistent with some electrophysiological reports (Mehta, Quirk, and Wilson 2000; Mehta, Barnes, and B. L. McNaughton 1997). However, changes in skewness and width were not the only cause of COM backward shifting, as the PFs end position also shifted backwards (Supplementary Fig. 2.4c-d). Interestingly, we noticed that in CA1 the population tended to shift forward during the first laps, with the global backward shift occurring around the 5th lap (Fig. 2.3e). We found that the delay in backward shifting was driven by instant PFs that tended to shift forward on early laps (Supplementary Fig. 2.15). It is worth restating here that CA3 shows few early-onset PFs on the initial laps which is when the forward shifting of instant CA1 PFs occurs. This suggests backward shifting in CA1 might require the presence of established CA3 PFs, which is why instant PFs initially shift forward.

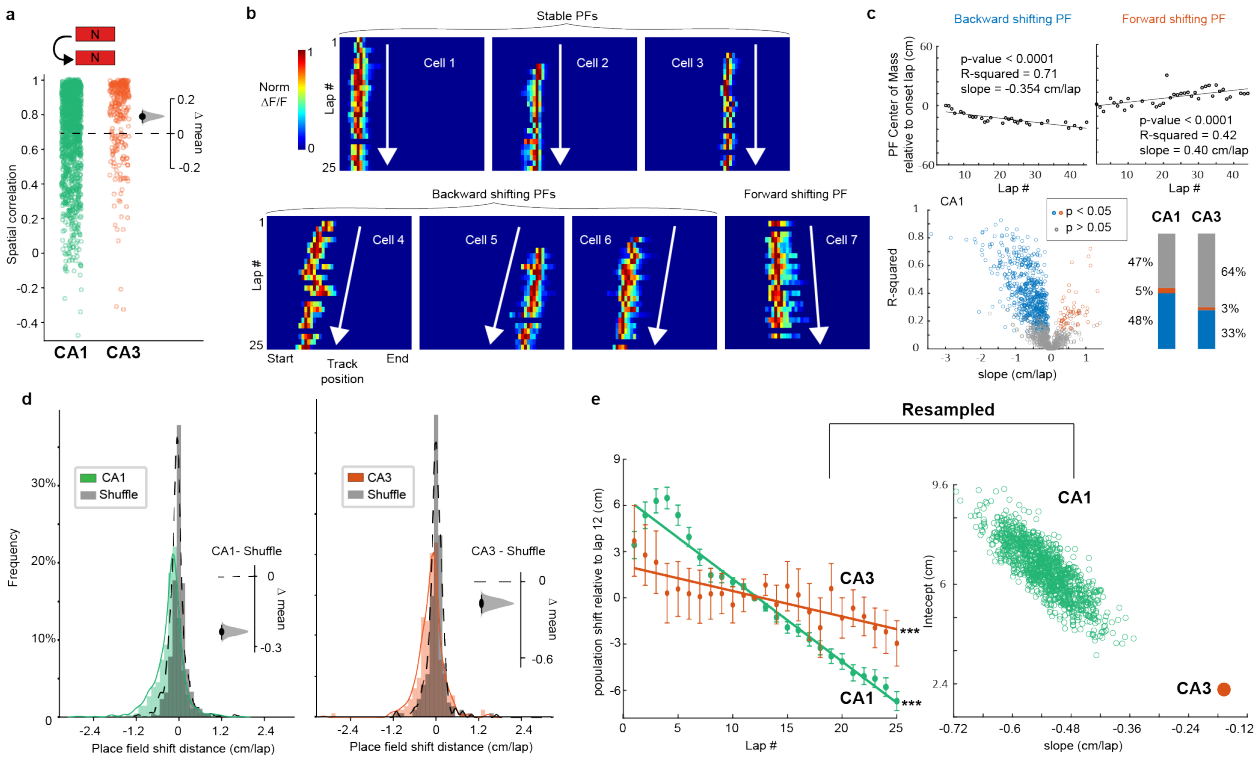

Figure 2.3: **CA3 place fields exhibit relative lap-by-lap stability while CA1 place fields shift with experience in novel environments:** **a**, Pearson's correlation coefficient of all neurons with place fields within N (average activity map in first 10 laps versus next 10 laps of session: CA1 n = 1238, CA3 n = 255 neurons). Bootstrapped mean difference (Δ) between CA1 and CA3 shown on the right. **b,** Example place cells with stable or shifting place fields (PFs) in N (lap-by-lap activity for the first 25 laps). White arrows depict the direction of shifting. **c,** Linear regression analysis on the center of mass (COM) of individual PFs (CA1 in N) shows a high number of significantly shifting PFs (blue and red dots and bars). The slope measures the direction and amplitude of the PF shift: for significantly shifting PFs, backward is blue, forward is red. CA3 has a lower proportion of significantly shifting PFs than CA1. **d,** Histograms of the COM difference between last and onset laps (5-lap weighted average, see Methods) normalized by the number of laps for each PFs in N for CA1 and CA3. Shuffling the lap numbers (grey distributions) reveals an overrepresentation of backward shifting PFs, as confirmed by the bootstrapped mean difference (Δ, insets). **e,** Population shift of COM. Left, Mean ± SEM, over all PFs, of 5-lap sliding average COM difference relative to lap 12 (see Methods), in N. CA1 (green) and CA3 (orange). Linear regression analysis (on all data points, not means) shows that the population of PFs shifts backwards significantly, both in CA1 and CA3. Linear regression, F-test, ***, $P < 0.001$, CA1, P= 3.13e-283, CA3, P= 1.31e-04. Right, The CA1 dataset was resampled 1000x using n = 175 PFs to match the number of CA3 PFs and the slope and intercept of the regression line was measured each time (green dots). CA1 slopes are always steeper than the CA3 slope indicating that the CA1 population shifts significantly faster than CA3.

2.3.3 Place field stability upon re-exposure to a novel environment across days in CA1 and CA3

Memory recall of spatial environments is generally thought to be supported by the reactivation of stable PFs upon re-exposures (Dupret et al. 2010; C. Kentros 2006; C. G. Kentros et al. 2004; McNamara et al. 2014). We therefore examined the same place cells upon re-exposure to N (specifically N2, see methods) across days (Fig. 2.4a). On N day 2, increased lap velocity on the first lap compared to the first lap on N day 1 revealed mice had become more familiar with N (Fig. 2.4b). We then quantified the spatial correlation of mean PFs identified on N day 1 with N day 2, which was on average significantly higher in CA3 (0.70 ± 0.04) than CA1 (0.49 ± 0.02) (Fig. 2.4c-f). The bimodal distribution of CA3 PF spatial correlations (Fig. 2.4d; bottom) helped categorize PFs as either stable ($R > 0.5$) or unstable ($R <= 0.5$). In all mice we found that CA3 had a higher fraction of stable PFs compared to CA1 (Fig. 2.4e). Interestingly, in CA1, we found a small but significant positive correlation between PF shifting on N day 1 and PF spatial correlation across days, suggesting that higher day-to-day PF stability is associated with more stable trial-to-trial PF dynamics upon the first exposure to a novel environment (Supplementary Fig. 2.16). We then compared the PF onset laps of stable PFs on day 2 (re-emergence, Fig. 2.4g, left) with PFs that newly formed on day 2, which included both unstable PFs from day 1 (Fig. 2.4g, middle) and PFs that appeared for the first time on day 2 (Fig. 2.4g, right). We found that stable PFs re-emerged earlier in the session than newly formed PFs, and this difference was much more apparent in CA3 than CA1 (Fig. 2.4h, right). Further, a high proportion of CA1 PFs are continuously forming even as the environment becomes familiar. Lastly, similar to day 1, the vast majority of new PFs in CA3 emerge gradually after a delay with very few instant PFs (Fig. 2.4h, bottom-middle and bottom-right) whereas the CA1 again shows a much higher proportion of instant PFs on day 2 (Fig. 2.4h, top-middle and top-right). This reveals that stable CA3 PFs are retrieved much faster than new PFs emerge during

re-exposure on day 2, whereas stable and new PFs in CA1 show similar emergence dynamics.

2.3.4 Lap-by-lap dynamics across days

We first asked if there was any evidence of continuous PF shifting of the population occurring offline between sessions separated by a day. We found no such evidence as the distribution of PF shift distance between the end of the session on day 1 and the start of the session on day 2 was not skewed (Fig. 2.5a). This indicates that COM shifting reflects experience-dependent processes that occur during ongoing familiarization but do not continue offline. However, when considering only stable PFs that on day 1 showed statistically significant backward shifting, we found they tended to reset on day 2 toward their original position on the early laps of day 1 (Fig. 2.5b, Supplementary Fig. 2.17). Therefore, although shifting does not continue offline, offline processes may be involved in resetting PFs back towards their original position. We then asked whether the PF shifting dynamics we had observed on day 1 in N continued upon re-exposure on day 2. The few stable PFs that exhibited significant shifting on both days did not change much on average, but the direction and amplitude of individual PF shifts were not correlated across days (Fig. 2.5c). At the population level, which was thus mostly driven by newly shifting PFs, we found that CA1 PFs on average shifted backwards like on day 1, before stabilizing after lap 15 (Fig.2.5d). The CA3 map shifted less than CA1 (Fig. 2.5d, right). In contrast to day 1, we observed a decrease in PF width over the first laps in CA1, but not CA3, and little change in skewness with population dynamics indistinguishable between CA1 and CA3 (Supplementary Fig. 2.14).

Formally comparing dynamics on N day 1, N day 2 and very familiar environments (F), we found that CA1 population backward shifting slowed down and stabilized with familiarization across days (Fig. 2.6a, c). Stabilization also tended to occur earlier with the level of familiarity: in contrast to day 1, a plateau was reached on day 2 after 15 laps, and

only after 12 laps in F. Shifting of the CA3 map showed a similar trend than CA1 although changes with familiarization across days were less obvious (Fig. 2.6b, d), in part because shifting dynamics were already slow on day 1. Resampling the CA3 data revealed extensive overlap in the population shift across conditions, indicating similar dynamics, (Fig. 2.6d, right). This analysis also revealed that the population becomes more homogeneous with familiarization across days (smaller variance in the slope distribution). Finally, in CA1, PF skewness and width tended to evolve and stabilize with familiarization, whereas the CA3 population did not show clear dynamics despite homogenizing across days (Supplementary Fig. 2.14). These results suggest that lap-wise PF dynamics are enhanced by novelty and decrease as a function of familiarity in CA1, and these PF changes are less apparent in CA3.

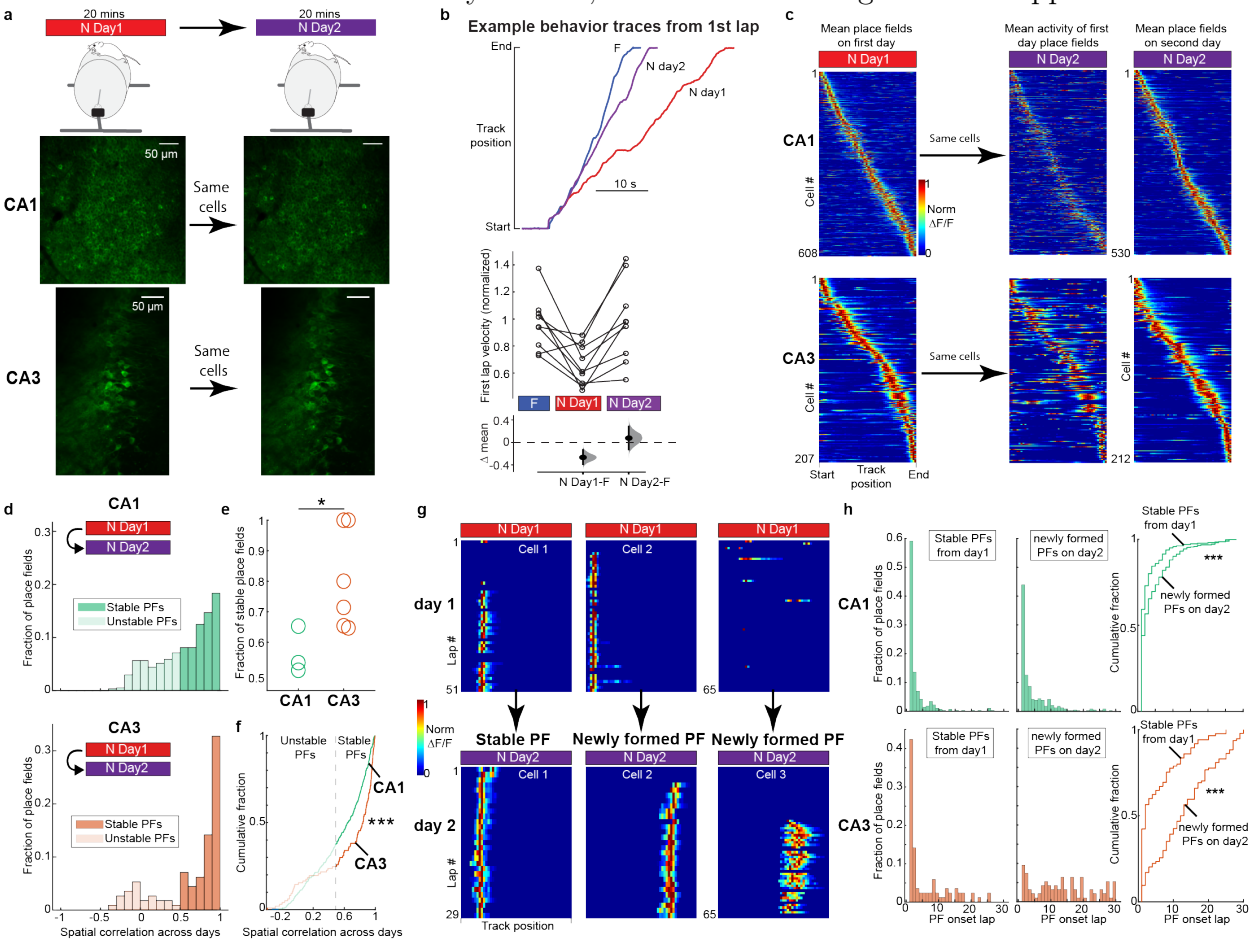

Figure 2.4: **CA3 place fields exhibit higher stability across days than CA1 place fields and rapidly reappear upon re-exposure to the environment.**

Figure2.4, continued: **a**, Experimental setup. Top: mice are recorded for 20 min in N across 2 days. Bottom: example field of view from one imaging plane from CA1 and CA3 across 2 days showing the same cells. scale bar = $50\mu m$. **b,** Top, example mouse behavior showing track position for the first lap in F (blue), N day 1 (red) and N day 2 (purple). Bottom, summary across all mice of first lap velocity in F, N day1 and N day2. Lap velocities were normalized to the mean velocity in F in each mouse (n = 11 mice). Bootstrapped mean difference (Δ) between F and N day 1, and F and N day 2. Note that lap velocity is only different on N day 1. **c,** Left: mean place fields in N on day 1 sorted by track position. Middle: mean activity of the same neurons on the left on day 2 in N. Right: mean place fields in N on day 2 sorted by track position. **d,** Histograms of Pearson's correlation coefficient of average activity map across days in N. Spatial correlations greater than 0.5 were considered stable place fields and less than 0.5 unstable. CA1 n = 409, CA3 n = 113 neurons with PFs in both sessions. **e,** Fraction of stable place fields across days per mouse in CA1 and CA3. Wilcoxon rank sum test, two-sided. *, $P < 0.05$, P = 0.0476. **f,** Cumulative fraction plots of Pearson's correlation coefficient in N across days in CA1 and CA3 from the same data shown in (c). Wilcoxon rank sum test, two-sided. ***, $P < 0.001$, P = 6.85e-04. **g,** Example of a stable place field (left), an unstable place field with a newly formed place field on day 2 (middle) and a newly formed place field on day 2 (right). Place field transients shown lap-by-lap for all laps in N on day 1 and day 2 from the same 3 cells. **h,** Histograms of place field onset laps in N on day 2 for stable place fields (left), and newly formed place fields (middle) in CA1 (top) and CA3 (bottom). Right: cumulative fraction plots of histogram data. Wilcoxon rank sum test, two-sided. ***, $P < 0.001$, CA1, P= 1.76e-05, CA3, P= 6.70e-10. CA1 stable n = 251 PFs, newly formed, n = 333 PFs, CA3 stable n = 72 PFs, newly formed, n = 94 PFs.

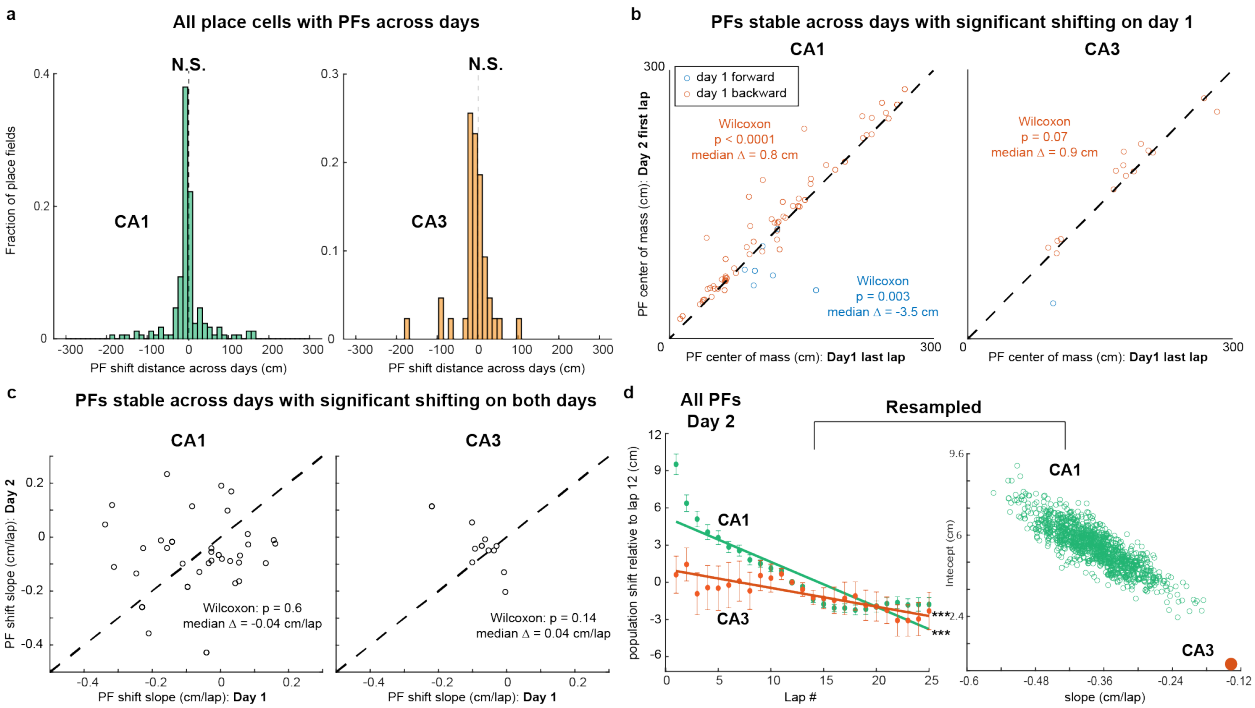

Figure 2.5: **Place field shifting resets and continues upon first re-exposure to N on day 2. : a,** Histogram of place field (PF) shifts across days for CA1 (left, n =171 PFs) and CA3 (right, n = 43 PFs). The shifts were calculated as the difference between each PF's center of mass (COM) of the last active lap on day 1 and first active lap in day 2. Only place cells with PFs on both days are included. Wilcoxon signed rank test, two-sided. N.S., P ¿ 0.05. **b,** Comparison of COM position at the end of day 1 and COM position at the start of day 2 for PFs with day-to-day correlation ¿ 0.5 and significant shifting on day 1 (see Fig. 2.3c). Dashed diagonal: identity line. On day 2, PFs tend to reset towards the direction opposite of shifting on day 1. Two-sided Wilcoxon sign-rank test on Day 2-Day 1 difference from 0 for backward and forward shifting (P-values and median in panel). **c,** Comparison of PF shifting slope on both days. No clear correlation is observed, but the Day 2-Day 1 difference is not significantly different from 0 (Wilcoxon sign-rank, two sided: P-values and medians in panel) and individual PF shifting was slow (close to 0 cm/lap) on both days. **d,** Population shift of PF COM. Left, Mean ±SEM, over all PFs, of 5-lap sliding average COM difference relative to lap 12 (see Methods), in N day2. CA1 (green; n = 371 PFs from 3 mice) and CA3 (orange; n = 84 PFs from 6 mice). Linear regression, F-test, ***, $P < 0.001$ CA1, P= 2.69e-196, CA3, P= 0.00011161. The resampling analysis (1000 random resamples matching the CA3 sample size) shows that CA1 slopes are always steeper than the CA3 slope, indicating that on day 2 the CA1 population shifts backward faster than CA3.

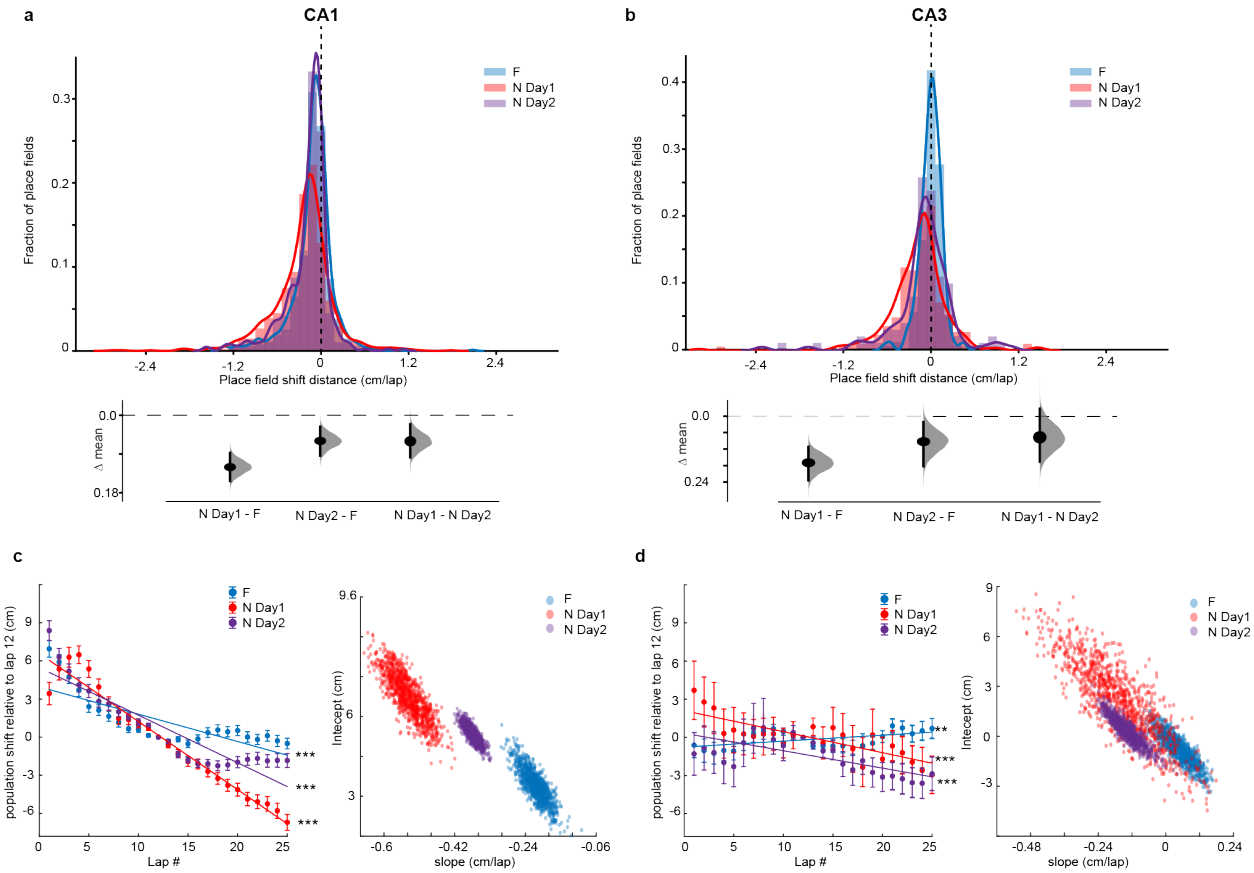

Figure 2.6: **Population backward shifting slows down with familiarization across days:** **a**,Top, histograms of $COM_{last\_lap} - COM_{onset\_lap}$ (session shift defined as in Fig. 2.3d) in Familiar (F), N day 1 and N day 2, for CA1. Bottom, Bootstrapped mean difference (Δ) between the three conditions. **b,** Same as a for CA3. **c,** Population shift of PF COM. Left, Mean $\pm$SEM, over all PFs, of 5-lap sliding average COM difference relative to lap 12 (see Methods), comparing CA1 population shifts in F (blue), N day 1 (red) and N day 2 (purple). Linear regression, F-test, ***, $P < 0.001$,F, P= 3.08e-86, NDay1, P= 3.13e-283, NDay2, P= 2.69e-196. The resampling analysis uses a number of PFs equal to 80 percent of the number of PFs in the condition with lowest number of PFs (1000 resamples). The lack of distribution overlap between conditions indicates dynamics are significantly different. **d,** Same as c for CA3. Overlap in the slope distributions suggests that population dynamics are similarly flat (slopes close to 0) although CA3 PFs shifting become more homogeneous (smaller variance) with familiarization. Linear regression, F-test, ***, $P < 0.001$, F, P= 0.005, NDay1, P= 1.31e-04, NDay2, P= 0.00011161.

2.4 Discussion

We used 2-photon calcium imaging of large populations of dorsal CA1 and CA3 pyramidal neurons to measure and compare the emergence, shifting dynamics, and longitudinal stability of PFs in novel environments with trial-to-trial resolution. We found that PFs emerge faster in CA1 but place cells are constantly renewed across exposures whereas they emerge later in CA3 with less turnover across exposures. After emergence, the location of the PFs is not always stable, sometimes showing prominent backward or forward shifting from lap-to-lap. The average spatial representation in the hippocampus shifts backwards, with a faster shift in CA1 than CA3. This backward shifting slows down with familiarization across days. These findings support the idea that CA3 and CA1 perform distinct functions during familiarization to a novel environment, and CA1 does not simply inherit spatial information from CA3 during this form of spatial learning. They also constrain the potential mechanisms explaining how spatial representations emerge, evolve, and reactivate in the hippocampus.

Consistent with previous reports, we observed hippocampal PFs that emerged instantly in a novel environment (on the very first trial) and others that emerged after multiple trials (delayed onset PFs) (Sheffield and Dombeck 2019; Sheffield, Adoff, and Dombeck 2017; Frank, Stanley, and Brown 2004). Interestingly, the proportion of instant PFs was much lower in CA3 than CA1 (Fig. 2.2). Although to our knowledge this is the first time the trial-to-trial emergence of CA3 PFs has been reported in completely novel environments, a related study did compare the emergence of PFs in CA3 and CA1 in a familiar linear belt with novel sensory cues added (Geiller et al. 2017). This study found 2 types of place cells: 1) landmark vector (LV) cells that have multiple instant PFs locked to sensory cues and 2) place cells with single PFs with a mix of instant and delayed-onset PFs that emerge when novel sensory cues are added. Interestingly, they found 10 times more LV cells in CA1 than CA3. Because PFs in LV cells emerged instantly, the larger proportion of LV cells in CA1 is consistent with our finding that CA1 has more instant PFs than CA3. We confirmed that

CA1 has a lot more place cells with multiple PFs than CA3 (10-15 % in N and F in CA1 vs 1-2 % in CA3), but, in contrast to LV cells, only a fraction of them had instant PFs (31 % in CA1 in N, comparable to the 27 % instant PFs of single-PF place cells). There was no difference between multi- and single-PF place cells in the distribution of onset laps (2-sample KS-test $p = 0.4$ in N, CA1). This might be due to differences in paradigms. For instance, in contrast to the global remapping and emergence of PFs distributed across the whole track that we see in new environments, adding a cue to a familiar environment only induces partial remapping and PF emergence near cues (Geiller et al. 2017).

Rapid PF emergence in a novel environment in CA1 is thought to rely on a combination of strong, spatially tuned excitatory inputs that do not need to be potentiated (Sheffield and Dombeck 2019) and high neuronal excitability, either from novelty-induced disinhibition (Pedrosa and Clopath 2020) or from intrinsic properties (low firing threshold, bursting propensity) (Epsztein, Brecht, and A. K. Lee 2011). CA3 is the main source of excitatory inputs to CA1 and is known to drive CA1 spatial representations in a majority of neurons, at least in familiar environments (Davoudi and Foster 2019). It was thus surprising to find that instant PFs were much less prevalent in CA3 than CA1 (Fig. 2.2). The simplest explanation is that CA1 instant PFs are not inherited from CA3 inputs during initial exploration. Indeed, not all CA1 place cells are necessarily driven by CA3 (Davoudi and Foster 2019) as CA1 receives other sources of spatially modulated inputs (entorhinal cortex (Latuske et al. 2018), CA2 (Mankin, Diehl, et al. 2015), non-imaged subareas of CA3 (Hunsaker, Rosenberg, and Kesner 2008), nucleus reuniens (Dolleman-van der Weel et al. 2019)), but the emergence dynamics of spatial representations in these areas are not currently known. Alternatively, CA1 instant PFs could be driven by the few CA3 neurons with instant PFs if those neurons have a high degree of divergence to CA1. Low dendritic inhibition in CA1 pyramidal cells upon initial exposure to novel environments could serve to amplify the low number of CA3 inputs (Sheffield, Adoff, and Dombeck 2017; Cohen, Bolstad, and A. K. Lee 2017; Nitz and

B. McNaughton 2004). Delayed onset CA3 neurons as well as neurons with unstable spatial modulation could also partially contribute to CA1 instant PFs since some of them are active on early trials.

After PF emergence, PF properties (position, width, shape) evolve with familiarization and their dynamics have been used as a proxy to study the synaptic plasticity mechanisms supporting spatial representations in the hippocampus (I. Lee, Rao, and Knierim 2004; Mehta, Quirk, and Wilson 2000; Mehta, Barnes, and B. L. McNaughton 1997). Initial reports showed that, in a familiar environment, the population of CA1 PFs shifts backwards with experience, a phenomenon consistent with Hebbian rules (Mehta, Quirk, and Wilson 2000; Mehta, Barnes, and B. L. McNaughton 1997) and dependent on NMDA-receptors (Ekstrom et al. 2001). Later electrophysiological studies compared lap-by-lap shifting dynamics in CA1 versus CA3 under different familiarity levels (Geiller et al. 2017; I. Lee, Rao, and Knierim 2004; Roth et al. 2012). Despite discrepancies across studies attributable to different ways of defining novelty, our results are generally consistent with these studies, especially with (Roth et al. 2012) who used completely new distal and proximal cues. We observed significant backward shifting of the population of PFs on day 1 of a new virtual environment in CA1, and to a lesser extent CA3, with the shift slowing down with familiarization across days (Figs. 2.3, 2.5, 2.6 3, 5, 6). Consistent with most reports (Roth et al. 2012; Mehta, Quirk, and Wilson 2000; Mehta, Barnes, and B. L. McNaughton 1997), we found that CA1 was still backward shifting in very familiar environments, but not CA3 (Fig. 2.6).

Population backward shifting was initially reported to coincide with increased negative skewness and enlargement of PFs (Mehta, Quirk, and Wilson 2000; Mehta, Barnes, and B. L. McNaughton 1997). However, in contrast to backward shifting, skewness and width dynamics are inconsistent across studies (I. Lee, Rao, and Knierim 2004; Roth et al. 2012), suggesting a heterogeneity of mechanisms leading to backward shifting (I. Lee, Rao, and Knierim 2004; Yu et al. 2006). Our data indicates that population backward shifting in CA1

in a novel environment is due to a combination of PF expansion, skewness changes and pure translation of the PF (Supplementary Figs. 2.10, 2.14). These dynamics were dependent on familiarity, with changes in skewness closely matching population backward shifting. We did not detect clear dynamics in PF width or skewness in CA3, revealing a dissociation in mechanisms supporting population shifting between CA3 and CA1.

In addition to the population trend, we characterized shifting dynamics in individual PFs, revealing that half of PFs show significant linear shifts in CA1, mostly backward, compared to only a third in CA3 (Fig. 2.3c). PFs with large shifts tended to be less stable across days (Supplementary Fig. 2.16), suggesting that the same mechanisms may underly lap-by-lap and day-to-day stability. On the other hand, PFs that significantly shifted on N day 1 but were stable across days tended, upon re-exposure on day 2, to reset their location toward their original position on day 1 (Fig. 2.5b, Supplementary Fig. 2.17). This reset opposite of the direction of shifting shows that the plasticity underlying lap-by-lap shifting does not continue offline and is thus experience-dependent (Mehta, Quirk, and Wilson 2000). It also shows that lap-by-lap plasticity does not necessarily cause long-term changes in PFs. Together, these findings suggest that the effects of weak lap-by-lap plasticity decay offline (resetting PFs across exposures), whereas strong lap-by-lap plasticity, although not necessary, may promote remapping across sessions.

Interestingly, we found that PFs did not shift backward in CA1 for the first few trials in the novel environment, they actually shifted forward on average (Supplementary Fig. 2.15). This fits with the idea that synapses from CA3 place cells could be necessary to initiate backward shifting in CA1, as only a very small number of CA3 PFs emerge on initial laps in the novel environment. As more CA3 PFs emerge those synapses may undergo asymmetric plasticity, such as spike-timing-dependent plasticity (STDP) (Buchanan and Mellor 2010) and behavioral time-scale plasticity (BTSP) (Magee and Grienberger 2020; Bittner, Milstein, et al. 2017), which could start backward shifting in CA1 (Magee and Grienberger 2020; I.

Lee, Rao, and Knierim 2004; Roth et al. 2012; Mehta, Quirk, and Wilson 2000; Ekstrom et al. 2001). Indeed, both STDP and BTSP are known to occur at CA3-CA1 synapses of pyramidal neurons (Magee and Grienberger 2020; Buchanan and Mellor 2010; Bittner, Milstein, et al. 2017) but other synapses could also be involved.

A classic STDP rule fits well with the extent of backward shifting we observe across laps (Mehta, Quirk, and Wilson 2000; Yu et al. 2006) as it can potentiate synapses activated up to 20 milliseconds prior to postsynaptic firing, which, based on the average running speed we observed, would maximally shift PFs backwards by 0.5 cm/lap, approximately what we see in CA1 on N day 1. However, STDP is not always asymmetric at CA3-CA1 synapses, depending on induction protocols (Buchanan and Mellor 2010). Moreover, the relevance of this type of time-dependent plasticity in vivo has been called into question as synaptic changes might just be too weak to yield an effect on single trials (J. Lisman and Spruston 2010; Graupner, Wallisch, and Ostojic 2016). On the other hand, BTSP induces larger synaptic changes (Bittner, Milstein, et al. 2017) and may thus be more likely to produce visible shifting effects over single trials. However, BTSP requires plateau potentials associated with burst firing, and those may not happen on most laps (Cohen, Bolstad, and A. K. Lee 2017; Bittner, Grienberger, et al. 2015), which may be necessary to see continuous linear shifts like we observed. BTSP can also lead to potentiation of synapses activated several seconds prior to burst firing, which could induce larger PF shifting than observed here. In addition, BTSP has only been found at CA3-CA1 synapses so far and may not occur in CA3 pyramidal neurons even though CA3 shows some backward shifting, albeit less than CA1. Lastly, there is evidence that cholinergic input from the medial septum could play a role in regulating backward shifting, at least in CA1 (Fattahi et al. 2018). It is therefore not yet clear which mechanisms are driving backward shifting in CA1 and CA3 place cells. The mechanisms supporting forward shifting in some neurons is also unknown. Our careful characterization of the shifting phenomenon in both CA1 and CA3 will constrain future

computational models to clarify how hippocampal physiology supports plasticity of spatial representations.

The reinstatement of the same place code upon re-exposure to the same environment is generally thought to provide a neural substrate for remembering the environment (Dupret et al. 2010; C. Kentros 2006; C. G. Kentros et al. 2004; McNamara et al. 2014). Single unit recordings supported this idea by showing place cells remain stable over long periods (Thompson and Best 1990). However, recent evidence from calcium imaging of large ensembles of place cells has shown that many place cells in CA1 are unstable across exposures to the same environment (Mankin, Diehl, et al. 2015; Sheffield and Dombeck 2015; Hainmueller and Bartos 2018; Ziv et al. 2013; Kinsky et al. 2018; Rubin et al. 2015; Jeantet and Cho 2012; Mankin, Sparks, et al. 2012). Rather than a deterioration in the memory representation of the environment, such remapping may serve a function and has been proposed to encode distinct episodes that occur in the same environment separated by time or small changes in environment (Mankin, Diehl, et al. 2015; Rubin et al. 2015; Mankin, Sparks, et al. 2012; Colgin, E. I. Moser, and M.-B. Moser 2008; Wood, Dudchenko, Robitsek, et al. 2000; Krishnan, Cherian, and Sheffield 2020; Anderson and Jeffery 2003; Hasselmo and Eichenbaum 2005; Cai et al. 2016). This remapping might therefore allow the animal to create independent representations of different episodes associated with the same environment and favor mnemonic discrimination of those episodes (Allegra et al. 2020; Antoine David Madar 2018). Our data support this idea as the average PF correlation in CA1 across days in a novel environment was 0.49 $\pm$0.02 (see methods) revealing considerable remapping across days (Fig. 2.4). This value is higher than what is reported in a recent study using methods similar to ours (0.2) (Hainmueller and Bartos 2018). This discrepancy could come from differences in environment complexity which has been shown to influence PF stability and reliability (Hainmueller and Bartos 2018; Bourboulou et al. 2019), although no differences were observed between moderate and enriched visual environments, only impoverished

environments showed reduced stability (Hainmueller and Bartos 2018). Differences in the experimental paradigm could also factor in: they switched repeatedly back and forth between novel and familiar environments within a single recording session, whereas our mice switched only once, defining only two different episodes (familiar and novel). Increased remapping due to repetitive switching, which defines several episodes, is consistent with the hypothesis of CA1 tracking distinct episodes.

A constantly changing place code in the hippocampus could nevertheless be problematic as information about the familiarity of the environment would be lost. CA3 has long been theorized to have a stable code to support memory recall through pattern completion via recurrent connections (Kesner and Rolls 2015). We show that CA3 place cells are indeed more stable across exposures to a novel environment than CA1 place cells. To our knowledge the only other study to track CA3 place cells across days in a novel environment did not observe higher stability in CA3 (0.1 spatial correlation in their study versus 0.7 reported in Fig. 2.4) (Hainmueller and Bartos 2018). In addition to differences of task design stated above, this discrepancy could be explained by their inability to distinguish between CA3 and CA2 cells, as CA2 cells are known to have unstable place coding properties (Mankin, Diehl, et al. 2015). Another related study did find a similar effect as we report here in familiar environments (Mankin, Sparks, et al. 2012) and concluded that CA3 provides a highly stable representation of space and context but little information about time, whereas CA1 is selectively required to integrate CA3 spatial/contextual and CA2 temporal information over hours and days. We add to this framework by showing that the reactivation of stable place cells in CA3 occurs rapidly (on the first traversal) upon re-exposure to the environment. This is consistent with the idea of the CA3 recurrent connectivity being the support of pattern completion through discrete attractors, CA3 activity rapidly settling in the correct attractor basin upon re-exposure (Knierim and Zhang 2012). Transition dynamics from one attractor to the next likely depend on specific connectivity and excitability properties: identifying

the characteristics of recurrent neural network models that would fit the fast transition we observed will be essential to understand the elusive mechanisms of hippocampal remapping.

Overall, the differences in emergence, shifting, and stability of PFs in CA1 and CA3 suggest distinct roles and mechanisms at play in these hippocampal subnetworks to support spatial memories. Instant CA1 PFs could mediate the ability of the hippocampus to rapidly represent episodes on a single trial, a feature of episodic memory (S. W. Lee, O'Doherty, and Shimojo 2015). The backward shifting of the PF population during ongoing experience could allow CA1 to gradually better predict future locations within an environment before physically arriving at those locations (Magee and Grienberger 2020; Stachenfeld, Botvinick, and Gershman 2017; Abbott and Blum 1996). CA1, therefore, rapidly generates unique representations of the world that are then continuously updated by exploratory experience to predict the near future (where am I going?). In parallel, the CA3 gradually forms representations with stable trial-to-trial dynamics, thus encoding location in the present moment (where am I currently?). This function seemingly extends across time as relatively stable CA3 spatial representations are rapidly reinstated upon re-exposure to the same environment, possibly to support memory recall through pattern completion. Remapping of CA1 spatial representations across days may instead serve to separate events occurring in the same environment into distinct memory episodes (Clewett, DuBrow, and Davachi 2019). This framework is depicted in a conceptual model in Supplementary Fig. 2.18.

2.5 Methods

2.5.1 Subjects

All experimental and surgical procedures were in accordance with the University of Chicago Animal Care and Use Committee guidelines. For this study, 10-12 week old C57BL/6J wild-type (WT) male mice (23-33g) (4 WT for CA1 population imaging, Jackson Lab 000664) and

C57BL/6-Tg(Grik4-cre)G32-4Stl/J (7 for CA3 population imaging, Jackson Lab, 006474) were individually housed in a reverse 12 hr light/dark cycle. Male mice were used over female mice due to the size and weight of the headplates (9.1 mm x 31.7 mm, 2 g) which were difficult to firmly attach on smaller female skulls. All training and experiments were conducted during the animal's dark cycle.

2.5.2 Mouse surgery and virus injection

Mice were anesthetized (1-2% isoflurane) and injected with 0.5 mL of saline (intraperitoneal injection) and 0.45 mL of Meloxicam (1-2 mg/kg, subcutaneous injection). For CA1 population imaging, a small (0.5-1.0 mm) craniotomy was made over the hippocampus CA1 (1.7 mm lateral, -2.3 mm caudal of Bregma). A genetically encoded calcium indicator, AAV1-CamKII-GCaMP6f (Addgene, #100834) was injected into CA1 (75 nL) at a depth of 1.25 mm below the surface of the dura using a beveled glass micro pipette. For CA3 population imaging, the craniotomy was made over the CA3 (2.0 mm lateral, -1.7 mm caudal of Bregma). A Custom made Cre-dependent AAV virus: AAV1-CamKII-flex-GCaMP6f (made by Vigene) was injected (two injection sites at least 100 µm apart within the craniotomy, 75 nl at each site) at a depth of 1.9 mm below the surface of the dura. After injection, the site was covered up using dental cement (Metabond, Parkell Coropration) and a metal head plate (Atlas Tool and Die Works). Water scheduling began the following day (0.8-1 mL per day and continued through all training and experiments). Around 7 days later, mice underwent another surgery to implant a hippocampal window as previously described15. Following implantation, the head-plate was reattached with the addition of a head-ring cemented on top of the head-plate which was used to house the microscope objective and block out ambient light. For CA3 mice, because the cannula window was implanted at an angle (15 degrees) relative to the horizontal plane, we bent the two ends of the head plate to match this angle so that the head plate and cannula were on the same plane. We could then change the angle

of our microscope objective to be perpendicular to this plane. Post-surgery mice were given 2-3 ml of water/day for 3 days to enhance recovery before returning to the reduced water schedule (0.8-1.0 ml/day).

2.5.3 Behavior and virtual reality (VR) switching

To navigate in the VR environment, animals ran on a treadmill surrounded by 5 LED screens. (Sheffield, Adoff, and Dombeck 2017; Aronov, Nevers, and Tank 2017). VR environments (one training environment, which served as the familiar environment, F, and two novel environments: N1 and N2) were created using VIRMEn (Mukamel, Nimmerjahn, and Schnitzer 2009). Each environment contained a 3-meter long linear track enriched with different distal and proximal 3D visual cues. 4 µL water rewards were delivered at the end of the track in all environments. During training, which began at least 5 days after window implantation, mice were placed in F for 30-40 mins each day and learned to run and lick the water reward in F. After each lap traversal, mice were teleported back to the beginning of the track. Before teleportation, a short VR pause of 1.5 s was implemented to allow for water consumption and to help distinguish laps from one another rather than them being continuous. Once mice reached the criterion $>$ 2 laps per min that remained stable for 2-3 days (usually around 10-14 days after the start of training), imaging commenced.

2.5.4 Two-photon imaging

Imaging was done using a laser scanning two-photon microscope (Neurolabware). The microscope consisted of an 8 KHz resonant scanning module (Thorlabs), a 16x/0.8 NA/3 mm WD water immersion objective (MRP07220, Nikon). GCaMP6f was excited at 920 nm with a femtosecond-pulsed two photon laser (Insight DS+Dual, Spectra-Physics) and the fluorescence was collected using a GaAsP PMT (H11706, Hamamatsu). The microscope is customized to tilt the objective, which we tilted to be perpendicular to the CA3 head plate

angle but kept vertical for CA1 imaging. Stray light from the VR monitor was blocked from entering the objective lens by a dark rubber tube attached to the implanted head ring and the objective. Laser average power after the objective was 60 mW for CA1 imaging and 120 mW for CA3 to gain similar baseline florescence levels in the CA1 or CA3 FOV. Scanbox (Neurolabware) was used for microscope control and data acquisition. Time series videos were acquired at around 11 Hz for each of the 3 imaging planes (using an electronic lens) to maximize the number of neurons imaged in each mouse. The PicoScope Oscilloscope (PICO4824, Pico Technology) collected the signal from the microscope to synchronize frame acquisition timing with behavior (see below).

2.5.5 Imaging Sessions

Each mouse that reached the behavior criterion was carefully checked for expression under the two-photon microscope. Each mouse used in this study had healthy-looking GCaMP6f expression (resting fluorescence absent from the nucleus; fast transient kinetics; no signs of misshaped somas). On experimental day1: fields of view (FOV) were chosen that maximized the number of neurons across three planes. Imaging and behavior recordings started right before mice entered the VR. Mice ran at least 20 laps in F which took at least 10 min. After which the mice were instantaneously switched to a novel environment (N1). Mice then ran at least 35 laps in N1 and were recorded for at least 20 min and then placed back in their home cage. Experimental day 2: a similar procedure whereby mice were exposed to F first and then switched to a novel environment, but this novel environment (N2) was different from the first novel environment (N1). The FOVs were not necessarily the same as day1. After imaging, more than one averaged FOV was saved to be the reference for day 3 imaging in order to align the planes and record from the same cells the following day. Experimental day 3: The same FOVs were carefully matched to the previous day FOVs. Once imaging started, mice were directly exposed to N2 and ran for at least 29 laps and recorded for 20

min. Mice behavior including treadmill running speed, position, and licking were collected using the PicoScope Oscilloscope to synchronize with the imaging.

2.5.6 Image processing and ROI selection

Time-series movies for multi-plane recordings were acquired using interleaved frames (1st, 4th, 7th... frames belong to plane 1; 2nd, 5th, 8th... frames belong to plane 2: 3rd ,6th, 9th... frames belong to plane 3). Each multi-plane time series was then split into separate time series movies. Same plane movies from Day1 in F and N1 were concatenated into one movie, as were Day 2 single plane movies in F and N2, and Day 2 N2 and Day 3 N2 single plane movies (for across days analysis of the same cells). Movement artifacts are corrected by customized MATLAB scripts based on whole frame cross correlation. For multiday imaging datasets (Day 2 N2 and Day 3 N2 concatenation), motion correction was applied before concatenation and then Fiji (ImageJ) was used to correct any rotational displacement between the two movies. The concatenated movies were then motion corrected again to assure the best alignment (Fig. 2.4). Regions of interest (ROIs) were defined using customized MATLAB scripts from the Dombeck lab (Tampuu et al. 2019) (parameters: mu = 0.6, 150 principal components, 150 independent components, s.d. threshold = 2.5, s.d. smoothing width = 1, area limits = manually chose for each FOV). For each ROI, baseline corrected $\Delta F/F$ traces across time, filtered for significant calcium transients were then generated as previously described (Sheffield and Dombeck 2015; Sheffield, Adoff, and Dombeck 2017; Dombeck et al. 2010). In brief, slow time scale changes in the fluorescence time series were removed by examining the distribution of fluorescence in a +/-5 second interval around each sample time point and subtracting the 8% percentile value. The baseline and σ were calculated from the fluorescence time series that did not contain large transients. Fluorescence transients were then identified as events that started when fluorescence deviated 2σ from the corrected baseline, and ended when it returned to within 0.5σ of baseline. The

baseline-subtracted neuron fluorescence traces were then subjected to analysis of the ratio of positive- to negative-going transients of various amplitudes and durations. We used this analysis to identify significant transients with <1% false positive error rates and generated the significant transient-only traces that were used for all subsequent analysis. Calcium transient analysis: After extracting significant calcium transients, we analyzed and compared some basic characteristics of these transients across CA1 and CA3. Transient peaks: the maximum value for each transient from each neuron. Transient duration: the duration of each transient calculated at half peak from each neuron. Transient frequency: the frequency of significant transients from each neuron.

2.5.7 Behavior analysis

First, immobile and backward moving periods were removed by identifying instantaneous velocity signals slower than 0.2 cm/s. Second, to calculate the mean lap velocity on each lap, we divided the track length (3 m) by the time taken to finish the lap. Third, to then calculate normalized mean lap velocity (Fig. 2.1b; Fig. 2.4b), we took the mean lap velocity on each lap and divided it by the mean velocity of the first 3 laps in F.

2.5.8 Defining Place fields

Because mice ran continuously and consistently in all conditions, we included all laps and transients for place field identification. The 3 m track was divided into 50 bins (6 cm per bin). The mean $\Delta F/F$ was calculated as a function of virtual track position for 50 position bins for each lap, which formed a 50 by N laps matrix. Potential place fields were first identified as contiguous points of this matrix in which all of the points were greater than 15% of the difference between the peak $\Delta F/F$ value (from all 50 bins) and the baseline value (mean of the lowest 12 out of 50 $\Delta F/F$ values). The potential place field had to satisfy the following criteria to be defined as a significant place field: 1. The field width must be $>$ 20 cm and

< 150 cm. 2. The field must have at least one value bigger than 0.1 $\Delta F/F$. 3. The mean in field $\Delta F/F$ value must be > 3 times the mean out of field $\Delta F/F$ value. 4. Significant calcium transients must be present on at least 15 laps out of all the laps that the mouse traversed. Potential place field regions that met these criteria were then defined as place fields if their P value from boot strapping was < 0.05, as described previously (Dombeck et al. 2010). Place fields from cells that have multiple place fields used the same criteria and were treated independently. Transients that occurred outside of the defined place field region were removed for analysis of each specific field. The resultant place fields were then used in all subsequent analysis unless specified.

2.5.9 Histology and brain slices imaging

We checked the CA3 expression of some of the Grik4-cre mice to ensure the GCaMP expression was restricted to CA3. Mice were anaesthetized with isoflurane and perfused with 10 ml PBS followed by 20 ml 4% paraformaldehyde in PBS. The brains were removed and immersed in 30% sucrose solution overnight before being sectioned at 50 µm-thickness on a cryostat. The brain slices were then collected on glass slides and mounted with a mounting media with DAPI (SouthernBiotech DAPI-Fluoromount-G Clear Mounting Media,010020). The whole brain slices were imaged under 10X with a Caliber I.D. RS-G4 Large Format Laser Scanning Confocal microscope from the Integrated Light Microscopy Core at the University of Chicago.

2.5.10 Spatial Correlation

To measure place field spatial correlation across environments, we found place cells that had place fields in either environment and then calculated the Pearson's correlation coefficient between the mean activity along the track (in 50 bins) for all laps in two environments. To measure the place field correlation within environment, we divided the session up onto two

halves based on the total number of laps completed. We then calculated the mean activity along the track for each half and calculated the Pearson's correlation coefficient. For cells with multiple place fields, only the first place field on the track was included. To measure place field spatial correlation across days, we found place cells that had place fields in both days and then calculated the Pearson's correlation coefficient between the mean activity along the track (in 50 bins) for the last 10 laps in N day 1 and first 10 laps in N day 2.

2.5.11 Place field onset lap

To determine place field onset lap (Fig. 2.2c-e, Fig. 2.4h), starting from lap 1 we searched lap-by-lap for a lap with a significant calcium transient present within the boundaries of the future place field calculated from all the laps in the session. Once the lap was found, we would then search for significant calcium transients on each of the next 5 laps. If 3 of the 6 laps had significant calcium transients within the place field boundaries, that would be considered the place field onset lap, if not, we move to the next lap and repeated the analysis. If we changed this criterion and instead used 2 out of 6 laps or 4 out of 6 laps to define place field onset lap, the differences in distributions we observed between CA1 and CA3 remained. To control for the different numbers of laps that the mouse ran in F and N, the comparison in Fig. 2d only included the first 25 laps in F and N. If we instead included the later laps in N, the result did not change.

2.5.12 Place field COM and spatial precision

To calculate the spatial precision, we first calculated the somatic transient center of mass (COM) on each traversal along the linear track. We measured $\Delta F/F$ in each bin. We then used the following equation to calculate the COM for each traversal n (COMn):

$$COM_n = \frac{\sum_i DF_i \cdot x_i}{\sum_i DF_i} \tag{2.1}$$

Where DF_i is the somatic $\Delta F/F$ in bin i and $x_i is$ the distance of bin i from the start of the track. We then calculated the weighted average COM (COMw) from all traversals n (COMn from each traversal was weighted by the peak transient $\Delta F/F$ on that traversal (An)):

$$COM_w = \frac{\sum_n A_n \cdot COM_n}{\sum_n A_n} \tag{2.2}$$

Spatial precision (Sheffield and Dombeck 2015) (SP) was then calculated as follows (inverse of the COM standard deviation):

$$SP = \frac{1}{\sqrt{\frac{\sum_n A_n (COM_n - COM_w)^2}{\sum_n A_n}}} \tag{2.3}$$

2.5.13 Out/in place field firing ratio

This was computed as the ratio between the mean $\Delta F/F$ in bins outside the place field and the mean $\Delta F/F$ in bins within the place field.

2.5.14 Position Decoding Analysis

Based on a recent study (Ho et al. 2019), we chose to use the long short-term memory (LSTM) neural network model to test whether representations in CA1 were better at decoding position on the first lap of N than CA3 representations. Considering the differences in number of place fields we measured in CA1 and CA3 (more PFs in CA1 than CA3), as well as the amount of data required to build a useful LSTM model, we grouped data from all CA1 and CA3 mice that ran more than 45 laps in N2, and matched the number of cells used from CA1 and CA3 to build the models. To match the data from different mice and use the decoders to decode position on a lap-by-lap basis, we first changed the time-series based data to position based data: the 3 m track was divided into 100 bins (3 cm per bin). The mean $\Delta F/F$

was calculated as a function of virtual track position for 100 position bins for each lap. By doing this, data within and across mice became the same length by lap. CA1 data were then grouped into one dataset and CA3 data grouped into another dataset. The decoding data was restricted to periods when the animals were running. To test decoding ability on the first lap in N, we first tested different parameters (LSTM model network structure and the number of place cells used to build the models) to make sure that the two decoders had similar decoding ability in the later laps (validation set) (Supplementary Fig. 2.9). We chose a one-layer LSTM decoder with 1024 units to decode the animals' position from the input of 200 place cells. When building a model, 200 place cells were randomly chosen from the entire CA1 or CA3 place cell population, the data from the 6th to 35th laps were used to train the decoder to decode the animals' position on the track which had been divided to 50 bins. The 36th to 40th lap data were used as the validation set. The decoders were then used to decode the animals' position on the first lap based on the place cell activity on this lap. We repeated this procedure 20 times for CA1 and CA3 and compared the predicting error on the first lap between the regions. The predicting error was calculated as the mean of the absolute difference between the prediction position and the animals' real position on the first lap. We also built a naïve Bayes decoder with the same data, though the decoding ability is not as good as the LSTM decoder for the validation set, we got the same result as the LSTM decoder for the first lap position decoding (that is the CA1 is better at decoding position on the first lap compared to CA3) (Supplementary Fig. 2.9).

2.5.15 Place Field Shifting

To calculate population place field shifting (Fig. 2.3e, 2.5d, 2.6c-d), we first calculate the COM for all place fields on each lap with a sliding window of 5 laps (the COMw of the current and 4 next laps). The 5-lap sliding average was done for smoothing purposes but the same trends were observed without smoothing. For each place field, lap-wise shift was

computed as the difference between lap 12 and current lap. We could then calculate the average shifting over the population of place fields on each lap. Only place fields with place field activity on lap 12 and a place field onset lap ¡ 20 were included. Also, due to the onset of place fields on different laps, the number of samples that contribute to the mean on each lap is different. Note that we also used the 5-lap COM weighted average method in Fig. 2.3d.

2.5.16 Place Field Skewnes

Place field skewness is calculated as the third statistical moment of the place field. For lap n:

$$Skewness_n = \sum_i \frac{DF_i}{\sum_i DF_i} \cdot \frac{(x_i - COM_n)^3}{\sigma^3} \tag{2.4}$$

where σ is the place field's "standard deviation":

$$\sqrt{\sum_i \frac{DF_i}{\sum_i DF_i} \cdot (x_i - COM_n)^2} \tag{2.5}$$

To calculate population place skewness trend, we first calculate the skewness for all place fields on each lap. Then we took each place field and aligned them together by the actual laps.

2.5.17 Place field width

Place field width on each lap is calculated as the difference between the first and last bin with in-field activity. We then normalized the lap-wise width to the mean PF width for each PF. Notice, for COM shift and reset, PF skewness and width analyses, most PFs near start or end of the track were excluded if they were clipped, using the following criterion: if the distance between one track edge and PF COM was at least 1 bin shorter than the other half

of the PF, the PF was excluded. For cells with multiple place fields, only the first PF on the track was included.

2.5.18 Statistical analysis

Error in the text and figures are presented as mean ±S.E.M, unless stated otherwise. We used either an estimation approach or null-hypothesis testing to compare data (described in figure legends). To generate Gardner-Altman estimation plots, which highlight the effect size, we used the Data Analysis with Bootstrapped-coupled ESTimation (DABEST) package(Ho et al. 2019) (available on GitHub: https://github.com/ACCLAB/DABEST-python). To assess the uncertainty of the effect size, the mean difference between two distributions and its 95 % confidence interval were bootstrapped. For null-hypothesis testing, Wilcoxon rank-sum test, Wilcoxon signed-rank test or Kolmogorov-Smirnov 2 sample test were applied. $P < 0.05$ was chosen to indicate statistical significance and P-values in figures are indicated as follows: *, $P < 0.05$, **, $P < 0.01$, ***, $P < 0.001$, N.S. not significant. For data tested with the estimation approach, we also used the null-hypothesis testing to confirm any differences. For linear regressions of the population slopes (e.g. Fig. 2.3e left), the p-value for the t-statistics to test whether the slope was significantly positive or negative were reported following the same approach reported above. To compare the population dynamics of different conditions, we performed exact testing based on Monte-Carlo resampling (1000 re-samples with sample size matching the lower sample size condition) as detailed in legends. To assess the shifting dynamics in single PFs, we performed linear regression on the lap-wise COM_n relative to onset lap (Fig. 2.3c), and significance was assessed with an F-test.

2.5.19 Data and Software

Data processing and analysis was performed using custom written scripts in MATLAB (2018a) or Python (3.7).

2.6 Supplementary

2.6.1 Supplementary figures

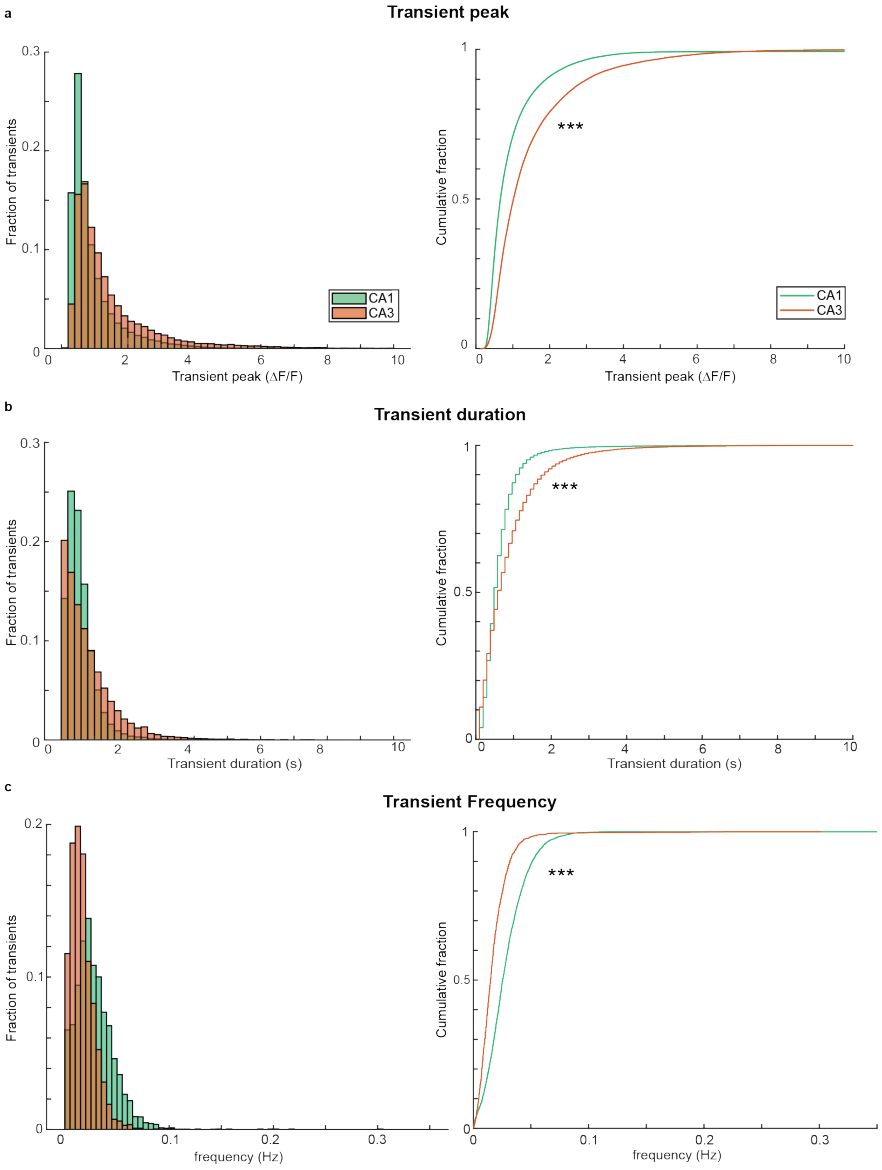

Figure 2.7: **Calcium transient properties in CA1 and CA3. a,** Left, histogram of the Calcium transient peaks for CA1 (green) and CA3 (orange). Right, the corresponding cumulative fraction plot. Wilcoxon rank sum test, two-sided, ***, $P < 1e-100$. **b,** Left, histogram of the Calcium transient durations calculated at 50% of the peak. Right, the corresponding cumulative fraction plot. Wilcoxon rank sum test, two-sided, ***, $P < 1e-100$. **c,** Left, histogram of Calcium transient frequencies. Right, the corresponding cumulative fraction plot. Wilcoxon rank sum test, two-sided, ***, $P < 1e-100$

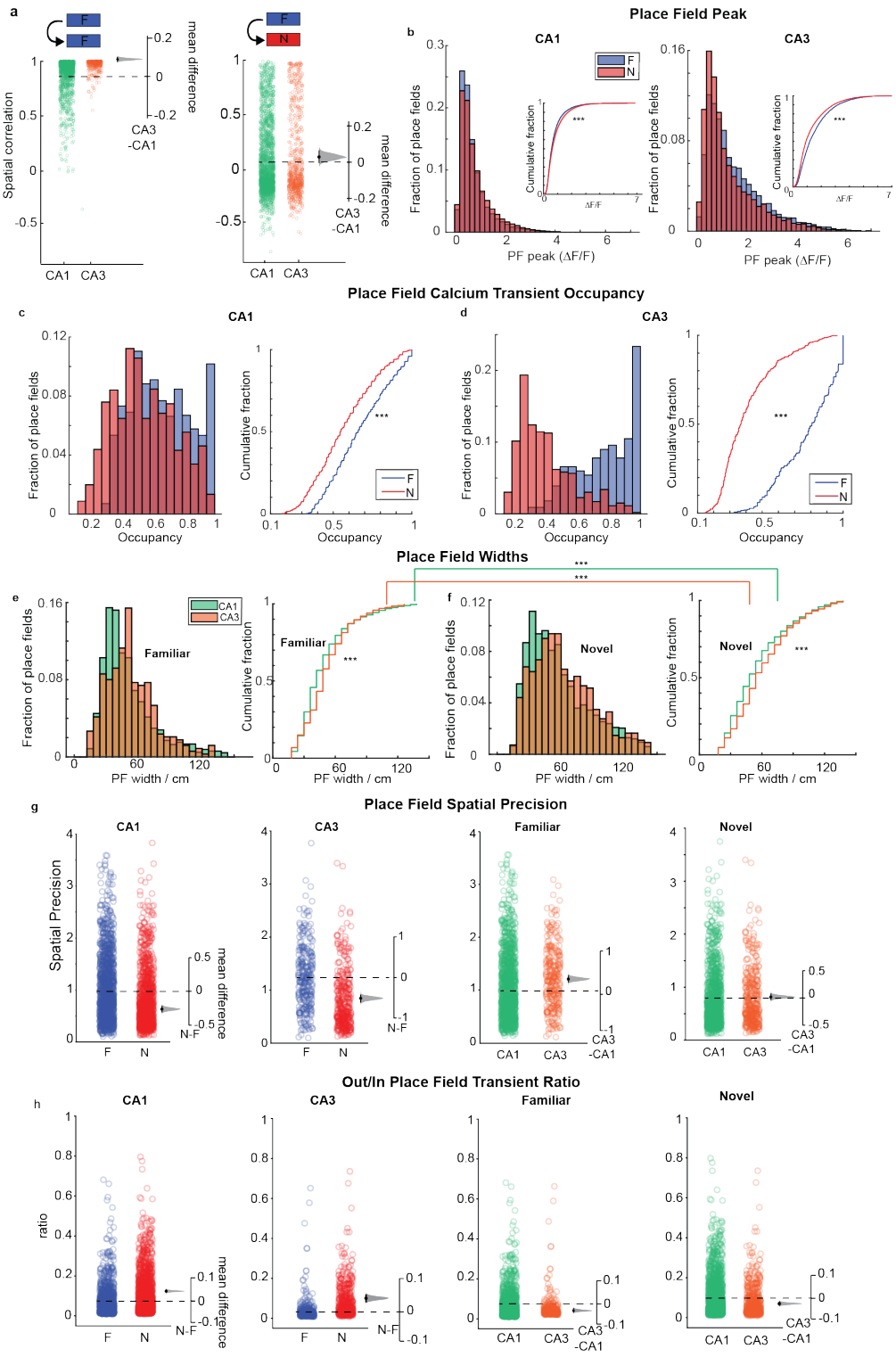

Figure 2.8: **Place field properties in familiar and novel environments in CA1 and CA3.**

Figure2.8, continued. **a,** Pearson's correlation coefficient of each cell's mean place field (PF) between CA1 and CA3 within familiar (F) sessions (left) and between F and novel (N) sessions (right). Bootstrapped mean difference (Δ) shown on the right of each plot. Note CA3 PFs are much more stable within F than CA1 PFs. **b,** Histogram of each PFs peak activity for CA1 (left) and CA3 (right) in F (red) and N (blue). Insets show cumulative fraction plots. Wilcoxon rank sum test, two-sided, ***, $P < 0.001$; CA1, P = 4.5e-56, CA3, P = 8.4e-79. **c,** Left, histogram of PF Calcium transient occupancy (percentage of laps with PF activity) in F (red) and N (blue) in CA1. Right, corresponding cumulative fraction plot. Wilcoxon rank sum test, two-sided, ***, $P < 0.001$, P = 4.5e-56. d, Same plots as (c) in CA3, P = 3.1e-95. Note the striking difference in transient occupancy in N versus F in CA3. The lower transient occupancy in N is largely due to delayed PF formation in N in CA3 (See Fig. 2.2). e, Histogram of each PFs width in CA1 (green) and CA3 (orange) in the familiar environment. Right, corresponding cumulative fraction plot. Wilcoxon rank sum test, two-sided, ***, $P < 0.001$, CA1-CA3 F, P = 7.1e-4, CA1-CA3 N, P = 4.9e-5, CA1 F-N, P = 3.2e-15, CA3F-N, P = 2.6e-6. f, Same plots as (e) but in N. g, Spatial precision of each PF in CA1 (left) and CA3 (middle left) in F (blue) and N (red). Same data are also compared across CA1 and CA3. Bootstrapped mean difference (Δ) shown on the right of each plot. Note that PFs in N are less precise than in F in both CA1 and CA3, and CA3 PFs in F are more precise than CA1 PFs in F. h, Ratio of out versus in PF activity for CA1 (left) and CA3 (middle left) in F (blue) and N (red). Same data are also compared in F (middle right) and N (right) across CA1 and CA3. Bootstrapped mean difference (Δ) shown on the right of each plot. Note that PFs in N have more out-of-field firing than F in both regions but CA3 has less out-of-field firing than CA1.

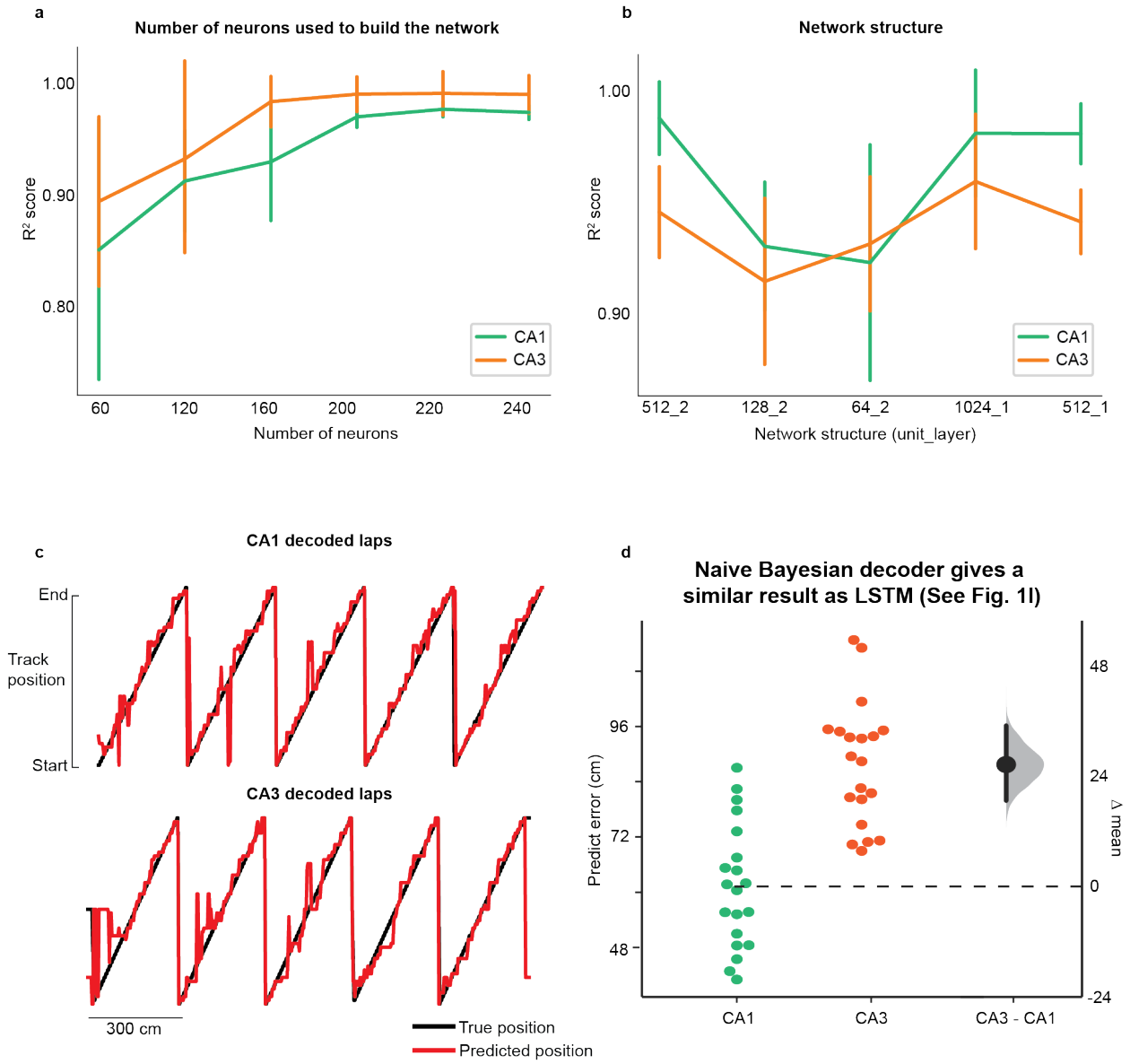

Figure 2.9: **Long-Short-Term-Memory (LSTM) and Bayesian decoding of animal position.** **a,** Mean LSTM decoder performance ±SEM versus the number of place cells that were used to build the decoder. The network structure for all the decoders are the same, a one-layer 1024-unit neuronal network. **b,** Mean decoding performance ±SEM versus the network structure for the decoder. All decoders were trained with 200 place cells. **c,** Example mouse showing true track position (black) on laps 36-40 and the predicted position (red) decoded by a Naïve Bayesian decoder. Note the LSTM decoder (Fig. 2.2f) did a much better job than the Bayesian decoder. **d,** Average predicted error for the first lap in the novel environment for CA1 and CA3. Each dot represents the decoding error for one decoder trial built based on the activity of 200 randomly chosen place cells from CA1 (green) or CA3 (orange) data. n = 20 decoder trails. Bootstrapped mean difference (Δ) shown on the right of each plot.

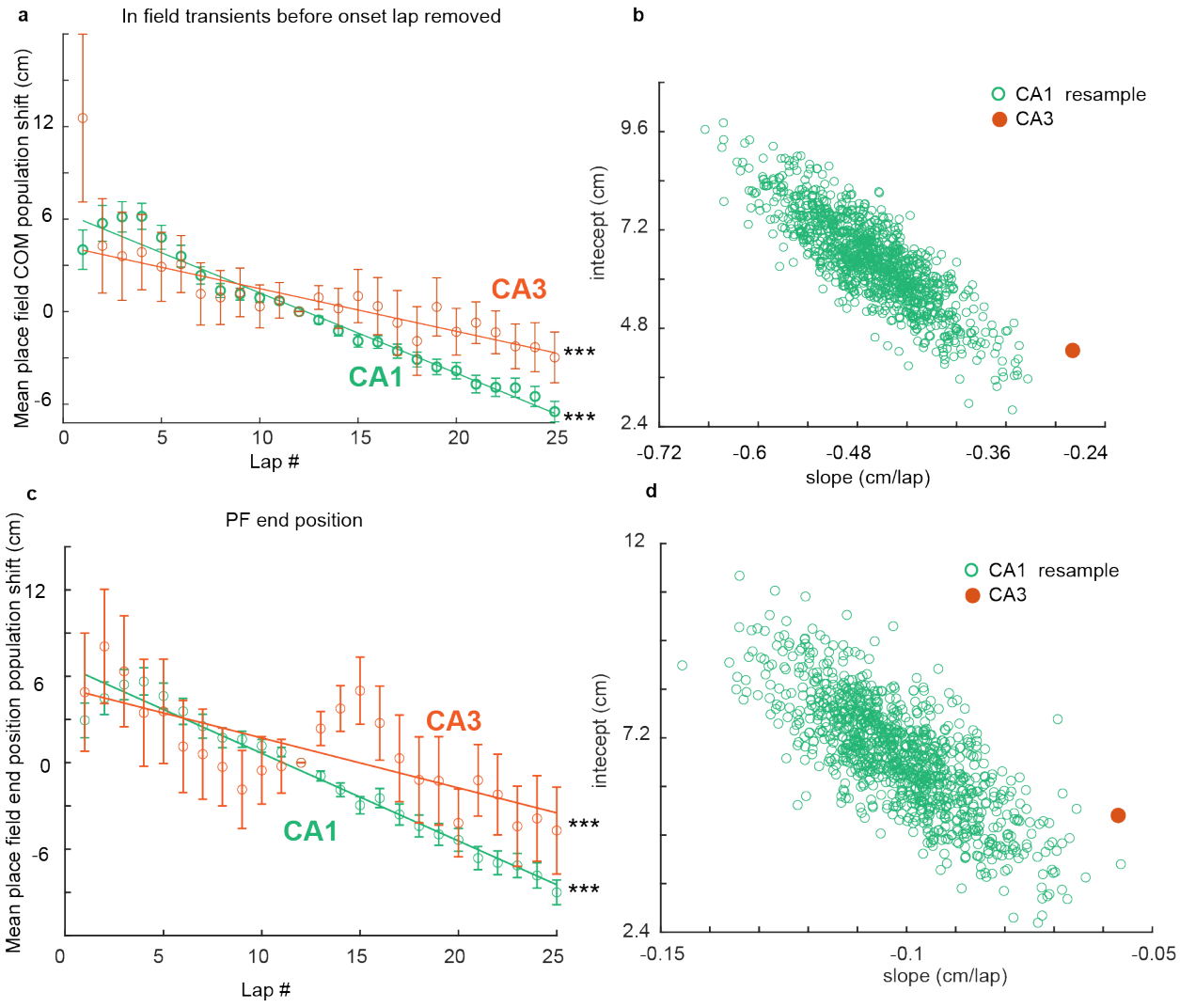

Figure 2.10: **Population backward shifting is still observed when transients that occur prior to place field emergence are removed and when place field position on each lap is defined by the location of the calcium transient end point. a,** Population shift of COM. Mean ±SEM from all place fields (PFs) using a 5-lap sliding average. COM difference is relative to lap 12. All in-field transients that occurred prior to PF onset lap have been removed. Linear regression, F-test, ***, $P < 0.001$, CA1, $P < 1e-100$, CA3, P = 1.5e-7. b, Resampling analysis (1000 resamples) associated to (a) shows CA1 backward shifting is still significantly faster than in CA3. c, Population PF shift on each lap not defined by the COM but by the location of the end of the calcium transient. Mean ±SEM from all PFs using a 5-lap sliding average. COM difference relative to lap 12. This shows that the location of the end position of the PF shifts backward in both CA1 and CA3. Linear regression, F-test, ***, $P < 0.001$, CA1, $P < 1e-100$, CA3, P = 9.9e-6. d, same as (b) but associated to (c): CA1 population shifting slopes are still significantly more negative than CA3 (P = 0.001).

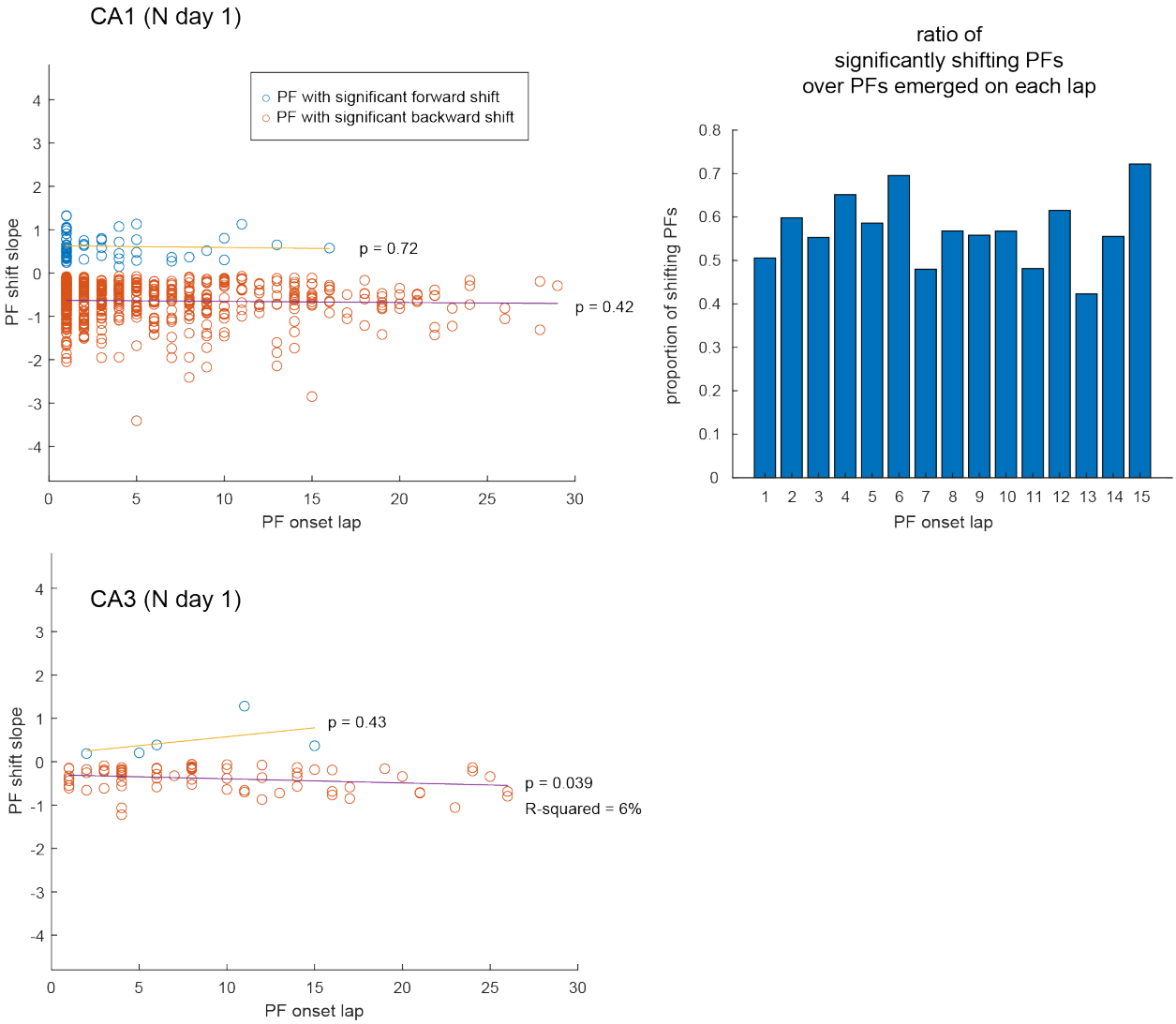

Figure 2.11: **Lap-by-lap shifting is not related to the timing of PF emergence.** Place field (PF) shift slope is defined as in Fig. 2.3c. Only significantly shifting PFs (regression P ¡ 0.05) are included. No correlation between PF onset lap and the amplitude of their shifting dynamics is observed in CA1, and only weakly in CA3 where the sample size is low. Note that, in CA1, the higher number of shifting PFs with early onset is simply due to the higher number of PFs emerging in early laps. The proportion of shifting PFs (Right panel) stays stable throughout the first 15 laps (later laps not shown because number of shifting PFs ¡ 10). Linear regression, F-test.

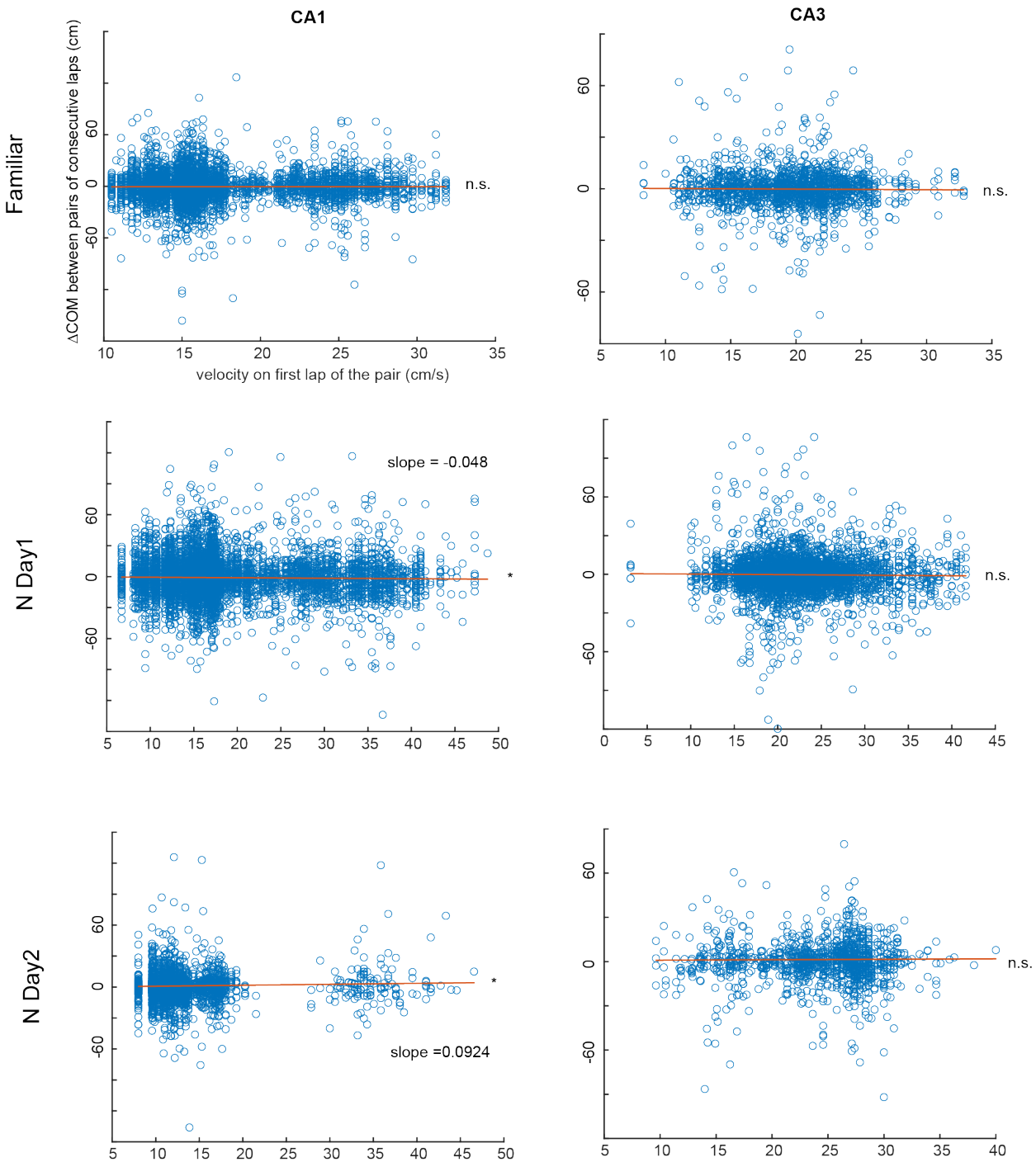

Figure 2.12: **Relationship between place field shifting and lap velocity.** For all place fields (PFs), all differences in COM position between consecutive laps (ΔCOM) are plotted against the velocity on the first lap of the pair (similar results when velocity on second lap is used instead). This analysis does not reveal an obvious relationship between velocity and shifting and clearly shows that large lap-to-lap shifts are not due to higher velocities. Linear regression, F-test.

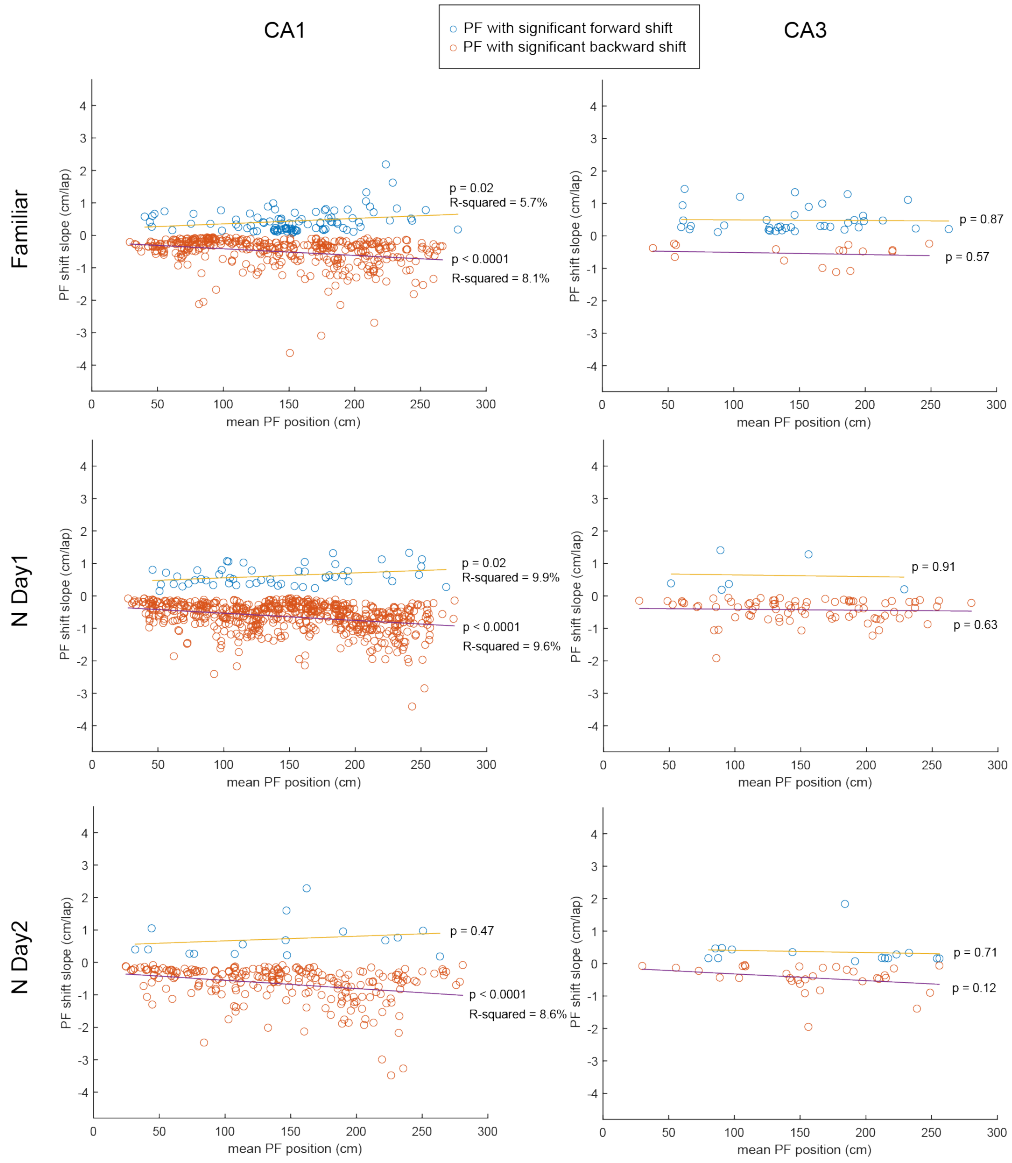

Figure 2.13: **Place field shifting is weakly correlated to place field position.** Each data point corresponds to the shifting slope of a single place field (PF) from the regression analysis on the PF COM lap-by-lap position (see Fig. 2.3c). Only PFs with regression $P - value < 0.05$ are included. In CA1, PF shifting amplitude is weakly but significantly correlated with the PF mean COM position in each recording day and environment. PFs with a large forward or backward shift are biased toward the end of the track. No correlation is detected in CA3 but the number of shifting PFs is much lower. Linear regression, F-test.

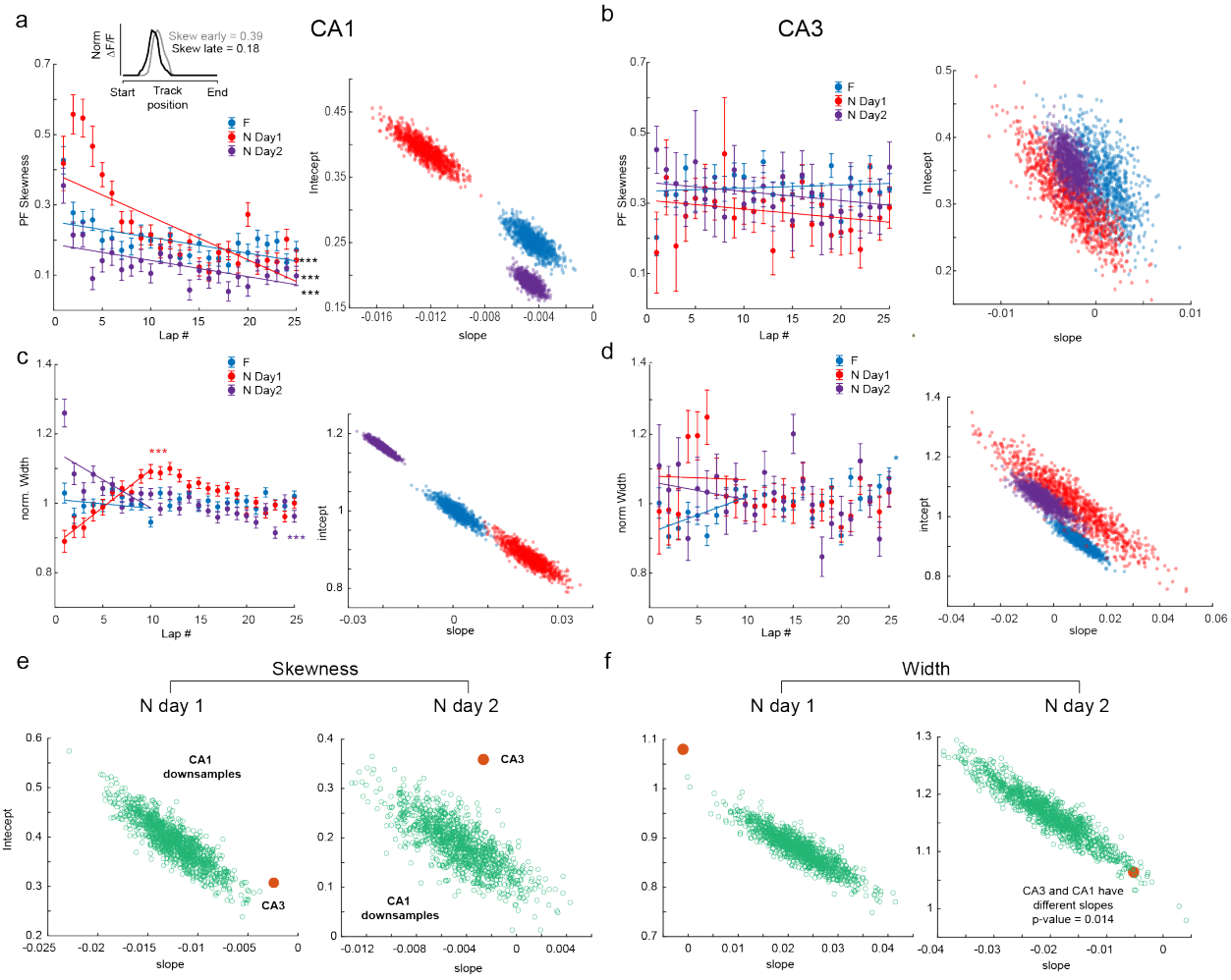

Figure 2.14: **Lap-by-lap change of place field skewness and width.**

a, Left, Lap-wise mean ±SEM skewness over all place fields (PFs) recorded in a given condition. Linear regression (on data points, not means) shows a decrease in positive skewness with experience, especially in N day 1. Inset: representative example PF that shifted backward, became less positively skewed and wider (early = lap 1-5 average fluorescence activity, late = lap 25-30 average). Right, resampling analysis as in Fig. 2.6c: slopes are significantly different from N day 1 to N day 2 and stay similar in a very familiar environment (F). Overall, these results suggest that PFs become less skewed over the first 10 laps in N and seem to stabilize afterwards, with slow population change upon re-exposure. Linear regression, F-test, ***, $P < 0.001$, F, P = 9.09e-10, N Day1, P = 9.59e-39, N Day2, P = 9.06e-8.

Figure2.14, continued. b, same as (a) for CA3. Distribution spread is wide, suggesting less homogeneity in the population of PFs. Overlap in distributions show dynamics do not change significantly with familiarization. Linear regression, F-test, F, P = 0.40, N Day1, P = 0.28 N Day2, P = 0.23. **c-d,** Same as (a) for the lap-wise PF width normalized to width averaged over all laps for each PF (i.e. 1 means that the width is the same as the average PF width). This normalization controls for large variations in individual PF width and allows direct comparison with (Mehta, Barnes, and B. L. McNaughton 1997). In CA1, PF width increases over first 10 laps in N but decreases on second day and is stable in F. CA3 does not show clear population dynamics, although PFs become more homogeneous with familiarization across days. Linear regression fit to data points from the first 10 laps only. Linear regression, F-test, ***, $P < 0.001$. CA1 F, P = 0.20, N Day1, P = 3.88e-16 N Day2, P = 1.12e-10CA3: F, P = 0.001, N Day1, P = 0.90, N Day2, P = 0.50. **e-f,** Resampling analysis as described in Fig. 2.3e. CA3 and CA1 PF width and skewness dynamics (slopes) are significantly different on day 1, but only widths are different on day 2.

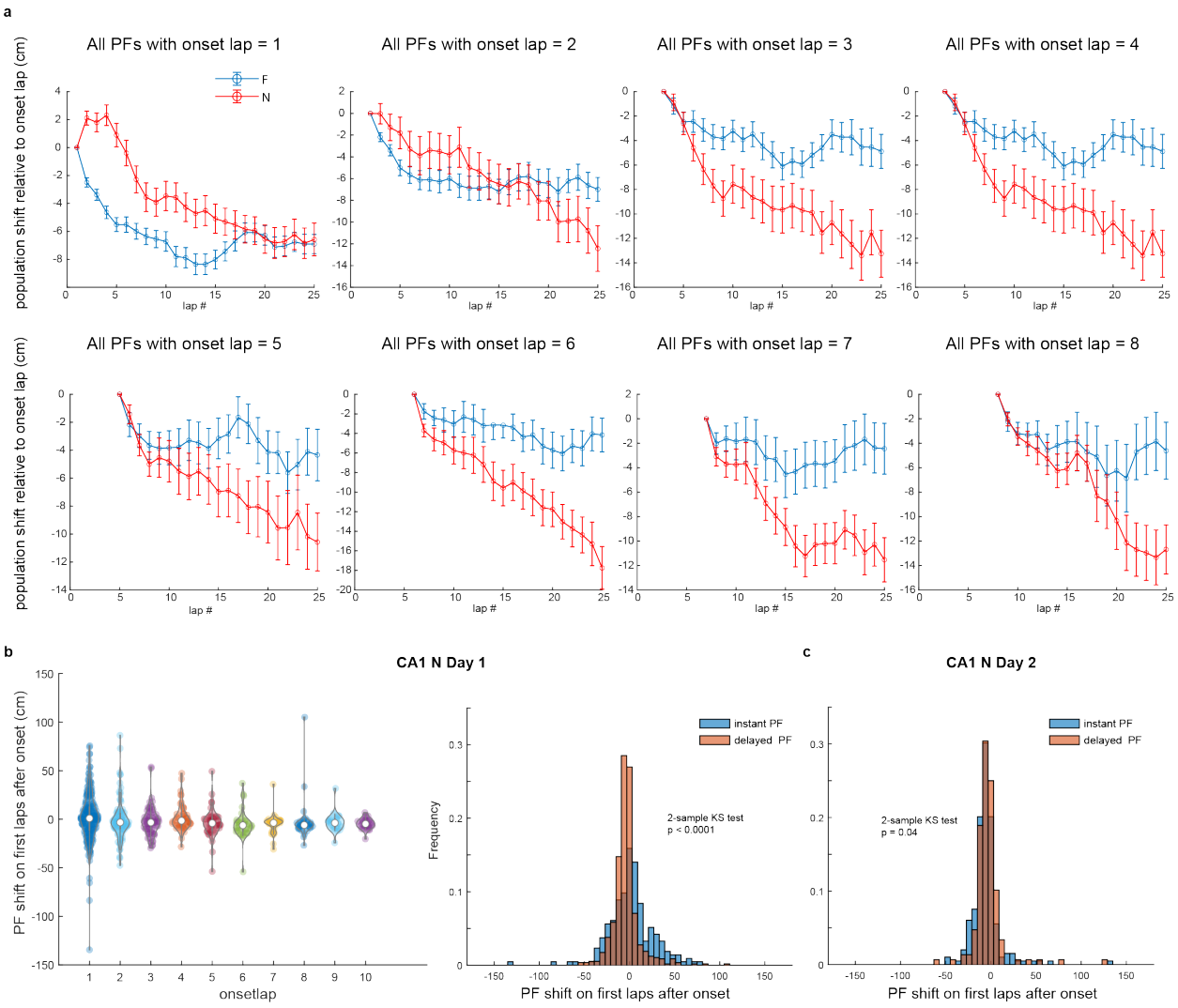

Figure 2.15: **CA1 forward shifting during first laps is driven by instant-onset place fields.** **a,** Mean ±SEM, for all place fields (PFs), of 5-lap rolling average center of mass (COM) difference relative to onset lap, in novel (N) and familiar (F) environments. Forward population shifting during first laps after onset is only seen for instant PFs (onset lap = 1). **b,** Left, difference between 5-lap rolling average COM at onset lap and next lap, for each PFs, as a function of onset lap (not showing onset lap > 10). The median is above 0 for instant PFs, not the other groups. Right, same as b but combining all delayed PFs together for comparison with instant PFs. Distributions are significantly different, with more early forward shifting PFs in the instant PFs group. **c,** The effect seen in b disappears on day 2. Distributions are only mildly different and not because of a higher number of early forward shifting PFs in the instant onset group.

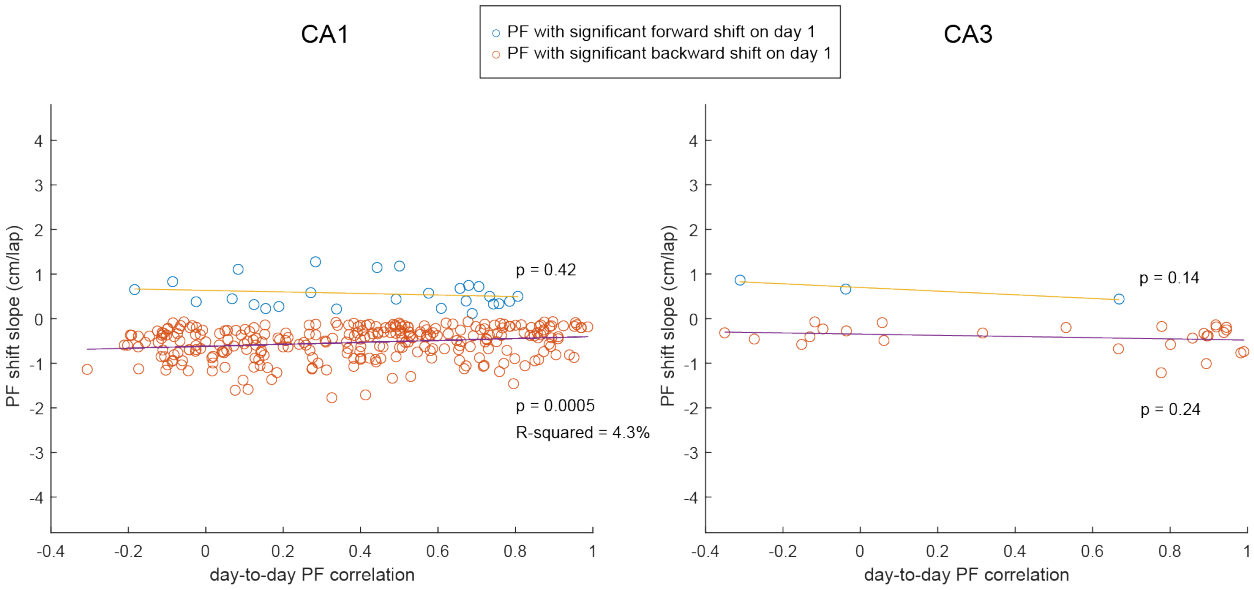

Figure 2.16: **CA1 place field stability across days is correlated to lap-by-lap stability on day 1.** Place field (PF) shift slope is defined as in Fig. 2.3c. Only significantly shifting PFs (regression $P < 0.05$) are included. In CA1, there is a weak correlation (linear regression) between day-to-day stability and day 1 lap-by-lap dynamics for backward shifting PFs, suggesting that PFs that are stable across days are also more stable from lap-to-lap on day 1. Although not significant, this trend is seen for forward shifting PFs too. In CA3, PFs do not shift as much (see Fig. 2.3), resulting in a low sample size and no apparent correlation. Linear regression, F-test.

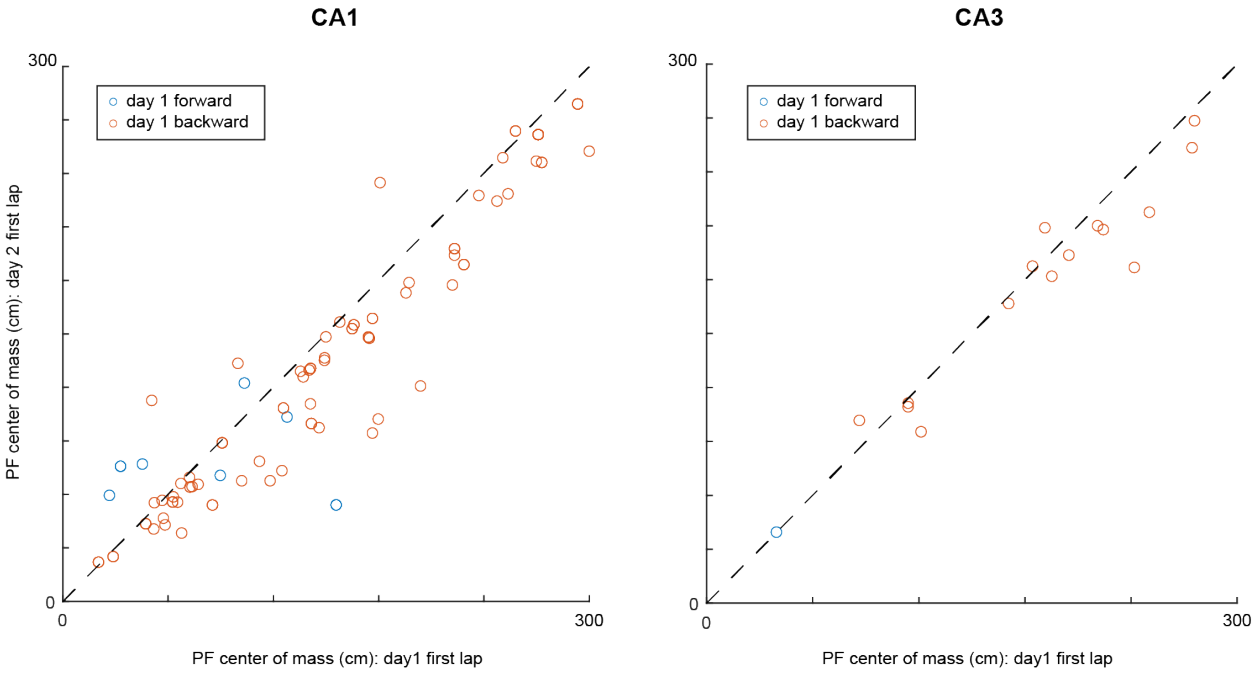

Figure 2.17: **On day 2, shifting place fields do not necessarily reset to their exact initial position on day 1.** Place field (PF) shift slope is defined as in Fig. 2.3c. Selected PFs (day-to-day correlation > 0.5 and significant shifting on day 1) are the same as in Fig. 2.5b. 2.18

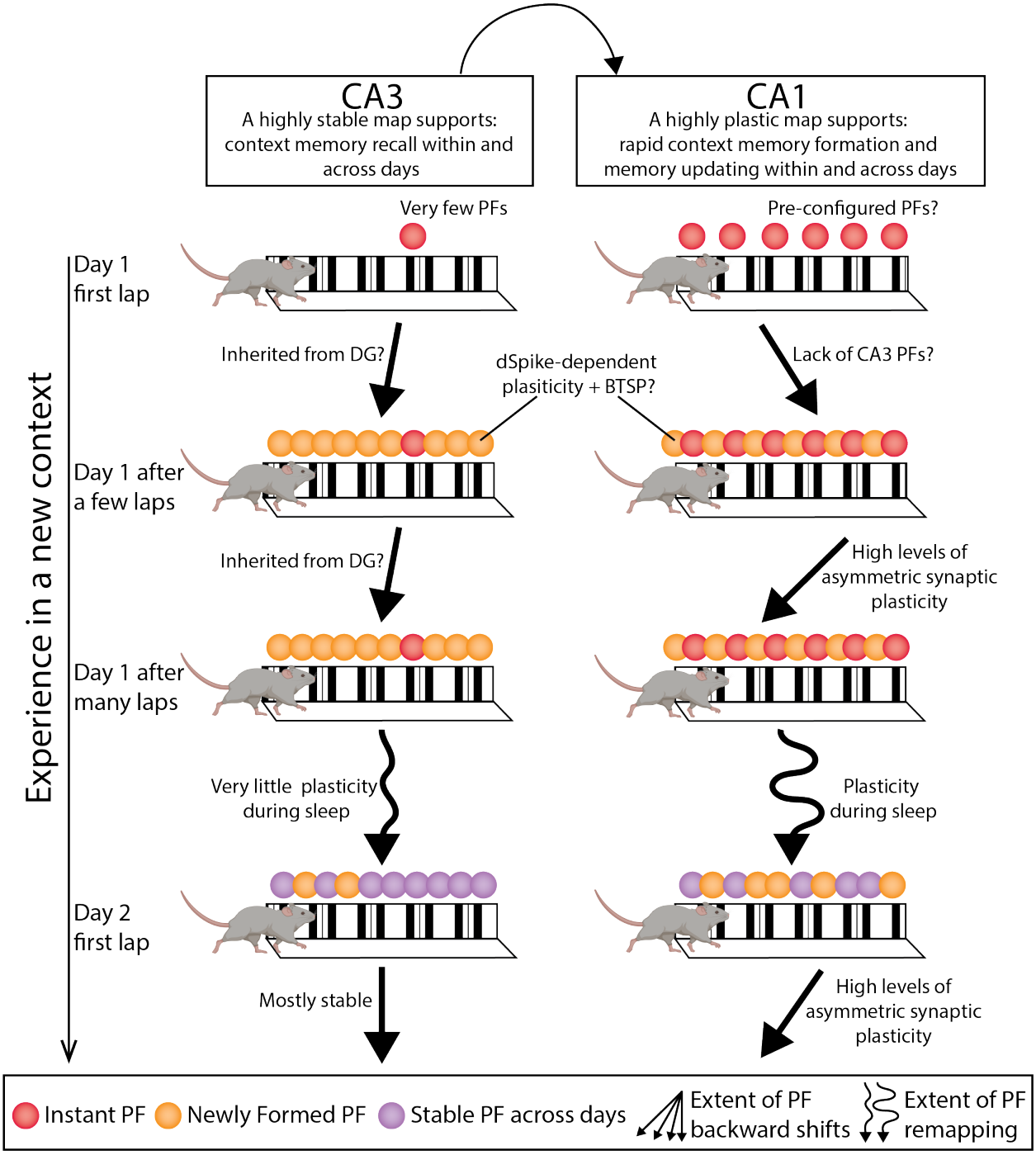

Figure 2.18: **Conceptual model.**

In a new context, place fields (PFs) in CA1 instantly appear on the first traversal (red circles). These PFs do not require experience-dependent synaptic plasticity and so are likely pre-configured. Instant PFs are lacking in CA3. Instant PFs in CA1 initially shift forward

Figure 2.18, continued. for the first 1-4 laps, possibly due to the lack of CA3 PFs. Within the first few laps in the new context, new PFs appear in both CA1 and CA3 (orange circles). We partially know how these PFs form in CA1, but it remains unknown whether the same mechanisms are at play in CA3. In CA1, these PFs form through local dendritic spikes (dSpikes) that induce synaptic potentiation through an NMDA receptor mechanism (Sheffield, Adoff, and Dombeck 2017). This process occurs during the silent period when these cells are not firing. On the lap where the PF first appears, in some or many of these cells, behavioral timescale synaptic plasticity (BTSP) further strengthens synapses more globally throughout the neuron through burst firing associated with plateau potentials generated in the dendrites by coincident input from CA3 and Entorhinal cortex (Bittner, Milstein, et al. 2017). Throughout experience the newly formed PFs shift backwards and develop NMDA-dependent negative skewness in CA1 likely through asymmetric synaptic plasticity at the CA3-CA1 synapse. CA3 PFs show only a small amount of backward shifting and no increase in negative skewness, suggesting they may inherit their shifts from their inputs. Across days, PFs in CA1 undergo partial remapping, which likely involves synaptic plasticity that occurs during sleep when place cell sequences are known to be reactivated. CA3 PFs are much more stable across days. Throughout experience on day 2, a reduced but still very significant level of backward shifting occurs in CA1 with even less backward shifting in CA3. These PF dynamics in CA1 and CA3 likely support distinct roles in memory processing. We suggest that the CA1 rapidly forms a memory of a new context that supports single trial learning, and continuously updates this memory throughout ongoing experience. This updating - in the form of backward shifting PFs - may enable the CA1 to predict the near future regarding where in the context the animal is about to visit. The partial remapping across days in CA1 may also be another form memory updating by separating memory representations of experiences that occur in the same context on different days or at different times. On the other hand, animals need to recognize where they are and recall whether they are in a

context they have experienced before. CA3 PFs seem to support this memory process by maintaining stable PFs within and across days.

Acknowledgements

We thank D. Dombeck for comments on the manuscript, C. Cherian for helpful manuscript edits, and members of the Sheffield lab for manuscript comments and useful discussions. Funding: This work was supported by: The Whitehall Foundation, The Searle Scholars Program, The Sloan Foundation, The University of Chicago Grossman Institute for Neuroscience start-up funds, and the NIH (1DP2NS111657-01). Author contributions (CRediT): Conceptualization: MS, Data curation: CD, Formal Analysis: CD, AM, MS, Funding acquisition: MS, Investigation: CD, Methodology: MS, CD, AM, Project administration: CD, Software: CD Supervision: MS, AM, Validation: AM, MS, Visualization: CD, AM, MS, Writing – original draft: MS, CD, Writing - review and editing: AM, MS, CD. **Competing interests:** Authors declare no competing interests

Data availability: Raw data is available upon request. Processed data for analysis are available on GitHub:
(https://github.com/Candong/Distinct_CA1_CA3.git).
Scripts used for data analysis and processed data are available on GitHub:
(https://github.com/Candong/Distinct_CA1_CA3.git) .

CHAPTER 3

SYNCHRONIZED CO-ACTIVATION EVENTS ACROSS CA1 AND CA3 ARE ASSOCIATED WITH CONTEXTUAL FEAR MEMORY FORMATION AND RECALL

This chapter is a draft for an ongoing study of 'Synchronized co-activation events in CA1 and CA3 are important for contextual fear memory formation and recall', in which I will be the first author. The work is included with permission from all authors.

3.1 Abstract

Episodic memories—memories of experiences in time and space— form through associations made in the hippocampus between distinct stimuli within specific contexts. In a contextual fear conditioning (CFC) paradigm, optogenetic activation of 'engram cells' - neurons that are activated and "tagged" during induction of CFC - in hippocampal CA1, CA3 or Dentate Gyrus can sufficiently trigger retrieval of the contextual fear-memory. The existence of "engram-cells" in different hippocampal sub-networks suggests that the intact hippocampus is critical for episodic memory formation and recall. However, how the anatomically connected but functionally distinct sub-networks in the hippocampus, such as CA3 and CA1, coordinate the information to support memory formation and recall remains unknown. This question can only be solved by studying the cross-network interactions during memory formation and recall. Here, we implemented a novel behavioral and imaging paradigm for CFC in virtual reality where simultaneous two-photon calcium imaging of the hippocampal CA1 and CA3 was performed. Head-fixed mice navigating virtual contexts underwent fear conditioning and fear memory recall was assessed across multiple days until fear memory extinction, all while simultaneously imaging both CA1 and CA3. We observed CFC behaviors in head-fixed mice in virtual reality similar to freely moving animals. We identified

co-activated neuronal ensembles independently within CA1 and CA3 and also across CA1 and CA3 during contextual fear memory formation and recall. Interestingly, across regions synchronized events were associated with fear memory encoding and recall, suggesting synchronized activity across hippocampal sub-networks is a feature of memory encoding and recall in the hippocampus.

3.2 Introduction

The hippocampal formation and its connected sub-networks are critical for encoding and recall of episodic memory in humans and other mammalian species (Eichenbaum 2017; Rolls 2018; Scoville and Milner 1957). Recent studies have shown that in a contextual fear conditioning (CFC) paradigm, which causes the formation of an episodic-like memory (Pause et al. 2013), optogenetic activation of neurons in hippocampal CA1, CA3 or Dentate Gyrus that are "tagged" during induction of CFC can trigger retrieval of a context-specific fear-memory (X. Liu et al. 2012; Ramirez et al. 2013; Josselyn, Köhler, and Frankland 2015). The existence of "engram-cells" in different hippocampal sub-networks suggests that the intact hippocampus is critical for episodic memory formation and recall. Supporting this, sub-populations of hippocampal principal neurons are specifically tuned to contextual cues (location, reward, time etc.) (O'Keefe and Dostrovsky 1971; Gauthier and Tank 2018; MacDonald et al. 2011; Knudsen and Wallis 2021). These neurons also show 'offline' reactivation, indicating a role in memory encoding and memory consolidation (Pavlides and Winson 1989; Skaggs and B. L. McNaughton 1996; Wu et al. 2017; Buhry, Amir H Azizi, and Cheng 2011). It is natural to consider the engram cells and the contextual cue-tuned neurons to be the same population of hippocampal neurons, however, recent studies have indicated that engram cells and contextual-tuned cells are not necessarily the same (Tanaka et al. 2018; Ghandour et al. 2019). The relationship between engram cells and contextual tuned neurons remains unclear. Investigating the real-time neural dynamics of hippocampal neurons during contextual fear

memory formation and recall should shed light on this question.

Another intriguing question in studying episodic memory is how the sub-networks in the hippocampus coordinate information to support memory formation and recall. The CA1 sub-network is considered the main output of the hippocampus and the CA3 sub-network is the main input region to CA1. (Förster, Zhao, and Frotscher 2006) . Although engram cells exist in both CA1 and CA3 plus CA3 neurons heavily project to CA1, the neural dynamics in the two regions are different during novel spatial experiences and familiarization of contexts, indicating distinct functional roles during memory formation and recall (Tonegawa et al. 2015; Josselyn, Köhler, and Frankland 2015; Dong, Antoine D Madar, and Sheffield 2021; S. Leutgeb, J. K. Leutgeb, et al. 2004). How the anatomically connected yet functionally distinct sub-networks coordinate information to support memory formation and recall remains unknown. This question can only be answered by studying the neuronal dynamics of the two sub-networks at the same time and determining the cross-network interactions during memory formation and recall.

In this work, we implemented a novel behavioral paradigm for CFC in virtual reality combined with functional two-photon co-imaging of the hippocampal CA1 and CA3. In this paradigm head-fixed mice navigate virtual contexts and undergo contextual fear conditioning and subsequent contextual fear memory recall across multiple days. We observed CFC behaviors in head-fixed mice similar to freely moving animals (X. Liu et al. 2012). Recent studies have shown that co-active neurons in the hippocampus is related to contextual fear memory encoding (Malvache et al. 2016; Y.-Z. Liu et al. 2017; Rajasethupathy et al. 2015). Here, we measured and analyzed the CA1 and CA3 population activity across days throughout CFC and recall. We found co-active neuron ensembles independently in both regions. We found a higher proportion of CA3 neurons participated in a co-active event than in CA1 whereas CA1 had a higher frequency of co-active events than CA3. Among these co-active events, we found some of them were synchronized across CA1 and CA3, indicating possible

functional connections between CA1 and CA3 ensembles. Intriguingly, we found that these synchronous CA1-CA3 events were higher in frequency during fear memory formation and recall, suggesting they play a role in the formation and recall of these memories. Supporting this idea, we found that in a subset of animals that did not show a strong contextual fear memory had formed, there was a much lower frequency of CA1-CA3 synchronous events. This finding might indicate that contextual fear memory formation and recall requires CA1-CA3 synchronization. Such synchronization might play an important role in the induction of synaptic plasticity across hippocampal sub-networks to support memory processing in the hippocampus.

3.3 Materials and Methods

3.3.1 Subjects

All experimental and surgical procedures were in accordance with the University of Chicago Animal Care and Use Committee guidelines and were approved by IACUC. For this study, 10-12 week old C57BL/6-Tg(Grik4-cre)G32-4Stl/J (9 animals for analysis in figure 1-3, 5 animals for analysis in figure4 and supplementary figure 1, 4 animals for animals in figure 5 and supplementary figure 2.). All training and experiments were conducted during the animal's dark cycle.

3.3.2 Mouse surgery and virus injection

Mice were anesthetized (1-2% isoflurane) and injected with 0.5 mL of saline (intraperitoneal injection) and 0.45 mL of Meloxicam (1-2 mg/kg, subcutaneous injection). To prepare animals for CA1-CA3 populational co-imaging, a small (0.5-1.0 mm) craniotomy was made over the hippocampus CA1 and CA3 area (a triangle center around 1.6 mm lateral, -2.3 mm caudal of Bregma). A genetically encoded calcium indicator, AAV1-CamKII-GCaMP6f

(Addgene, #100834) was injected into CA1 (75 nL) at around 1.65 mm lateral, -1.65 mm caudal of Bregma and with a depth of 1.3 mm below the surface of the dura using a beveled glass micropipette. After CA1 injection, custom-made Cre-dependent AAV virus: AAV1-CamKII-flex-GCaMP6f (made by Vigene) was injected to CA3 (220 nl) at around 2.4 mm lateral, -1.7 mm caudal of Bregma and with a depth of a depth of 1.75 mm below the surface of the dura. After injection, the exposed skull was covered up using dental cement (Metabond, Parkell Corporation) and a metal head plate (Atlas Tool and Die Works). Water scheduling began the following day (0.8-1 mL per day and continued through all training and experiments). Around 7 days later, mice underwent another surgery to implant a hippocampal window as previously described (Sheffield, Adoff, and Dombeck 2017). Following implantation, the head-plate was reattached with the addition of a head ring cemented on top of the head plate which was used to house the microscope objective and block out ambient light. For this experiment, because the cannula window was implanted at an angle (15 degrees) relative to the horizontal plane, we bent the two ends of the head plate to match this angle so that the head plate and cannula were on the same plane. We could then change the angle of our microscope objective to be perpendicular to this plane. Post-surgery mice were given 2-3 ml of water/day for 3 days to enhance recovery before returning to the reduced water schedule (0.8-1.0 ml/day).

3.3.3 Behavior and virtual reality (VR) switching:

To navigate in the VR environment, animals ran on a treadmill surrounded by 5 LED screens (Sheffield, Adoff, and Dombeck 2017; Heys, Rangarajan, and Dombeck 2014). VR environments (one training environment refer to F, two novel environments, Ctrl and CFC and two backup novel environment to replace the Ctrl and CFC if the animal didn't run in the original two) were created using VIRMEN (Aronov and Tank 2014). Each environment contained a 2-meter long linear track enriched with different distal and proximal 3D visual

cues. Animals were first trained in a familiar environment with rewards for around 10-14 days with 4 µL water rewards delivered at the end of the track. Once animals' running achieved a lap rate of > 4 laps/minute, mice were trained in the same familiar environment with a custom-made wearable tail shock apparatus ("tailcoat") to habituate the mice to the sensation they would feel during fear conditioning. Water reward was removed if the animal ran well with the tailcoat. Those that maintained running speed after the addition of the tailcoat and removal of water reward, continued to the experiment stage. The tailcoat is made of conductive mesh wrapped around soft denim cloth that is in contact with the mouse's tail. Two alligator clips that are connected to a shock generator (Precision animal shocker, Harvard Bioscience) hold the tailcoat on the mouse's tail.

3.3.4 Two-photon imaging

Imaging was done using a laser scanning two-photon microscope (Neurolabware). The microscope consisted of an 8 kHz resonant scanning module (Thorlabs), and a 16x/0.8 NA/3 mm WD water immersion objective (MRP07220, Nikon). GCaMP6f was excited at 920 nm with a femtosecond-pulsed two-photon laser (Insight DS+Dual, Spectra-Physics) and the fluorescence was collected using a GaAsP PMT (H11706, Hamamatsu). The microscope is customized to tilt the objective, which we tilted to be perpendicular to the CA3 head plate angle. Laser average power after the objective was set at 80 mW for CA1 imaging and 120 mW for CA3 plane during multi-plane imaging. Scanbox (Neurolabware) was used for microscope control and data acquisition. Because the distance between CA1 and CA3 may vary across animals and we need to control the same recording frequency, time series videos were acquired at around 11 Hz for each of the 3 imaging planes (using an electronic lens) to maximize the number of neurons imaged in each mouse. Later, 2 planes with the most CA1 and CA3 neurons from each animal were selected to be used (usually top and bottom planes). A PicoScope Oscilloscope (PICO4824, Pico Technology) collected the signal from

the microscope to synchronize frame acquisition timing with behavior (see below).

3.3.5 Imaging sessions

Each mouse used in this study had healthy-looking GCaMP6f expression (resting fluorescence absent from the nucleus; fast transient kinetics; no signs of misshaped somas) in both CA1 and CA3. On experimental day0: field of view (FOV) was chosen that maximized the number of CA1 or CA3 neurons across three planes. Imaging and behavior recordings started right before mice entered the VR. Mice ran at least 10 laps in Ctrl (novel environment on this day) in about 6 min. After which the mice were instantaneously switched to the CFC environment (novel environment on this day). Mice then ran at least 10 laps in CFC in about 6min and then were placed back in their home cage. After imaging, more than one averaged FOV was saved to be the reference in order to align the planes and record from the same cells the following day. Experimental day 1: The same FOVs were carefully matched to the previous day's FOVs. Mice were exposed to Ctrl environment first and then switched to the CFC environment. After this, animals were delivered 6 one-second-long 1mA tail shocks at 1-minute intervals while animals kept navigating in the CFC, so the shocking position on the 2-meter track was pseudo-random. Experimental day 2: The same FOVs were carefully matched to the previous day's FOVs. Once imaging started, mice were first exposed to Ctrl and recorded for 6 min and then the animals were directly exposed to the CFC environment and recorded for another 6 min. Mice behavior including treadmill running speed, position, shock and licking was collected using the PicoScope Oscilloscope to synchronize with the imaging.

3.3.6 Image processing and ROI selection

Time-series movies for multi-plane recordings were acquired using interleaved frames (1st, 4th, 7th... frames belong to plane 1; 2nd, 5th, 8th... frames belong to plane 2: 3rd ,6th,

9th... frames belong to plane 3). So that the video of the CA1 and CA3 planes were processed separately. Movement artifacts were removed using rigid and non-rigid transformations and assessed to ensure the absence of drifts in the z-direction. To combine multi-day datasets, imaging planes acquired from each day were first motion-corrected separately. ImageJ (NIH) was then used to align the motion-corrected images relative to each other by correcting for any rotational displacements. The images across all days were then stitched together and motion-corrected again as a single movie in Suite2p (Pachitariu et al. 2017).

Regions of interest (ROIs) were also defined using Suite2p and manually inspected for accuracy. For each ROI, baseline-corrected δF/F traces across time, filtered for significant calcium transients were then generated as previously described (Dombeck et al. 2010; Sheffield and Dombeck 2015; Sheffield, Adoff, and Dombeck 2017). In brief, slow time scale changes in the fluorescence time series were removed by examining the distribution of fluorescence in a ± 5 second interval around each sample time point and subtracting the 8% percentile value. A suite2p baseline removing function and a Savitzky–Golay filter (with order = 3 and frame length = 7) were used to further denoise the signal. The baseline and σ were calculated from the fluorescence time series that did not contain large transients. Fluorescence transients were then identified as events that started when fluorescence deviated 2 σ from the corrected baseline and ended when it returned to within 0.5σ of baseline. The baseline-subtracted neuron fluorescence traces were then subjected to analysis of the ratio of positive- to negative-going transients of various amplitudes and durations. We used this analysis to identify significant transients with $< 1\%$ false-positive error rates and generated the significant transient-only traces that were used for all subsequent analyses. Calcium transient analysis: After extracting significant calcium transients, we analyzed and compared some basic characteristics of these transients across CA1 and CA3. Transient peaks: the maximum value for each transient from each neuron. Transient duration: the duration of each transient calculated at the half peak from each neuron. Transient frequency: the

frequency of significant transients from each neuron.

3.3.7 Histology and brain slices imaging

We checked the GCaMP6f expression in CA1 and CA3 for all the animals we imaged in to ensure the GCaMP expression was restricted to CA1 and CA3. Animals that didn't show correct expression were excluded. Mice were anesthetized with isoflurane and perfused with 10 ml PBS followed by 20 ml 4% paraformaldehyde in PBS. The brains were removed and immersed in 30% sucrose solution overnight before being sectioned at 50 µm-thickness on a cryostat. The brain slices were then collected on glass slides and mounted with a mounting media with DAPI (SouthernBiotech DAPI-Fluoromount-G Clear Mounting Media,010020). The whole brain slices were imaged under 10X with a Caliber I.D. RS-G4 Large Format Laser Scanning Confocal microscope from the Integrated Light Microscopy Core at the University of Chicago.

3.3.8 Behavior analysis

We detected animals' freezing and backward movement behavior on recall days. Animals' freezing periods were defined as periods of time that are longer than 1 second during which animals' moving velocity is lower than 1cm/s. Animals' backward movement was defined as more than 0.5 second of continuously backward movement (velocity < 0 cm/s).

3.3.9 Co-activation detection

To analyze the activity of the neuron co-activation in each animal, we did the following steps. 1. Compute the onset, offset, peak and duration of each transient. 2. Create a hundred times shuffle matrix for the neuron population by doing interval shuffling for each neuron (randomly reordering intervals between events for each cell). 3. Compare the number of transient peaks within a 0.5s time window in real data and shuffle data distribution for

each time point. If the number of peaks in real data is bigger than the 95 percentile of the shuffling data, then this time point and all subsequent contiguous time points that reach the standard are grouped as a co-activation event. 4. Sometimes the neurons are very active and multiple co-activation events are grouped as one event. So we calculate the average activity of the neuron ensemble that participated in the co-activation event. We find the peaks for the mean activity during the long co-activation period and separate the event into small events based on the peak width. 5. For each sub-event we calculate the number of neurons that participated in the event, events with more than 3 neurons co-activated will be labeled as a co-activation event. Both CA1 and CA3 were analyzed with this same procedure. The onset, offset and duration of the co-activation event as well as the neuron ensemble for each event were saved for later analysis.

3.3.10 synchronization co-activation detection

To find the synchronization co-activation in CA1 and CA3, we compare the onset and offset between CA1 and CA3 co-activation events. For events where the CA3 event ends before the CA1 event ends and more than 50% of the event duration overlaps in either network is labeled as a pair of synchronized co-activation events.

3.3.11 Statistics

We used null-hypothesis testing to compare data (described in figure legends). For null-hypothesis testing, Wilcoxon rank-sum test, student t-test and one-way ANOVA were applied. $P < 0.05$ was chosen to indicate the statistical significance and P-values in the figures are indicated as follows: , $P < 0.05$, , $P < 0.01$, , $P < 0.001$, N.S. not significant. For data tested with the estimation approach, we also used the null hypothesis testing to confirm any differences.

3.4 Results

3.4.1 CFC Paradigm in the Virtual Reality environment

We designed a new behavior paradigm that allows animals to navigate in the virtual reality (VR) environment meanwhile experiencing CFC shocks through a shock box that delivered shocks to the animals' tail (Fig. 3.1a). Different from previous fear conditioning methods in a virtual reality environment, which deliver air puff to the animal face and measure change of the amount of licking for reward (Lovett-Barron et al. 2014; Rajasethupathy et al. 2015), our setup mimics the classic CFC experimental paradigms (X. Liu et al. 2012), ensuring the results will be more comparable with previous studies.

Head-fixed, water-restricted mice were trained to run in VR environment with a water reward. Once the animals were used to running in the VR, the reward was removed and a tailcoat that conducts electrical shocks was introduced to the animals. If animals run well with the tailcoat (at least 10 laps in 5 minutes), they were introduced to two novel environments (Ctrl and CFC) on experiment day 0 (Fig. 3.1b). On experiment day 1 (shock day), mice first revisited the two environments, afterwards, six electrical tail shocks were delivered at 1mA amplitude for 1 second with a time interval of 1 minute to the animals in the CFC environment(Fig. 3.2a). Animals showed a vigorous increase in running speed immediately after the shock delivery, indicating that the animals felt the noxious stimulus and were running to avoid it (Fig. 3.2a-bottom,c). On experiment day 2 (recall day), mice revisited the two environments in the order of Ctrl and then CFC environment. Animals that went through the CFC paradigm generally showed typical 'freezing' behavior, consistent with what has been observed in real-world CFC experiments(Fig. 3.2a-b, right) (X. Liu et al. 2012; Chaaya et al. 2019). Because the animals were head-fixed and running on a one dimension treadmill, we also noticed a specific backward moving behavior when the animals were re-exposed to the CFC environment on recall day, indicating fear of the en-

vironment (Fig. 3.2b, right). 7 out of 9 animals showed an increase in freezing count, the number of freezing, during the first 3 minutes in the CFC environment compared to in the Ctrl environment. A higher freezing count in the CFC environment indicates contextual fear memory recall happens when the animals first enter the CFC environment (Fig. 3.2d). This fear behavior in VR CFC is consistent with real world CFC providing us with the ability to study contextual fear memory in head-fixed mice which is compatible with large-scale 2-photon population recordings of the same cells across days that real-world CFC studies are not (Y.-Z. Liu et al. 2017; Jimenez et al. 2020).

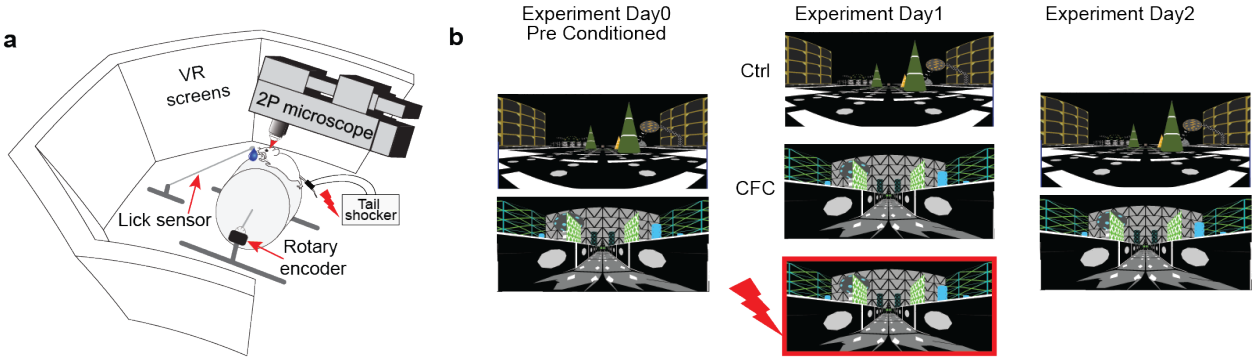

Figure 3.1: **Experimental Setup. a,** Depiction of the virtual reality (VR) setup and the tail chock setup. **b,** Scheme of the experimental paradigm. Two environments (Ctrl and CFC) were introduced to the animals during the experiments.

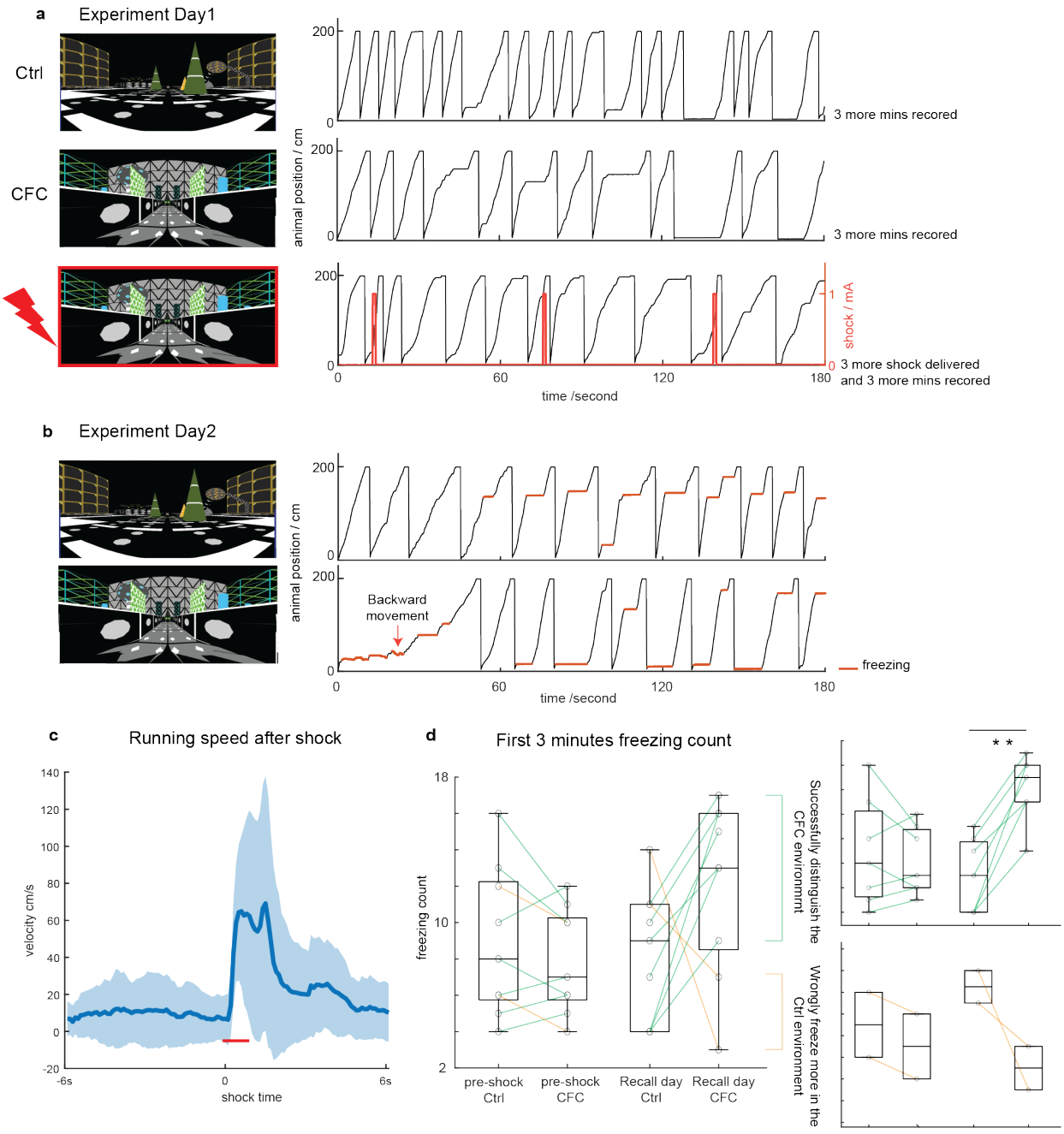

Figure 3.2: **VR CFC paradigm induces similar behavioral responses as real-world CFC.**

a, Left, depiction of experiment day1 (shock day) paradigm. Right, example animal behavior shows track position versus time in Ctrl environment (top), CFC environment (middle) and CFC environment during shocks (bottom). **b,** Left, depiction of experiment day2 (recall day) paradigm. Right, example animal behavior shows track position versus time in Ctrl

Figure3.2, continued. environment (top), and CFC environment (bottom). **c,** Running velocity vs time aligned to shock onset (time = 0) during the shock session on shock day. (n=9 animals, shaded area, ±STD, red,shock period). **d,** Freezing counts vs condition during the first 3 minutes. Left, all 9 animals; Right, animals grouped by either increased or decreased (top or bottom) freezing count in the CFC environment. (n=9 animals; green, increased freezing in the CFC environment,n=7; red. increased freezing in the Ctrl environment, n=2) Top right, one-way ANOVA with Tukey HSD post hoc test. **p¡0.01, p=0.0026)

3.4.2 Co-imaging of hippocampal CA1 and CA3 neurons

Simultaneously recording from CA1 and CA3 during CFC is required to study the cross-subnetwork interactions between hippocampal CA1 and CA3. To tackle this, we applied a multiplane imaging technique to record both dorsal CA1 and CA3a (referred to as CA3 from here on) simultaneously (Fig. 3.1a, top). To do so, we expressed GCaMP6f only in hippocampal CA1 and CA3 by using a cre mouse line named 'Grik4-cre', which limits the cre expression only in CA3 neurons(Nakazawa et al. 2002). We then restricted the expression of GCaMP6f in CA1 by adjusting the position of the viral injection to be as far away from CA2 as possible. Furthermore, to confirm that we are not recording from hippocampal CA2, we checked the GCaMP6f expression in brain slices of each animal after experiments (Fig. 3.1a, bottom). Additionally, we compared the size of the regions of interests (ROIs) in CA1 and CA3 to once again confirm that we were indeed only recording CA1 and CA3. (Fig. 3.1b, see methods). We found bigger ROI sizes in CA3 than in CA1 (Fig. 3.1c), which is consistent with previous anatomical studies(Attili et al. 2019). To our knowledge, this is the first time CA1/CA3 has been simultaneously functionally imaged under 2-photon in vivo without removing any hippocampal tissue (Redman et al. 2022).

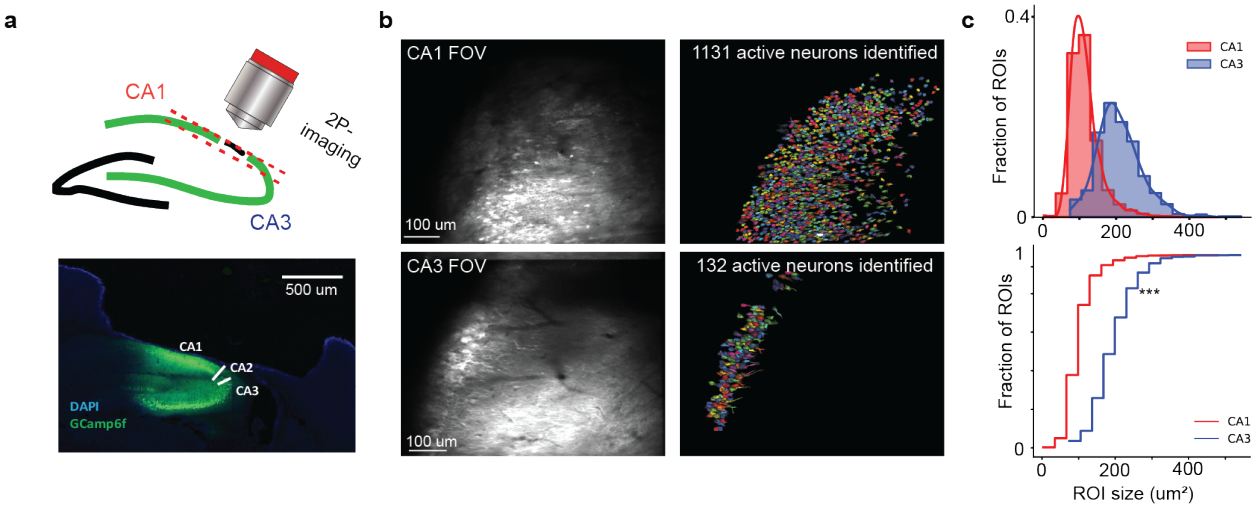

Figure 3.3: **Co-imaging of hippocampal CA1 and CA3 neurons. a,** Top, depiction of CA1-CA3 co-imaging. Multi-plane imaging was applied during recording, the CA1 field of view (FOV) is the top plane and the CA3 FOV is the bottom plane. Bottom, example brain slice that shows GCaMP6f (green) expression in the CA1 and CA3 region but not the CA2 region. **b,** Left, example FOV from the same animal of CA1 (top) and CA3 (bottom). Right, the regions of interest (neurons) that were detected from the example FOVs (CA1, 1131 active neurons; CA3, 132 active neurons). **c,** .Top, histogram of the size ditribution of the CA1 (red) and CA3 (blue) ROIs. Bottom, Cumulative fraction plots for the size of the size of the CA1 (red) and CA3 (blue) ROIs. Wilcoxon rank sum test, two-sided. ***, $P < 0.001$

3.4.3 Co-activation of neuron ensembles in hippocampal CA1 and CA3

To study the hippocampal CA1 and CA3 neuronal dynamics, we first analyzed the neuronal activity of CA1 and CA3 separately. Although the mice were navigating in VR without reward and wearing tail coats, the hippocampal place fields (PFs) looked similar to traditional VR navigation-induced PFs (Sheffield and Dombeck 2015; Dombeck et al. 2010), (Fig.3.6 a). This result granted us the confidence to further analyze the neuronal data. A previous study has reported that hippocampal CA1 neurons show co-activation during navigation, but focusing on when animals were not moving (Malvache et al. 2016). We also observed co-activation in both CA1 and CA3 regions before, during shock and during recall session (Fig. 3.3 a) but during aniaml movements and stoppings. We referred to the group of neurons

that participate in a co-active event as a co-active ensemble, although with different names across different studies and the standard for selecting the events were varied (Malvache et al. 2016; Sweis et al. 2021; Rajasethupathy et al. 2015; Gillespie et al. 2021). We first tested the co-active events frequency in CA1 and CA3. We found that the frequency of co-active events is higher in CA1 than in CA3 (Fig.3.3 b), which is consistent with the finding that CA1 neurons are in general more active than CA3 neurons when animals navigate in environments (Mizuseki et al. 2012; Dong, Antoine D Madar, and Sheffield 2021). Interestingly, although we noticed higher co-activation frequency in CA1, we found a higher percentage of CA3 neurons that participate in a co-activate event (Fig. 3.3 c, Fig. 3.6 b). This fits with the fact that hippocampal CA3 neurons are more recurrently connected and form an associative network, which might increase the recruitment of more CA3 neurons into the co-active ensemble (Le Duigou et al. 2014). Moreover, we found both CA1 and CA3 had an increase in the number of neurons participating in co-active ensembles during the shock session on the shock day, although the frequency of events remained unchanged (Fig. 3.3 d, Fig. 3.6 c)). Our result indicates contextual fear associations in the hippocampus are encoded by recruiting more neurons into co-active ensembles in both CA1 and CA3.

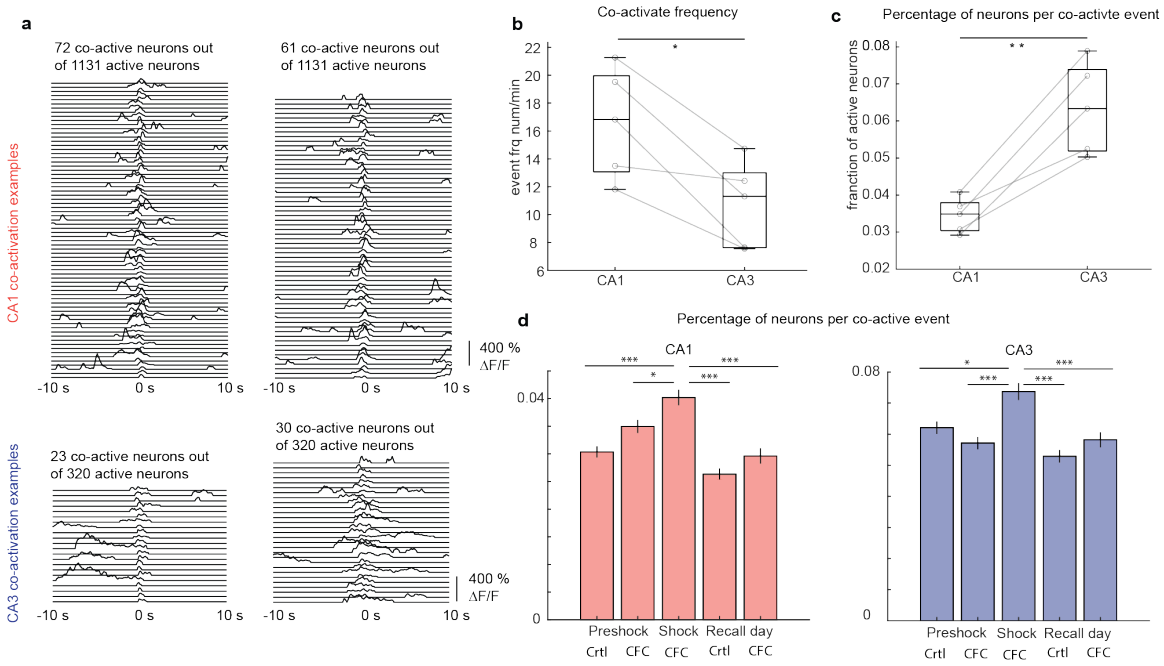

Figure 3.4: **Co-activation of neuron ensembles in hippocampal CA1 and CA3. a,** Top, Two example traces of CA1 co-active events, the peak of the mean co-activated neurons activity is set to be time = 0s. Bottom, example traces for CA3 co-active events. Calcium signals that didn't pass the significant criteria have been set to zero, see methods for details. **b,** Co-active event frequency (number of events per minute) in CA1 and CA3 compared in an animal by animal manner. (n=5 animals, * $p < 0.05$, p=0.0319, paired t-test) **c,** Average percentage of neurons participate in CA1 and CA3 co-active events compared in an animal by animal manner. (n=5 animals, ** $p < 0.01$, p=0.0012, paired t-test) **d,** Bar plot for a percentage of neurons participating in CA1 (left) and CA3 (right) co-active events, x-axis is each specific session. (errorbar,±SEM. One-way ANOVA, stats detail(sample size, p-value, etc.) see table 3.1 for CA1, table 3.2 for CA3

3.4.4 Synchronized co-activation in hippocampal CA1 and CA3

The co-activation in the hippocampus has been viewed as one of the mechanisms for memory consolidation and recall and is governed by Hebbian plasticity rules(Buhry, Amir H Azizi, and Cheng 2011; Dupret et al. 2010; Foster 2017; Hwaun and Colgin 2019; Nakashiba et al. 2009). As our study and previous studies have shown, co-activation events exist in both hippocampal CA1 and CA3, however, what is happening between CA1 and CA3 during co-activation events is unknown. Benefiting from our CA1-CA3 co-imaging setup, we had

the chance to answer this question. We noticed around 10 20 % of co-activation events were synchronized across CA1 and CA3 subnetworks. Although calcium imaging lacks the time resolution to determine if CA3 co-active ensembles drive CA1 co-active ensembles, we surmise that it is more likely that the synchronization events are triggered by CA3 co-activation, due to the CA1 to CA3 pathway is not monosynaptic and are not likely to trigger population co-activation.

We then tested if these synchronized co-activation events in CA1 and CA3 are related to the animals' behavior on the recall day since the behavioral readout of the animal indicates if it successfully remembered the context specific fearful experience. Interestingly, we found that the animals' behavior was correlated with the amount of synchronized co-activation events in the Ctrl and CFC environment (Fig. 3.5 b, c). Animals who froze more in the CFC environment also had a higher count of synchronization co-activation events in the CFC environment, and the one animal who froze more in the Ctrl environment also had more synchronization co-activation events in the Ctrl environment. We also found a consistent trend between the animal's freezing behavior on recall day and CA1-CA3 synchronized co-activation on the previous day during fear conditioning (Fig. 3.5 d). Notice that this relationship is specific to CA1-CA3 synchronized co-activation, the number of independent co-activation events in CA1 or CA3 was not related to animal behavior (Fig. 3.7 b,c). The increased synchronized co-activation events during both fear memory encoding and memory recall indicates that synchronization between CA1 and CA3 might be essential for contextual fear memory formation and recall. Through this network synchrony within the hippocampus new memories may be encoded and subsequently retrieved.

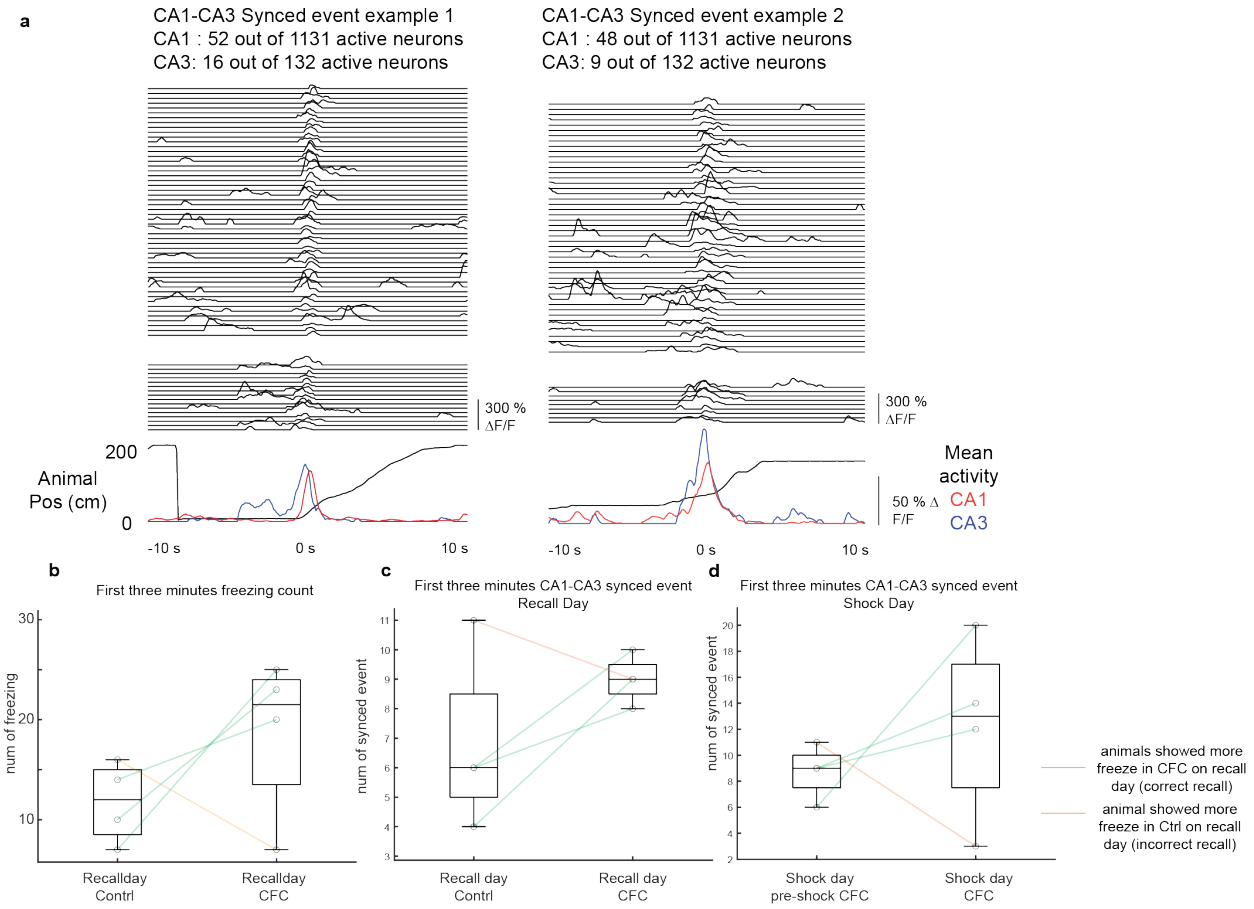

Figure 3.5: **Synchronized co-activation in hippocampal CA1 and CA3.** **a,** Two examples of synchronized co-activation events in hippocampal CA1 and CA3 aligned with the animal behavior. Top,CA1 traces; middle, CA3 traces; bottom, animal position on the track aligned with the mean activity of the synchronization co-activation ensembles in CA1 (red) and CA3 (blue). The peak of the mean co-activated neurons activity is set to be time = 0s. Calcium signals that didn't pass the significant criteria have been set to zero, see methods for details. **b,** Freezing counts during the first 3 minutes when animals navigating in Ctrl and CFC environments. (n= 4 animals; green, more freezing in the CFC environment, n=2; orange, more freezing in the Ctrl environment, n=1) **c,** Number of CA1-CA3 synchronization co-activation count in the first 3 minutes in Ctrl and CFC environments on recall day. (color code same as b) **d,** Number of CA1-CA3 synchronization co-activation count in the first 3 minutes in before and during shock in the CFC environment on shock day. (color code same as b)

3.5 Discussion & Future Direction

In this work, we implemented a novel behavioral paradigm for CFC where functional two-photon co-imaging of hippocampal CA1 and CA3 was performed in head-fixed mice navigating virtual contexts undergoing fear conditioning and during fear memory recall across multiple days. We observed contextual specific fearful behaviors in head-fixed mice similar to freely moving animals (X. Liu et al. 2012). To our knowledge, it is the first time the dynamics of the same group of neurons have been tracked across days simultaneously in CA1 and CA3 with 2-photon imaging during contextual fear conditioning. This study could provide the field with a new paradigm in which to investigate hippocampal memories.

We found co-activated neuron ensembles in CA1 and CA3 during pre-conditioning, shock and recall sessions. We noticed that a higher proportion of CA3 neurons participated in the co-activation than CA1 whereas CA1 had a higher frequency of co-activation event than CA3. In both regions, the co-activation ensemble proportion increased during fear memory formation (shock session), indicating fear memory encoding across these co-activation events. Among these co-activation events, we detected some synchronized co-activation events in CA1 and CA3, indicating a possible functional connection between these ensembles in CA1 and CA3. We found the synchronized CA1-CA3 co-activation frequency is higher during fear memory formation and recall if the animal expresses more fearful responses in the fear-conditioned environment than in the control environment and for animals that showed less fearful responses in the fear-conditioned environment, the frequency of synchronized events were lower. This finding might indicate that contextual fear memory formation and recall requires CA1-CA3 synchronization co-activation and might play important roles in the induction of hippocampal synaptic plasticity.

The recurrent connection in the hippocampal CA3 has been viewed as the anatomical evidence that CA3 supports memory recall through pattern completion (Kesner and Rolls 2015; Le Duigou et al. 2014). Previous computational modeling work and experimental work

also supports this idea (Panzeri et al. 2001; S. Leutgeb and J. K. Leutgeb 2007; Dong, Antoine D Madar, and Sheffield 2021). The associative network that exists in CA3 is consistent with our observation that co-activation events in CA3 recruit more neurons than in CA1. In contrast, the CA1 region receives input from multiply brain regions other than the CA3(such as entorhial cortex, ventral tegmental area, locus coeleus) , which might explain why co-activation events in CA1 are more frequent than CA3 (Tao et al. 2021a; Menno P Witter 2007). During the shock session, the percentage of neurons participating in co-activation events increased in both regions but not the event frequency, which might indicate the encoding of the aversive experience that could drive Hebbian plasticity (Magee and Johnston 1997).

Synaptic plasticity is thought to be the underlying mechanism of learning and memory (Martin, Grimwood, Morris, et al. 2000; Kandel et al. 2000). CA3 is the major excitatory projection to CA1, through the Shaffer collateral pathway, and has been viewed as the provider of the driving force for CA1 synaptic plasticity. Many insights regarding long-term potentiation (LTP) and long-term depression (LTD) were discovered through this connection (Bliss and Collingridge 1993). Previous studies regarding the sequential activation in the hippocampus during sleep or rest (replay events) suggest that co-activation is critical for memory consolidation, likely through activation of synaptic plasticity mechanisms (Girardeau, Cei, and Zugaro 2014; Ecker et al. 2022). The synced co-activation we discovered here was associated with contextual fear conditioning, a form of hippocampal-dependent memory formation. We hypothesize that CA3 neurons drive CA1 neuron activity during synched events to induce synaptic plasticity and thus memory formation. The association between animal freezing behavior and CA1-CA3 synced co-activation events support the idea that these events are involved in memory encoding. We observed that when animals are more afraid of the environment on recall day they exhibited more synchronized events on recall day. They also exhibited more synched events during the shock session the previous

day but not before shock. This indicates that the synchronized co-activation events are not only context-related but also fear-related.

There are several directions that are currently under investigation and will be included in the final version of a manuscript :

Previous co-activation studies in the hippocampus were highly focused on co-activation during sleep or rest and embedded within these co-activation were replay sequences based on the neurons' place field position, ignoring other hippocampal neurons (Foster 2017; Skaggs and B. L. McNaughton 1996; Dragoi and Tonegawa 2011; Pedrosa and Clopath 2020; Malvache et al. 2016). In our study, we found that co-activation events also happened during navigation, and not all the neurons participating in co-activation event were place cells (data not showed). Previous identification of co-activation events relied on co-detection of sharp-wave ripple (SWR) in the local field potential in the hippocampus, but SWRs do not occur when animals are running. This suggests the co-activation events described in this study are fundamentally different as they must occur independent from SWRs (Buzsáki 2015). Other interesting questions to study are the composition of the co-active ensembles and what the role of non-place cells are that participate in co-active events, given this study has shown that contextual information is not only encoded by place cells (Meshulam et al. 2017).

Contextual fear memory studies have identified engram cells in hippocampal subnetworks (DG, CA3 and CA1) (X. Liu et al. 2012; Y.-Z. Liu et al. 2017; Tonegawa et al. 2015). The relationship between engram cells and place cells has remain unclear (Goode et al. 2020). Some studies claimed that engram cells are not place cells (Tanaka et al. 2018), while other studies indicate place cells are essential for contextual memory encoding and recall(Ghandour et al. 2019). Our results indicate not all co-activated ensemble neurons are place cells. Maybe non-place-cell neurons that participate in synchronized co-activation events during memory recall are engram cells. If this could be provem, then we could show that although engram cells are not necessarily to be place cells, there are some functional connections between

engram cells and place cells because they are co-activated during memory formation.

In summary, we identified synchronized and non-synchronized co-activation of neuron ensembles in hippocampal CA1 and CA3 during contextual fear memory formation and recall. The synchronized co-activation events are related to fear memory encoding and recall. We will further analyze the neuronal composition of these ensembles and the relationship between co-activation and animal behavior (eg. running and freezing). We will also investigate co-activation of neuron ensembles across days across CA1 and CA3 to further understand the neuronal mechanisms for memory encoding and recall over longer timescales.

3.6 Supplemental Material

3.6.1 Supplementary figures

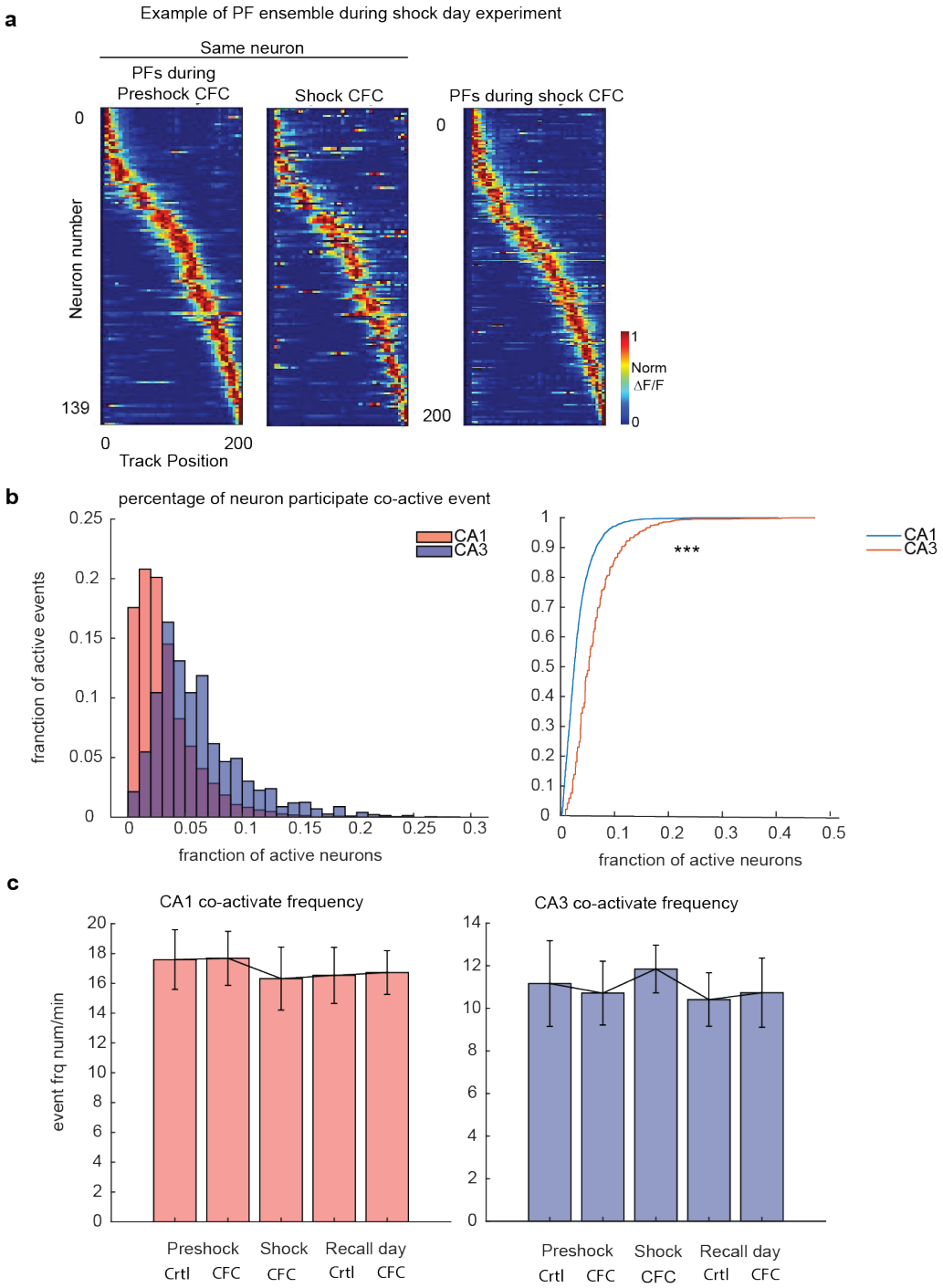

Figure 3.6: **PFs dynamics in CA1 and co-active event characters.**

Figure3.6, continued. a, Example PFs dynamics in CA1. Left, mean PFs sorted by track position in CFC environment before shock; middle, mean activity if the same neurons on the left during Shock; right, mean PF during shock sorted by track position. δ F/F activity is normalized to each neuron's maximum transient. **b,** Histogram (left) and cumulative fraction plots of the percentage of neurons are activated per co-active event in CA1 and CA3. (CA1, red, n= 4252 events from 5 animals; CA3, blue, n= 2690 events from 5 animals. Wilcoxon rank-sum test, two-sideded, ***, $p < 0.001$.) **c,** Bar plot for co-activate event frequency in CA1 (left) and CA3 (right), the x-axis is each specific session. (errorbar,±SEM. One-way ANOVA, stats detail see supplementary box.

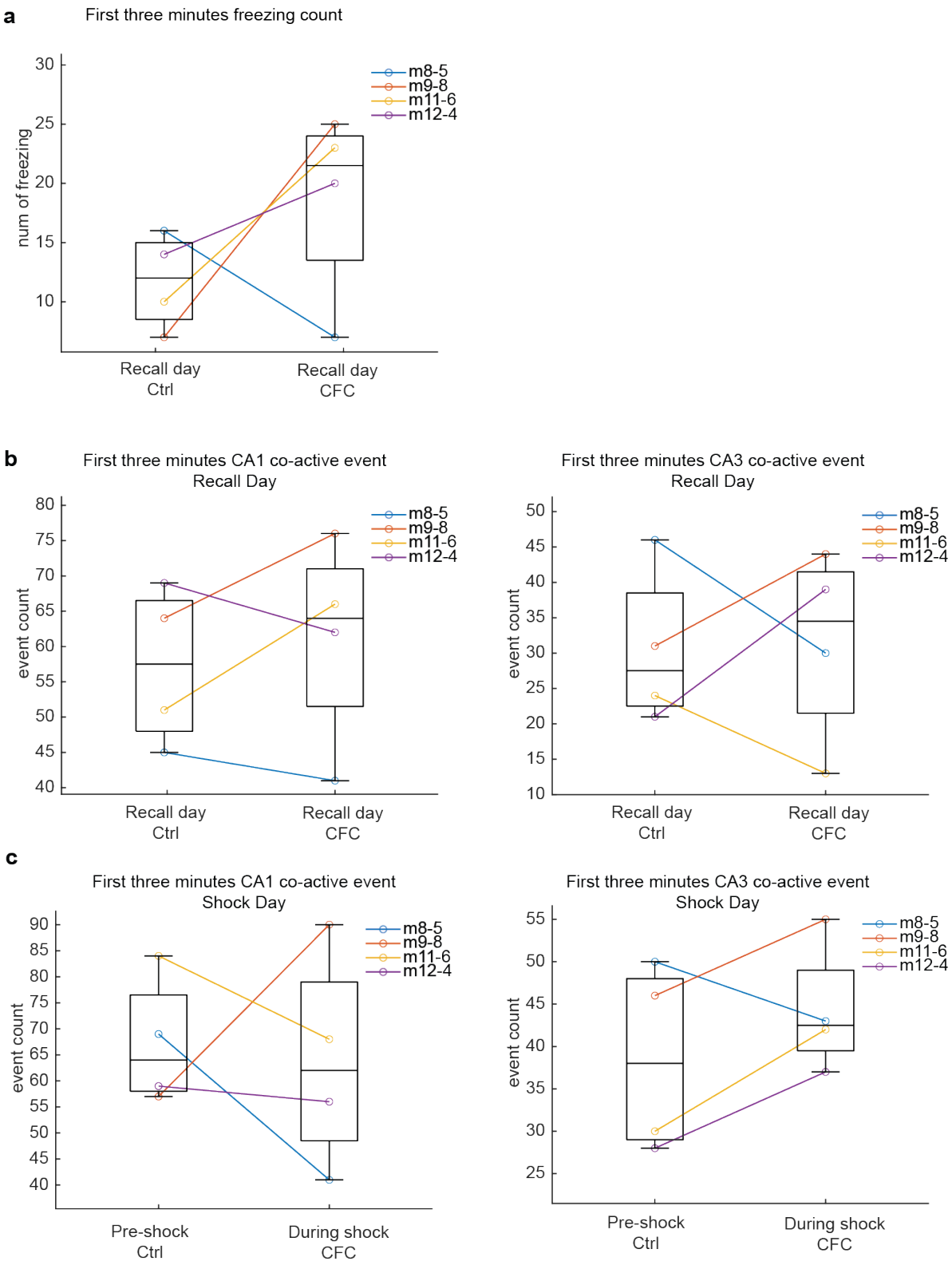

Figure 3.7: **Co-activate events in CA1 and CA3 on recall day and shock day.**

Figure 3.7, continued. a, Freezing counts during the first 3 minutes when animals navigating in Ctrl and CFC environments. (n= 4 animals, color-coded by animal ID consistent across this figure.) **b,** The number of CA1 (left) and CA3 (right) co-activate events count in the first 3 minutes in Ctrl and CFC environments on recall day. (n = 4 animals, color code same as a) **c,** Number of CA1 (left) and CA3 (right) co-activate events count in the first 3 minutes before and during shock in the CFC environment on recall day. (n = 4 animals, color code same as a)

3.6.2 Supplementary tables

Session	Session	p-value
pre-shock Ctrl	pre-schock CFC	0.0316
pre-shock Ctrl	shock	2.3664e-8
pre-shock Ctrl	recall Ctrl	0.1451
pre-shock Ctrl	recall CFC	0.9933
pre-shock CFC	shock	0.0125
pre-shock CFC	recall Ctrl	7.5037e-6
pre-shock CFC	recall CFC	0.0155
shock	recall Ctrl	7.6312e-14
shock	recall CFC	1.8899e-8
recall Ctrl	recal CFC	0.3971

Table 3.1: Multi comparison of proportion of neuron participates in the co-activation events in CA1 across different sessions

Session	Session	p-value
pre-shock Ctrl	pre-schock CFC	0.4922
pre-shock Ctrl	shock	0.0014
pre-shock Ctrl	recall Ctrl	0.0502
pre-shock Ctrl	recall CFC	0.7580
pre-shock CFC	shock	8.32144-7
pre-shock CFC	recall Ctrl	0.7279
pre-shock CFC	recall CFC	0.9975
shock	recall Ctrl	6.9411e-9
shock	recall CFC	2.123e-5
recall Ctrl	recal CFC	0.5702

Table 3.2: Multi comparison of proportion of neuron participates in the co-activation events in CA3 across different sessions

CHAPTER 4

CONCLUSION AND FUTURE DIRECTIONS

4.1 Summary of Findings

To study the role of hippocampal subnetwork CA1 and CA3 in memory formation and recall, we recorded the neural activity of these two regions independently or simultaneously during neutral or fearful contextual memory formation and retrieval. The two projects in this thesis analyzed the CA1 and CA3 network dynamics from different angles. In chapter 2, we systematically compared the neural dynamics of place cells, a sub-group of neurons in CA1 and CA3 during neutral novel environment navigation. In chapter 3, benefiting from the simultaneous CA1-CA3 recording, we study the whole CA1 and CA3 population dynamics with a contextual fear memory behavior paradigm. Here are the main findings:

Chapter 2: Distinct place cell dynamics in CA1 and CA3 encode experience in new environments

1. Novel environment exposure causes behavioral changes and global remapping in CA1 and CA3. Some PFs form after a delay in novel environments in CA1 and CA3, but instant PFs are much more prevalent in CA1. Indicating CA1 PFs rapidly respond to a novel environment.

2. In CA3 and CA1, more place fields showed backward shifting when the animals were exposed to a novel environment. CA3 PFs stabled down gradually and CA1 PFs kept shifting for a longer time.

3. Across days, CA3 place fields are highly correlated to their activities on day1, a smaller proportion of CA1 Place fields are stable across days

Chapter 3: Synchronized co-activation events across CA1 and CA3 are associated with contextual fear memory formation and recall

1. We found co-active neuron ensembles in both regions. We found a higher proportion

of CA3 neurons participated in a co-active event than in CA1 whereas CA1 had a higher frequency of co-active events than CA3.

2. Among these co-active events, we found that some were synchronized across CA1 and CA3, indicating possible functional connections between CA1 and CA3 ensembles. These synchronous CA1-CA3 events were higher in frequency during fear memory formation and recall, suggesting they play a role in the formation and recall of these memories.

4.2 Discussion and Future Directions

Mechanism of Place field formation

We observed hippocampal PFs emerged instantly in a novel environment (on the very first trial) and others that emerged after multiple trials (delayed onset PFs), consistent with previous studies (Sheffield and Dombeck 2019; Sheffield, Adoff, and Dombeck 2017; Frank, Stanley, and Brown 2004). Interestingly, the proportion of instant PFs was much lower in CA3 than in CA1. It was surprising given that CA3 is the main source of excitatory inputs to CA1 and is known to drive CA1 spatial representations in a majority of neurons, at least in familiar environments (Davoudi and Foster 2019). The simplest explanation is that CA1 instant PFs are not inherited from CA3 inputs during initial exploration. Indeed, not all CA1 place cells are necessarily driven by CA3 (Davoudi and Foster 2019) as CA1 receives other sources of spatially modulated inputs (entorhinal cortex (Latuske et al. 2018), CA2 (Mankin, Diehl, et al. 2015), non-imaged subareas of CA3 (Hunsaker, Rosenberg, and Kesner 2008), nucleus reuniens (Dolleman-van der Weel et al. 2019)), but the emergence dynamics of spatial representations in these areas are not clear. Alternatively, CA1 instant PFs could be driven by the few CA3 neurons with instant PFs if those neurons have a high degree of divergence to CA1. Low dendritic inhibition in CA1 pyramidal cells upon initial exposure to novel environments could amplify the low number of CA3 inputs (Sheffield, Adoff, and Dombeck 2017; Cohen, Bolstad, and A. K. Lee 2017; Nitz and B. McNaughton 2004). The

unstable spatial modulation could also partially contribute to CA1 instant PFs since some of them are active in early trials. To understand the underlying mechanism of PF emergence dynamics in CA1 and CA3, we could implement the recently developed due color imaging to simultaneously study multi-input on to one regions' place cells, for example, CA3 and EC axon onto CA1 neurons (Akerboom et al. 2013). We could consider using the technique in Chapter 3, to simultaneously study the place field emergence dynamics.

The mechanism of Place field development

During the process of familiarization with the novel environment, we found population-wise and single-neuron-wise shifting of place fields, dominantly to be backward shifting, indicates synaptic plasticity mechanism underlying the PF representation of familiarization. The two candidate asymmetric plasticity mechanisms are spike-timing-dependent plasticity (STDP) (Buchanan and Mellor 2010) and behavioral time-scale plasticity (BTSP) (Magee and Grienberger 2020; Bittner, Milstein, et al. 2017). It is yet clear which mechanisms are driving backward shifting in CA1 and CA3 place cells. Based on the behavior data and neural data, we are currently building a computational model that mimics the connectivity within CA1 and CA3 along with the animal running behavior to test if the STDP or BTSP could produce similar shifting dynamics in simulated neurons.

Place field dynamics during contextual fear memory formation

In chapter 3, we investigated CA1 and CA3 network dynamics by studying the co-activation events. However, given the task design, where the animals ran on a linear treadmill repeatedly, the data set we acquired will also be perfect for studying the relationship between place field dynamics and contextual fear memory. Although we briefly checked our data and were aware that not all co-activation cells are place cells, we haven't been able to determine the component of co-activation ensembles nor did we connect place field dynamics

with animal behavior. Although one study tried to connect fear memory retrieval with place field dynamics (Schuette et al. 2020), it basically studied the place field characters such as PF field size, and spatial information, without connecting with animal behavior, partially due to the animals were freely navigate the arena. A systematic study of place field dynamics during contextual fear memory formation and recall will bring new insight into the relationship between spatial representation and contextual fear memory.

Identification of co-activating ensembles in CA1 and CA3

The synchronized co-activation we discovered in Chapter 3 was associated with contextual fear conditioning and recall. We observed that when animals are more afraid of the environment on recall day they exhibited more synchronized events during the shock session and on recall day. The neuronal ensembles for the synchronized co-activation events could be the candidate of engram cells, the neurons identified by immediate early genes that could trigger fearful responses after animals undergo the contextual fear conditioning once activated. With the further development of genetics tools and optogenetics, there are two ways that we could testify to this assumption. A recent study showed that we can now label and visualize engram cells in vivo (Ghandour et al. 2019). With the current experiment setup, if we could proceed one step further to identify the engram cells in vivo, we could then determine the relationship between the engram cells and the synchronized co-activating neural ensembles. Another way to test is to selectively activate or inhibit these synchronized co-activation ensembles in a neutral context after contextual fear memory encoding. If the animals showed a fear response in the neutral environment, it indicates that these ensembles could be the engram cells.

Memory function is not only supported by hippocampal CA1 and CA3

In both projects of this thesis, we focused on studying the neural dynamics of dorsal hippocampal CA1 and CA3. Memory formation, storage and retrieval are not just dependent

on the CA1 and CA3. More brain regions, such as the ventral hippocampus, entorhinal cortex, dentate gyrus and prefrontal cortex, are shown to be critical components of the function of memory too(Jimenez et al. 2020; Sasaki, S. Leutgeb, and J. K. Leutgeb 2015; Eichenbaum 2017). How these connected brain regions work together to support memory function remains unclear. With the different methods we attempted to use in this thesis, we hope to bring some new angles to answer this ultimate question.

BIBLIOGRAPHY

Andersen, Per (1975). "Organization of hippocampal neurons and their interconnections". In: *The hippocampus*. Springer, pp. 155–175.

Scoville, William Beecher and Brenda Milner (1957). "Loss of recent memory after bilateral hippocampal lesions". In: *Journal of neurology, neurosurgery, and psychiatry* 20.1, p. 11.

O'Keefe, John and Jonathan Dostrovsky (1971). "The hippocampus as a spatial map: Preliminary evidence from unit activity in the freely-moving rat." In: *Brain research*.

O'Keefe, John and Dulcie H Conway (1978). "Hippocampal place units in the freely moving rat: why they fire where they fire". In: *Experimental brain research* 31.4, pp. 573–590.

O'keefe, John and Lynn Nadel (1979). "Précis of O'Keefe & Nadel's The hippocampus as a cognitive map". In: *Behavioral and Brain Sciences* 2.4, pp. 487–494.

Wood, Emma R, Paul A Dudchenko, and Howard Eichenbaum (1999). "The global record of memory in hippocampal neuronal activity". In: *Nature* 397.6720, pp. 613–616.

Sakurai, Y (2002). "Coding of auditory temporal and pitch information by hippocampal individual cells and cell assemblies in the rat". In: *Neuroscience* 115.4, pp. 1153–1163.

Eichenbaum, Howard (2014). "Time cells in the hippocampus: a new dimension for mapping memories". In: *Nature Reviews Neuroscience* 15.11, pp. 732–744.

Gauthier, Jeffrey L and David W Tank (2018). "A dedicated population for reward coding in the hippocampus". In: *Neuron* 99.1, pp. 179–193.

Knudsen, Eric B and Joni D Wallis (2021). "Hippocampal neurons construct a map of an abstract value space". In: *Cell* 184.18, pp. 4640–4650.

Sheffield, Mark EJ, Michael D Adoff, and Daniel A Dombeck (2017). "Increased prevalence of calcium transients across the dendritic arbor during place field formation". In: *Neuron* 96.2, pp. 490–504.

Dong, Can, Antoine D Madar, and Mark EJ Sheffield (2021). "Distinct place cell dynamics in CA1 and CA3 encode experience in new environments". In: *Nature communications* 12.1, pp. 1–13.

Ziv, Yaniv, Laurie D Burns, Eric D Cocker, Elizabeth O Hamel, Kunal K Ghosh, Lacey J Kitch, Abbas El Gamal, and Mark J Schnitzer (2013). "Long-term dynamics of CA1 hippocampal place codes". In: *Nature neuroscience* 16.3, pp. 264–266.

Rubin, Alon, Nitzan Geva, Liron Sheintuch, and Yaniv Ziv (2015). "Hippocampal ensemble dynamics timestamp events in long-term memory". In: *elife* 4, e12247.

Dupret, David, Joseph O'neill, Barty Pleydell-Bouverie, and Jozsef Csicsvari (2010). "The reorganization and reactivation of hippocampal maps predict spatial memory performance". In: *Nature neuroscience* 13.8, pp. 995–1002.

Robinson, Nick TM, Lucie AL Descamps, Lloyd E Russell, Moritz O Buchholz, Brendan A Bicknell, Georgy K Antonov, Joanna YN Lau, Rebecca Nutbrown, Christoph Schmidt-Hieber, and Michael Häusser (2020). "Targeted activation of hippocampal place cells drives memory-guided spatial behavior". In: *Cell* 183.6, pp. 1586–1599.

Pavlides, Constantine and Jonathan Winson (1989). "Influences of hippocampal place cell firing in the awake state on the activity of these cells during subsequent sleep episodes". In: *Journal of neuroscience* 9.8, pp. 2907–2918.

Wilson, Matthew A and Bruce L McNaughton (1994). "Reactivation of hippocampal ensemble memories during sleep". In: *Science* 265.5172, pp. 676–679.

Foster, David J and Matthew A Wilson (2006). "Reverse replay of behavioural sequences in hippocampal place cells during the awake state". In: *Nature* 440.7084, pp. 680–683.

Ólafsdóttir, H Freyja, Daniel Bush, and Caswell Barry (2018). "The role of hippocampal replay in memory and planning". In: *Current Biology* 28.1, R37–R50.

Pfeiffer, Brad E and David J Foster (2015). "Autoassociative dynamics in the generation of sequences of hippocampal place cells". In: *Science* 349.6244, pp. 180–183.

Squire, LR, L Genzel, JT Wixted, and RG Morris (2015). *Memory consolidation. Cold Spring Harb Perspect Biol 7 (8): a021766.*

Liu, Xu, Steve Ramirez, Petti T Pang, Corey B Puryear, Arvind Govindarajan, Karl Deisseroth, and Susumu Tonegawa (2012). "Optogenetic stimulation of a hippocampal engram activates fear memory recall". In: *Nature* 484.7394, pp. 381–385.

Ramirez, Steve, Xu Liu, Pei-Ann Lin, Junghyup Suh, Michele Pignatelli, Roger L Redondo, Tomás J Ryan, and Susumu Tonegawa (2013). "Creating a false memory in the hippocampus". In: *Science* 341.6144, pp. 387–391.

Tonegawa, Susumu, Xu Liu, Steve Ramirez, and Roger Redondo (2015). "Memory engram cells have come of age". In: *Neuron* 87.5, pp. 918–931.

Tanaka, Kazumasa Z, Hongshen He, Anupratap Tomar, Kazue Niisato, Arthur JY Huang, and Thomas J McHugh (2018). "The hippocampal engram maps experience but not place". In: *Science* 361.6400, pp. 392–397.

Ghandour, Khaled, Noriaki Ohkawa, Chi Chung Alan Fung, Hirotaka Asai, Yoshito Saitoh, Takashi Takekawa, Reiko Okubo-Suzuki, Shingo Soya, Hirofumi Nishizono, Mina Matsuo, et al. (2019). "Orchestrated ensemble activities constitute a hippocampal memory engram". In: *Nature communications* 10.1, pp. 1–14.

Allen, Timothy A and Norbert J Fortin (2013). "The evolution of episodic memory". In: *Proceedings of the National Academy of Sciences* 110.supplement_2, pp. 10379–10386.

Van Strien, NM, NLM Cappaert, and MP Witter (2009). "The anatomy of memory: an interactive overview of the parahippocampal–hippocampal network". In: *Nature reviews neuroscience* 10.4, pp. 272–282.

Tao, Sijue, Yihang Wang, Jundan Peng, Yang Zhao, Xiaobin He, Xuefeng Yu, Qing Liu, Sen Jin, and Fuqiang Xu (2021a). "Whole-brain mapping the direct inputs of dorsal and ventral CA1 projection neurons". In: *Frontiers in neural circuits* 15, p. 643230.

Strange, Bryan A, Menno P Witter, Ed S Lein, and Edvard I Moser (2014). "Functional organization of the hippocampal longitudinal axis". In: *Nature Reviews Neuroscience* 15.10, pp. 655–669.

Rolls, Edmund T (2018). "The storage and recall of memories in the hippocampo-cortical system". In: *Cell and tissue research* 373.3, pp. 577–604.

Teyler, Timothy J and Jerry W Rudy (2007). "The hippocampal indexing theory and episodic memory: updating the index". In: *Hippocampus* 17.12, pp. 1158–1169.

McHugh, Thomas J, Matthew W Jones, Jennifer J Quinn, Nina Balthasar, Roberto Coppari, Joel K Elmquist, Bradford B Lowell, Michael S Fanselow, Matthew A Wilson, and Susumu Tonegawa (2007). "Dentate gyrus NMDA receptors mediate rapid pattern separation in the hippocampal network". In: *Science* 317.5834, pp. 94–99.

Hainmueller, Thomas and Marlene Bartos (2020). "Dentate gyrus circuits for encoding, retrieval and discrimination of episodic memories". In: *Nature Reviews Neuroscience* 21.3, pp. 153–168.

Kesner, Raymond P and Edmund T Rolls (2015). "A computational theory of hippocampal function, and tests of the theory: new developments". In: *Neuroscience & Biobehavioral Reviews* 48, pp. 92–147.

Cayco-Gajic, N Alex and R Angus Silver (2019). "Re-evaluating circuit mechanisms underlying pattern separation". In: *Neuron* 101.4, pp. 584–602.

Goode, Travis D, Kazumasa Z Tanaka, Amar Sahay, and Thomas J McHugh (2020). "An integrated index: engrams, place cells, and hippocampal memory". In: *Neuron* 107.5, pp. 805–820.

Soltesz, Ivan and Attila Losonczy (2018). "CA1 pyramidal cell diversity enabling parallel information processing in the hippocampus". In: *Nature neuroscience* 21.4, pp. 484–493.

Li, X-G, P Somogyi, A Ylinen, and G Buzsáki (1994). "The hippocampal CA3 network: an in vivo intracellular labeling study". In: *Journal of comparative neurology* 339.2, pp. 181–208.

Guzman, Segundo Jose, Alois Schlögl, Michael Frotscher, and Peter Jonas (2016). "Synaptic mechanisms of pattern completion in the hippocampal CA3 network". In: *Science* 353.6304, pp. 1117–1123.

Rolls, Edmund T (2010). "A computational theory of episodic memory formation in the hippocampus". In: *Behavioural brain research* 215.2, pp. 180–196.

Treves, Alessandro, Ayumu Tashiro, Menno P Witter, and Edvard I Moser (2008). "What is the mammalian dentate gyrus good for?" In: *Neuroscience* 154.4, pp. 1155–1172.

Jackson, Meyer B (2013). "Recall of spatial patterns stored in a hippocampal slice by long-term potentiation". In: *Journal of neurophysiology* 110.11, pp. 2511–2519.

Lisman, John E and Anthony A Grace (2005). "The hippocampal-VTA loop: controlling the entry of information into long-term memory". In: *Neuron* 46.5, pp. 703–713.

Breton-Provencher, Vincent, Gabrielle T Drummond, and Mriganka Sur (2021). "Locus coeruleus norepinephrine in learned behavior: anatomical modularity and spatiotemporal integration in targets". In: *Frontiers in Neural Circuits*, p. 46.

Eichenbaum, Howard (2017). "Prefrontal–hippocampal interactions in episodic memory". In: *Nature Reviews Neuroscience* 18.9, pp. 547–558.

Jay, Thérèse M, Jacques Glowinski, and Anne-Marie Thierry (1989). "Selectivity of the hippocampal projection to the prelimbic area of the prefrontal cortex in the rat". In: *Brain research* 505.2, pp. 337–340.

Hoover, Walter B and Robert P Vertes (2007). "Anatomical analysis of afferent projections to the medial prefrontal cortex in the rat". In: *Brain Structure and Function* 212.2, pp. 149–179.

Hallock, Henry L, Arick Wang, and Amy L Griffin (2016). "Ventral midline thalamus is critical for hippocampal–prefrontal synchrony and spatial working memory". In: *Journal of Neuroscience* 36.32, pp. 8372–8389.

Place, Ryan, Anja Farovik, Marco Brockmann, and Howard Eichenbaum (2016). "Bidirectional prefrontal-hippocampal interactions support context-guided memory". In: *Nature neuroscience* 19.8, pp. 992–994.

Navawongse, Rapeechai and Howard Eichenbaum (2013). "Distinct pathways for rule-based retrieval and spatial mapping of memory representations in hippocampal neurons". In: *Journal of Neuroscience* 33.3, pp. 1002–1013.

Cheng, Sen (2013). "The CRISP theory of hippocampal function in episodic memory". In: *Frontiers in neural circuits* 7, p. 88.

Yau, Suk-yu, Ang Li, and Kwok-Fai So (2015). "Involvement of adult hippocampal neurogenesis in learning and forgetting." In: *Neural plasticity*.

Keller, Daniel, Csaba Erö, and Henry Markram (2018). "Cell densities in the mouse brain: a systematic review". In: *Frontiers in neuroanatomy* 12, p. 83.

Witter, Menno P (2007). "Intrinsic and extrinsic wiring of CA3: indications for connectional heterogeneity". In: *Learning & memory* 14.11, pp. 705–713.

Behabadi, Bardia F and Bartlett W Mel (2014). "Mechanisms underlying subunit independence in pyramidal neuron dendrites". In: *Proceedings of the National Academy of Sciences* 111.1, pp. 498–503.

Sheffield, Mark EJ and Daniel A Dombeck (2015). "Calcium transient prevalence across the dendritic arbour predicts place field properties". In: *Nature* 517.7533, pp. 200–204.

Lee, Inah, Geeta Rao, and James J Knierim (2004). "A double dissociation between hippocampal subfields: differential time course of CA3 and CA1 place cells for processing changed environments". In: *Neuron* 42.5, pp. 803–815.

Mehta, Mayank R, Michael C Quirk, and Matthew A Wilson (2000). "Experience-dependent asymmetric shape of hippocampal receptive fields". In: *Neuron* 25.3, pp. 707–715.

Buchanan, Katherine and Jack Mellor (2010). "The activity requirements for spike timing-dependent plasticity in the hippocampus". In: *Frontiers in synaptic neuroscience*, p. 11.

Bittner, Katie C, Aaron D Milstein, Christine Grienberger, Sandro Romani, and Jeffrey C Magee (2017). "Behavioral time scale synaptic plasticity underlies CA1 place fields". In: *Science* 357.6355, pp. 1033–1036.

Foster, David J (2017). "Replay comes of age". In: *Annu. Rev. Neurosci* 40.581-602, p. 9.

Hainmueller, Thomas and Marlene Bartos (2018). "Parallel emergence of stable and dynamic memory engrams in the hippocampus". In: *Nature* 558.7709, pp. 292–296.

Leutgeb, Stefan, Jill K Leutgeb, Alessandro Treves, May-Britt Moser, and Edvard I Moser (2004). "Distinct ensemble codes in hippocampal areas CA3 and CA1". In: *Science* 305.5688, pp. 1295–1298.

Parisi, German I, Ronald Kemker, Jose L Part, Christopher Kanan, and Stefan Wermter (2019). "Continual lifelong learning with neural networks: A review". In: *Neural Networks* 113, pp. 54–71.

Kitamura, Takashi, Sachie K Ogawa, Dheeraj S Roy, Teruhiro Okuyama, Mark D Morrissey, Lillian M Smith, Roger L Redondo, and Susumu Tonegawa (2017). "Engrams and circuits crucial for systems consolidation of a memory". In: *Science* 356.6333, pp. 73–78.

Latuske, Patrick, Olga Kornienko, Laura Kohler, and Kevin Allen (2018). "Hippocampal remapping and its entorhinal origin". In: *Frontiers in behavioral neuroscience* 11, p. 253.

Knierim, James J and Kechen Zhang (2012). "Attractor dynamics of spatially correlated neural activity in the limbic system". In: *Annual review of neuroscience* 35, p. 267.

Jeffery, Kathryn J (2011). "Place cells, grid cells, attractors, and remapping". In: *Neural plasticity* 2011.

Solstad, Trygve, Edvard I Moser, and Gaute T Einevoll (2006). "From grid cells to place cells: a mathematical model". In: *Hippocampus* 16.12, pp. 1026–1031.

Neher, Torsten, Amir Hossein Azizi, and Sen Cheng (2017). "From grid cells to place cells with realistic field sizes". In: *PLoS One* 12.7, e0181618.

Mankin, Emily A, Geoffrey W Diehl, Fraser T Sparks, Stefan Leutgeb, and Jill K Leutgeb (2015). "Hippocampal CA2 activity patterns change over time to a larger extent than between spatial contexts". In: *Neuron* 85.1, pp. 190–201.

Magee, Jeffrey C and Christine Grienberger (2020). "Synaptic plasticity forms and functions". In: *Annual review of neuroscience* 43, pp. 95–117.

Sheffield, Mark EJ and Daniel A Dombeck (2019). "Dendritic mechanisms of hippocampal place field formation". In: *Current opinion in neurobiology* 54, pp. 1–11.

Pedrosa, Victor and Claudia Clopath (2020). "The interplay between somatic and dendritic inhibition promotes the emergence and stabilization of place fields". In: *PLoS computational biology* 16.7, e1007955.

Freund, Tamas F and György Buzsáki (1996). "Interneurons of the hippocampus". In: *Hippocampus* 6.4, pp. 347–470.

Kentros, Clifford (2006). "Hippocampal place cells: the "where" of episodic memory?" In: *Hippocampus* 16.9, pp. 743–754.

Kentros, Clifford G, Naveen T Agnihotri, Samantha Streater, Robert D Hawkins, and Eric R Kandel (2004). "Increased attention to spatial context increases both place field stability and spatial memory". In: *Neuron* 42.2, pp. 283–295.

Frank, Loren M, Garrett B Stanley, and Emery N Brown (2004). "Hippocampal plasticity across multiple days of exposure to novel environments". In: *Journal of Neuroscience* 24.35, pp. 7681–7689.

Cohen, Jeremy D, Mark Bolstad, and Albert K Lee (2017). "Experience-dependent shaping of hippocampal CA1 intracellular activity in novel and familiar environments". In: *Elife* 6, e23040.

Epsztein, Jérôme, Michael Brecht, and Albert K Lee (2011). "Intracellular determinants of hippocampal CA1 place and silent cell activity in a novel environment". In: *Neuron* 70.1, pp. 109–120.

Geiller, Tristan, Mohammad Fattahi, June-Seek Choi, and Sébastien Royer (2017). "Place cells are more strongly tied to landmarks in deep than in superficial CA1". In: *Nature communications* 8.1, pp. 1–11.

Roth, Eric D, Xintian Yu, Geeta Rao, and James J Knierim (2012). "Functional differences in the backward shifts of CA1 and CA3 place fields in novel and familiar environments". In: *PloS one* 7.4, e36035.

Ekstrom, AD, J Meltzer, BL McNaughton, and CA Barnes (2001). "NMDA receptor antagonism blocks experience-dependent expansion of hippocampal "place fields"". In: *Neuron* 31.4, pp. 631–638.

Reijmers, Leon G, Brian L Perkins, Naoki Matsuo, and Mark Mayford (2007). "Localization of a stable neural correlate of associative memory". In: *Science* 317.5842, pp. 1230–1233.

Kinsky, Nathaniel R, David W Sullivan, William Mau, Michael E Hasselmo, and Howard B Eichenbaum (2018). "Hippocampal place fields maintain a coherent and flexible map across long timescales". In: *Current Biology* 28.22, pp. 3578–3588.

Jeantet, Yannick and Yoon H Cho (2012). "Evolution of hippocampal spatial representation over time in mice". In: *Neurobiology of learning and memory* 98.4, pp. 354–360.

Mankin, Emily A, Fraser T Sparks, Begum Slayyeh, Robert J Sutherland, Stefan Leutgeb, and Jill K Leutgeb (2012). "Neuronal code for extended time in the hippocampus". In: *Proceedings of the National Academy of Sciences* 109.47, pp. 19462–19467.

Nakazawa, Kazu, Michael C Quirk, Raymond A Chitwood, Masahiko Watanabe, Mark F Yeckel, Linus D Sun, Akira Kato, Candice A Carr, Daniel Johnston, Matthew A Wilson, et al. (2002). "Requirement for hippocampal CA3 NMDA receptors in associative memory recall". In: *science* 297.5579, pp. 211–218.

Colgin, Laura Lee, Edvard I Moser, and May-Britt Moser (2008). "Understanding memory through hippocampal remapping". In: *Trends in neurosciences* 31.9, pp. 469–477.

Muller, Robert U and John L Kubie (1987). "The effects of changes in the environment on the spatial firing of hippocampal complex-spike cells". In: *Journal of Neuroscience* 7.7, pp. 1951–1968.

Bostock, Elizabeth, Robert U Muller, and John L Kubie (1991). "Experience-dependent modifications of hippocampal place cell firing". In: *Hippocampus* 1.2, pp. 193–205.

Fyhn, Marianne, Torkel Hafting, Alessandro Treves, May-Britt Moser, and Edvard I Moser (2007). "Hippocampal remapping and grid realignment in entorhinal cortex". In: *Nature* 446.7132, pp. 190–194.

Mehta, Mayank R, Carol A Barnes, and Bruce L McNaughton (1997). "Experience-dependent, asymmetric expansion of hippocampal place fields". In: *Proceedings of the National Academy of Sciences* 94.16, pp. 8918–8921.

Dombeck, Daniel A, Christopher D Harvey, Lin Tian, Loren L Looger, and David W Tank (2010). "Functional imaging of hippocampal place cells at cellular resolution during virtual navigation". In: *Nature neuroscience* 13.11, pp. 1433–1440.

McNamara, Colin G, Álvaro Tejero-Cantero, Stéphanie Trouche, Natalia Campo-Urriza, and David Dupret (2014). "Dopaminergic neurons promote hippocampal reactivation and spatial memory persistence". In: *Nature neuroscience* 17.12, pp. 1658–1660.

Davoudi, Heydar and David J Foster (2019). "Acute silencing of hippocampal CA3 reveals a dominant role in place field responses". In: *Nature neuroscience* 22.3, pp. 337–342.

Hunsaker, Michael R, Jenna S Rosenberg, and Raymond P Kesner (2008). "The role of the dentate gyrus, CA3a, b, and CA3c for detecting spatial and environmental novelty". In: *Hippocampus* 18.10, pp. 1064–1073.

Dolleman-van der Weel, Margriet J, Amy L Griffin, Hiroshi T Ito, Matthew L Shapiro, Menno P Witter, Robert P Vertes, and Timothy A Allen (2019). "The nucleus reuniens of the thalamus sits at the nexus of a hippocampus and medial prefrontal cortex circuit enabling memory and behavior". In: *Learning & Memory* 26.7, pp. 191–205.

Nitz, Douglas and Bruce McNaughton (2004). "Differential modulation of CA1 and dentate gyrus interneurons during exploration of novel environments". In: *Journal of neurophysiology* 91.2, pp. 863–872.

Yu, X, James J Knierim, I Lee, and Harel Z Shouval (2006). "Simulating place field dynamics using spike timing-dependent plasticity". In: *Neurocomputing* 69.10-12, pp. 1253–1259.

Lisman, John and Nelson Spruston (2010). "Questions about STDP as a general model of synaptic plasticity". In: *Frontiers in synaptic neuroscience* 2, p. 140.

Graupner, Michael, Pascal Wallisch, and Srdjan Ostojic (2016). "Natural firing patterns imply low sensitivity of synaptic plasticity to spike timing compared with firing rate". In: *Journal of Neuroscience* 36.44, pp. 11238–11258.

Bittner, Katie C, Christine Grienberger, Sachin P Vaidya, Aaron D Milstein, John J Macklin, Junghyup Suh, Susumu Tonegawa, and Jeffrey C Magee (2015). "Conjunctive input processing drives feature selectivity in hippocampal CA1 neurons". In: *Nature neuroscience* 18.8, pp. 1133–1142.

Fattahi, Mohammad, Farnaz Sharif, Tristan Geiller, and Sébastien Royer (2018). "Differential representation of landmark and self-motion information along the CA1 radial axis: self-motion generated place fields shift toward landmarks during septal inactivation". In: *Journal of Neuroscience* 38.30, pp. 6766–6778.

Thompson, LT and PJ Best (1990). "Long-term stability of the place-field activity of single units recorded from the dorsal hippocampus of freely behaving rats". In: *Brain research* 509.2, pp. 299–308.

Wood, Emma R, Paul A Dudchenko, R Jonathan Robitsek, and Howard Eichenbaum (2000). "Hippocampal neurons encode information about different types of memory episodes occurring in the same location". In: *Neuron* 27.3, pp. 623–633.

Krishnan, Seetha, Chery Cherian, and Mark EJ Sheffield (2020). "Changing reward expectation transforms spatial encoding and retrieval in the hippocampus". In: *bioRxiv*.

Anderson, Michael I and Kathryn J Jeffery (2003). "Heterogeneous modulation of place cell firing by changes in context". In: *Journal of Neuroscience* 23.26, pp. 8827–8835.

Hasselmo, Michael E and Howard Eichenbaum (2005). "Hippocampal mechanisms for the context-dependent retrieval of episodes". In: *Neural networks* 18.9, pp. 1172–1190.

Cai, Denise J, Daniel Aharoni, Tristan Shuman, Justin Shobe, Jeremy Biane, Weilin Song, Brandon Wei, Michael Veshkini, Mimi La-Vu, Jerry Lou, et al. (2016). "A shared neural ensemble links distinct contextual memories encoded close in time". In: *Nature* 534.7605, pp. 115–118.

Allegra, Manuela, Lorenzo Posani, Ruy Gómez-Ocádiz, and Christoph Schmidt-Hieber (2020). "Differential relation between neuronal and behavioral discrimination during hippocampal memory encoding". In: *Neuron* 108.6, pp. 1103–1112.

Madar, Antoine David (2018). *Pattern separation in the hippocampus, in health and epilepsy*. The University of Wisconsin-Madison.

Bourboulou, Romain, Geoffrey Marti, François-Xavier Michon, Elissa El Feghaly, Morgane Nouguier, David Robbe, Julie Koenig, and Jerome Epsztein (2019). "Dynamic control of hippocampal spatial coding resolution by local visual cues". In: *Elife* 8, e44487.

Lee, Sang Wan, John P O'Doherty, and Shinsuke Shimojo (2015). "Neural computations mediating one-shot learning in the human brain". In: *PLoS biology* 13.4, e1002137.

Stachenfeld, Kimberly L, Matthew M Botvinick, and Samuel J Gershman (2017). "The hippocampus as a predictive map". In: *Nature neuroscience* 20.11, pp. 1643–1653.

Abbott, Laurence F and Kenneth I Blum (1996). "Functional significance of long-term potentiation for sequence learning and prediction". In: *Cerebral cortex* 6.3, pp. 406–416.

Clewett, David, Sarah DuBrow, and Lila Davachi (2019). "Transcending time in the brain: How event memories are constructed from experience". In: *Hippocampus* 29.3, pp. 162–183.

Aronov, Dmitriy, Rhino Nevers, and David W Tank (2017). "Mapping of a non-spatial dimension by the hippocampal–entorhinal circuit". In: *Nature* 543.7647, pp. 719–722.

Mukamel, Eran A, Axel Nimmerjahn, and Mark J Schnitzer (2009). "Automated analysis of cellular signals from large-scale calcium imaging data". In: *Neuron* 63.6, pp. 747–760.

Tampuu, Ardi, Tambet Matiisen, H Freyja Ólafsdóttir, Caswell Barry, and Raul Vicente (2019). "Efficient neural decoding of self-location with a deep recurrent network". In: *PLoS computational biology* 15.2, e1006822.

Ho, Joses, Tayfun Tumkaya, Sameer Aryal, Hyungwon Choi, and Adam Claridge-Chang (2019). "Moving beyond P values: data analysis with estimation graphics". In: *Nature methods* 16.7, pp. 565–566.

Pause, Bettina M, Armin Zlomuzica, Kiyoka Kinugawa, Jean Mariani, Reinhard Pietrowsky, and Ekrem Dere (2013). "Perspectives on episodic-like and episodic memory". In: *Frontiers in Behavioral Neuroscience* 7, p. 33.

Josselyn, Sheena A, Stefan Köhler, and Paul W Frankland (2015). "Finding the engram". In: *Nature Reviews Neuroscience* 16.9, pp. 521–534.

MacDonald, Christopher J, Kyle Q Lepage, Uri T Eden, and Howard Eichenbaum (2011). "Hippocampal "time cells" bridge the gap in memory for discontiguous events". In: *Neuron* 71.4, pp. 737–749.

Buhry, Laure, Amir H Azizi, and Sen Cheng (2011). "Reactivation, replay, and preplay: how it might all fit together". In: *Neural plasticity* 2011.

Skaggs, William E and Bruce L McNaughton (1996). "Replay of neuronal firing sequences in rat hippocampus during sleep following spatial experience". In: *Science* 271.5257, pp. 1870–1873.

Wu, Chun-Ting, Daniel Haggerty, Caleb Kemere, and Daoyun Ji (2017). "Hippocampal awake replay in fear memory retrieval". In: *Nature neuroscience* 20.4, pp. 571–580.

Förster, Eckart, Shanting Zhao, and Michael Frotscher (2006). "Laminating the hippocampus". In: *Nature reviews neuroscience* 7.4, pp. 259–268.

Malvache, Arnaud, Susanne Reichinnek, Vincent Villette, Caroline Haimerl, and Rosa Cossart (2016). "Awake hippocampal reactivations project onto orthogonal neuronal assemblies". In: *Science* 353.6305, pp. 1280–1283.

Liu, Yu-Zhang, Yao Wang, Weida Shen, and Zhiru Wang (2017). "Enhancement of synchronized activity between hippocampal CA1 neurons during initial storage of associative fear memory". In: *The Journal of Physiology* 595.15, pp. 5327–5340.

Rajasethupathy, Priyamvada, Sethuraman Sankaran, James H Marshel, Christina K Kim, Emily Ferenczi, Soo Yeun Lee, Andre Berndt, Charu Ramakrishnan, Anna Jaffe, Maisie Lo, et al. (2015). "Projections from neocortex mediate top-down control of memory retrieval". In: *Nature* 526.7575, pp. 653–659.

Heys, James G, Krsna V Rangarajan, and Daniel A Dombeck (2014). "The functional micro-organization of grid cells revealed by cellular-resolution imaging". In: *Neuron* 84.5, pp. 1079–1090.

Aronov, Dmitriy and David W Tank (2014). "Engagement of neural circuits underlying 2D spatial navigation in a rodent virtual reality system". In: *Neuron* 84.2, pp. 442–456.

Pachitariu, Marius, Carsen Stringer, Mario Dipoppa, Sylvia Schröder, L Federico Rossi, Henry Dalgleish, Matteo Carandini, and Kenneth D Harris (2017). "Suite2p: beyond 10,000 neurons with standard two-photon microscopy". In: *BioRxiv*, p. 061507.

Lovett-Barron, Matthew, Patrick Kaifosh, Mazen A Kheirbek, Nathan Danielson, Jeffrey D Zaremba, Thomas R Reardon, Gergely F Turi, René Hen, Boris V Zemelman, and Attila Losonczy (2014). "Dendritic inhibition in the hippocampus supports fear learning". In: *Science* 343.6173, pp. 857–863.

Chaaya, Nicholas, Angela Jacques, Arnauld Belmer, DJ Richard, SE Bartlett, AR Battle, and LR Johnson (2019). "Localization of contextual and context removed auditory fear memory within the basolateral amygdala complex". In: *Neuroscience* 398, pp. 231–251.

Jimenez, Jessica C, Jack E Berry, Sean C Lim, Samantha K Ong, Mazen A Kheirbek, and Rene Hen (2020). "Contextual fear memory retrieval by correlated ensembles of ventral CA1 neurons". In: *Nature communications* 11.1, pp. 1–11.

Attili, Sarojini M, Marcos FM Silva, Thuy-vi Nguyen, and Giorgio A Ascoli (2019). "Cell numbers, distribution, shape, and regional variation throughout the murine hippocampal formation from the adult brain Allen Reference Atlas". In: *Brain Structure and Function* 224.8, pp. 2883–2897.

Redman, William T, Nora S Wolcott, Luca Montelisciani, Gabriel Luna, Tyler D Marks, Kevin K Sit, Che-Hang Yu, Spencer Smith, and Michael J Goard (2022). "Long-term transverse imaging of the hippocampus with glass microperiscopes". In: *Elife* 11, e75391.

Sweis, Brian M, William Mau, Sima Rabinowitz, and Denise J Cai (2021). "Dynamic and heterogeneous neural ensembles contribute to a memory engram". In: *Current Opinion in Neurobiology* 67, pp. 199–206.

Gillespie, Anna K, Daniela A Astudillo Maya, Eric L Denovellis, Daniel F Liu, David B Kastner, Michael E Coulter, Demetris K Roumis, Uri T Eden, and Loren M Frank (2021). "Hippocampal replay reflects specific past experiences rather than a plan for subsequent choice". In: *Neuron* 109.19, pp. 3149–3163.

Mizuseki, Kenji, Sebastien Royer, Kamran Diba, and György Buzsáki (2012). "Activity dynamics and behavioral correlates of CA3 and CA1 hippocampal pyramidal neurons". In: *Hippocampus* 22.8, pp. 1659–1680.

Le Duigou, Caroline, Jean Simonnet, Maria T Teleñczuk, Desdemona Fricker, and Richard Miles (2014). "Recurrent synapses and circuits in the CA3 region of the hippocampus: an associative network". In: *Frontiers in cellular neuroscience* 7, p. 262.

Hwaun, Ernie and Laura Lee Colgin (2019). "CA3 place cells that represent a novel waking experience are preferentially reactivated during sharp wave-ripples in subsequent sleep". In: *Hippocampus* 29.10, pp. 921–938.

Nakashiba, Toshiaki, Derek L Buhl, Thomas J McHugh, and Susumu Tonegawa (2009). "Hippocampal CA3 output is crucial for ripple-associated reactivation and consolidation of memory". In: *Neuron* 62.6, pp. 781–787.

Leutgeb, Stefan and Jill K Leutgeb (2007). "Pattern separation, pattern completion, and new neuronal codes within a continuous CA3 map". In: *Learning & memory* 14.11, pp. 745–757.

Panzeri, Stefano, Edmund T Rolls, Francesco Battaglia, and Ruth Lavis (2001). "Speed of feedforward and recurrent processing in multilayer networks of integrate-and-fire neurons". In: *Network: Computation in Neural Systems* 12.4, pp. 423–440.

Magee, Jeffrey C and Daniel Johnston (1997). "A synaptically controlled, associative signal for Hebbian plasticity in hippocampal neurons". In: *Science* 275.5297, pp. 209–213.

Martin, SP, Paul D Grimwood, Richard GM Morris, et al. (2000). "Synaptic plasticity and memory: an evaluation of the hypothesis". In: *Annual review of neuroscience* 23.1, pp. 649–711.

Kandel, Eric R, James H Schwartz, Thomas M Jessell, Steven Siegelbaum, A James Hudspeth, Sarah Mack, et al. (2000). *Principles of neural science*. Vol. 4. McGraw-hill New York.

Bliss, Tim VP and Graham L Collingridge (1993). "A synaptic model of memory: long-term potentiation in the hippocampus". In: *Nature* 361.6407, pp. 31–39.

Ecker, András, Bence Bagi, Eszter Vértes, Orsolya Steinbach-Németh, Mária R Karlócai, Orsolya I Papp, István Miklós, Norbert Hájos, Tamás F Freund, Attila I Gulyás, et al. (2022). "Hippocampal sharp wave-ripples and the associated sequence replay emerge from structured synaptic interactions in a network model of area CA3". In: *Elife* 11, e71850.

Girardeau, Gabrielle, Anne Cei, and Michaël Zugaro (2014). "Learning-induced plasticity regulates hippocampal sharp wave-ripple drive". In: *Journal of Neuroscience* 34.15, pp. 5176–5183.

Dragoi, George and Susumu Tonegawa (2011). "Preplay of future place cell sequences by hippocampal cellular assemblies". In: *Nature* 469.7330, pp. 397–401.

Buzsáki, György (2015). "Hippocampal sharp wave-ripple: A cognitive biomarker for episodic memory and planning". In: *Hippocampus* 25.10, pp. 1073–1188.

Meshulam, Leenoy, Jeffrey L Gauthier, Carlos D Brody, David W Tank, and William Bialek (2017). "Collective behavior of place and non-place neurons in the hippocampal network". In: *Neuron* 96.5, pp. 1178–1191.

Akerboom, Jasper, Nicole Carreras Calderón, Lin Tian, Sebastian Wabnig, Matthias Prigge, Johan Tolö, Andrew Gordus, Michael B Orger, Kristen E Severi, John J Macklin, et al. (2013). "Genetically encoded calcium indicators for multi-color neural activity imaging and combination with optogenetics". In: *Frontiers in molecular neuroscience* 6, p. 2.

Schuette, Peter J, Fernando MCV Reis, Sandra Maesta-Pereira, Meghmik Chakerian, Anita Torossian, Garrett J Blair, Weisheng Wang, Hugh T Blair, Michael S Fanselow, Jonathan C Kao, et al. (2020). "Long-term characterization of hippocampal remapping during contextual fear acquisition and extinction". In: *Journal of Neuroscience* 40.43, pp. 8329–8342.

Sasaki, Takuya, Stefan Leutgeb, and Jill K Leutgeb (2015). "Spatial and memory circuits in the medial entorhinal cortex". In: *Current opinion in neurobiology* 32, pp. 16–23.

Cholvin, Thibault, Thomas Hainmueller, and Marlene Bartos (2021). "The hippocampus converts dynamic entorhinal inputs into stable spatial maps". In: *Neuron* 109.19, pp. 3135–3148.

Tao, Sijue, Yihang Wang, Jundan Peng, Yang Zhao, Xiaobin He, Xuefeng Yu, Qing Liu, Sen Jin, and Fuqiang Xu (2021b). "Whole-brain mapping the direct inputs of dorsal and ventral CA1 projection neurons". In: *Frontiers in neural circuits* 15, p. 643230.

Cheng, Sen and Loren M Frank (2008). "New experiences enhance coordinated neural activity in the hippocampus". In: *Neuron* 57.2, pp. 303–313.

Basu, Jayeeta and Steven A Siegelbaum (2015). "The corticohippocampal circuit, synaptic plasticity, and memory". In: *Cold Spring Harbor perspectives in biology* 7.11, a021733.

Canto, Cathrin B, Floris G Wouterlood, and Menno P Witter (2008). "What does the anatomical organization of the entorhinal cortex tell us?" In: *Neural plasticity* 2008.

Zemla, Roland and Jayeeta Basu (2017). "Hippocampal function in rodents". In: *Current opinion in neurobiology* 43, pp. 187–197.